

Arabidopsis NSE4 proteins act in somatic nuclei and meiosis to ensure
plant viability and fertility

Dissertation zur Erlangung des Doktorgrades der Naturwissenschaften

doctor rerum naturalium (Dr. rer. nat)

der Naturwissenschaftlichen Fakultät III- Agrar- und Ernährungswissenschaften,
Geowissenschaften und Informatik

der Martin-Luther-Universität Halle-Wittenberg

vorgelegt von

Herr M.Sc. Mateusz Zelkowski

geboren am 11.06.1988 in Lubań, Polen



verteidigt am 21.01.2019; Halle (Saale)

Gutachter:

- 1) Prof. Dr. habil. Andreas Houben
- 2) Prof. Dr. Monica Pradillo Orellana

Acknowledgements

I would like to thank my supervisors Prof. Dr. Andreas Houben and PD Dr. habil. Veit Schubert for giving me the opportunity to be a part of the Chromosome Structure and Function Group, and to have developed my PhD project. I would like to thank you both for guidance, advice, and supervision of this thesis.

I would like to thank very much my wife Kasia Zelkowska for supporting me at work and home. Thank you for this wonderful time in Germany and for being together!

I am sending special thanks to Dr. Dmitri Demidov, Dr. Inna Lermontova, Celia Municio, Dr. Steven Dreissig and Marek Marzec for all project discussions, ideas and great atmosphere in the lab.

I would like to thank our group technicians Oda Weiss, Katrin Kumke and Karla Mayer for their perfect technical assistance.

I would like to also thank all COMREC Maria Skłodowska – Curie program members, especially Prof. Dr. Juan L. Santos, Dr. Monica Pradillo and Pablo Parra Núñez for their help during my stay in Spain.

Niniejszą pracę dedykuję oraz dziękuję za ogromne wsparcie moim kochanym rodzicom Stanisławowi oraz Wiesławie Zelkowskim, babci Loni Zelkowskiej oraz rodzinie Szepietowskich. Ta praca nie jest tylko moja, ale również Wasza. Dziękuję!

Table of content

List of Figures.....	7
List of Tables	16
Abstract.....	18
Zusammenfassung.....	19
Abbreviations	21
1. Introduction.....	23
1.1 Chromatin organization.....	23
1.2 Chromatin dynamics in somatic and generative cell divisions	25
1.3 Structural maintenance of chromosomes (SMC) protein complexes.....	27
1.4 SMC5/6 structure	29
1.5 SMC5/6 localization.....	29
1.6 SMC5/6 function.....	31
1.7 The SMC5/6 complex of <i>Arabidopsis thaliana</i>	34
2. Materials	37
3. Methods.....	41
3.1 Plant materials and growth conditions	41
3.1.1 <i>Arabidopsis thaliana</i>	41
3.1.2 <i>Brassica rapa</i>	41
3.1.3 <i>Nicotiana benthamiana</i>	41
3.1.4 Surface sterilization of <i>A. thaliana</i> seeds	41
3.1.5 Plant crossings	42
3.2 Genetic material extraction	42

3.2.1	Isolation of plant genomic DNA	42
3.2.2	Isolation of plant RNA	43
3.2.3	Plasmid extraction from <i>E. coli</i> cells.....	43
3.2.4	Preparation of DNA for sequencing	43
3.3	Plant genotyping.....	44
3.4	Determination of the DNA, RNA and protein concentration.....	44
3.4.1	DNA and RNA concentration.....	44
3.4.2	Protein concentration.....	45
3.5	DNA restriction, dephosphorylation and ligation	45
3.5.1	DNA restriction	45
3.5.2	Plasmid dephosphorylation.....	46
3.5.3	Plasmid insert ligation	46
3.6	Bacteria transformation and selection	47
3.6.1	Heat shock transformation of <i>E. coli</i> DH5 α and BL21 (pLysS) strains	47
3.6.2	Electroporation of <i>A. tumefaciens</i>	48
3.7	Reverse transcription-PCR (RT-PCR)	48
3.8	Gene expression analysis by quantitative real time PCR.....	48
3.9	Plant transformation and selection	49
3.9.1	Floral dipping of <i>A. thaliana</i>	49
3.9.2	Transient transformation of <i>N. benthamiana</i>	49
3.10	Production of recombinant proteins	50
3.10.1	Recombinant proteins expression.....	50
3.10.2	Extraction of recombinant proteins	50

3.10.3	Purification of recombinant proteins	51
3.10.4	Recombinant protein dialysis	52
3.11	Antibody production	52
3.12	Polyacrylamide gel electrophoresis (PAGE).....	52
3.13	Western blot analysis	53
3.14	DNA gel electrophoresis	53
3.15	Microscopy.....	54
3.15.1	Alexander staining of pollen.....	54
3.15.2	Clearing of siliques	55
3.15.3	Seed setting analysis	55
3.15.4	Meiosis slide preparation.....	55
3.15.5	Fluorescent <i>in situ</i> hybridization (FISH).....	56
3.15.6	Indirect immunostaining.....	57
3.16	Counting of chiasmata.....	58
4.	Results	59
4.1	Characteristics of <i>A. thaliana Nse4</i> genes.....	59
4.1.1	<i>A. thaliana</i> encodes two <i>Nse4</i> gene variants	59
4.1.2	Transcription activity differs between <i>A. thaliana Nse4A</i> and <i>Nse4B</i>	63
4.1.3	<i>Nse4A</i> is co-expressed with cell division- and chromatin structure-specific genes	67
4.2	Functional analysis of <i>Nse4</i> genes	68
4.2.1	The complete inactivation of <i>Nse4A</i> is lethal	70
4.2.2	Complementation of the <i>nse4A</i> T-DNA insertion mutant GK-768H08 with wild-type <i>Nse4A</i>	72
4.2.3	Selection of a homozygous <i>nse4A/nse4B</i> T-DNA double mutant.....	73

4.2.4	<i>nse4A</i> mutants are reduced in size and branch number	74
4.2.5	The mutation of <i>Nse4A</i> , but not of <i>Nse4B</i> induces mitotic defects	76
4.2.6	The <i>Nse4</i> genes are essential for correct meiosis and fertility	77
4.2.7	<i>Nse4A</i> and <i>Nse4B</i> mutations result in impaired meiosis	79
4.2.8	The <i>Nse4A</i> mutation induces predominantly distal acentric fragments and which are not chromosome type-specific	82
4.3	Dynamics and localization of NSE4A in <i>A. thaliana</i>	86
4.3.1	Production of NSE3, NSE4A and SMC5 recombinant proteins in <i>E. coli</i>	87
4.3.2	Production of NSE3, NSE4A and SMC5 antibodies.....	89
4.3.3	Generation of transgenic <i>A. thaliana</i> plants expressing SMC5/6 complex proteins containing a fluorescence tag	90
4.4	Localization of NSE4A in somatic cells of <i>A. thaliana</i>	94
4.4.1	NSE4A localizes exclusively within the euchromatin of interphase nuclei	94
4.4.2	NSE4A is absent from chromatin during mitosis	95
4.5	Localization of NSE4A in meiosis.....	98
4.5.1	NSE4 is present during prophase I in <i>A. thaliana</i> and <i>B. rapa</i>	98
4.5.2	NSE4A::GFP signals are present in meiocytes of <i>A. thaliana</i> undergoing prophase I, prophase II and tetrad formation	101
5.	Discussion.....	103
5.1	<i>A. thaliana</i> encodes two <i>Nse4</i> variants	103
5.2	The specializations of the <i>Nse4</i> genes.....	104
5.3	<i>Nse4A</i> gene inactivation is lethal for <i>A. thaliana</i>	105
5.4	Does the impaired mitosis cause plant developmental defects?	106
5.5	Catalytic role of the SMC5/6 complex in somatic cells.....	107

5.6	Topological role of the SMC5/6 complex in somatic cells.....	108
5.7	In somatic cells NSE4A is localized within euchromatin.....	109
5.8	NSE4A is removed from chromatin during mitosis.....	110
5.9	<i>Nse4</i> is essential for proper male meiosis, fertility and seed development.....	112
5.10	Is SMC5/6 essential for homologous recombination intermediates?.....	114
5.11	NSE4::GFP is detectable at prophase I, II and the tetrads stage.....	115
5.12	Is NSE4A a synaptonemal complex component in plants?.....	116
5.13	The proposed function of NSE4 in plants.....	118
6.	Outlook.....	119
7.	References.....	120

List of Figures

Figure 1 Chromosome organization in eukaryotic organisms (modified from https://theory.labster.com/dna	24
Figure 2 Scheme of mitosis (De Mey et al., 1982).....	25
Figure 3 Scheme of meiosis (Lambing et al., 2017).....	26
Figure 4 Schematic draft of SMC ring structure (Nasmyth and Haering, 2005).....	28
Figure 5 Model of the SMC5/6 complex (modified from Jeppsson et al., 2014).....	29
Figure 6 Proposed meiotic function of the SMC5/6 complex. (A) In presence of functional SMC5/6 complexes accurate chromosome segregation occurs. (B) Lack or down-regulation of SMC5/6 function results in the accumulation of joint molecules including inter-homolog (IH) and inter-sister (IS) joint molecules (Verver et al., 2016).	32
Figure 7 Model of the <i>A. thaliana</i> SMC5/6 complex (Schubert, 2009).....	34
Figure 8 Schemata of the T-DNA genotyping experiment - localization of LP, RP and LB primers with PCR reaction products; wild type (wt) has unchanged genomic DNA (LP+RP); heterozygote (He) possesses one T-DNA insertion (LB+RP) and one unchanged gene copy (LP+RP), homozygote (Ho) has T-DNA insertion (LB+RP), in both gene copies. Adapted from http://signal.salk.edu/tdnaprimers.2.html	44
Figure 9 BSA standard curve and concentration formula.....	45
Figure 10 Gene models of <i>A. thaliana Nse4A</i> and <i>Nse4B</i> . Exons are shown as blue boxes, introns as lines. UTRs are shown in grey.	59
Figure 11 Amino acids sequence alignment between full length NSE4A and NSE4B of <i>A. thaliana</i> . (*) identical amino acids, (: and .) similar amino acids, (-) missing amino acids. The yellow box marks the NSE4-C domain. The alignment was performed by the Clustal Omega 2.1 software (https://www.ebi.ac.uk/Tools/msa/clustalo/).	60

Figure 12 The phylogenic relationships of the putative *Nse4* orthologues in plants. Red and green boxes indicate the *Nse4A* and *Nse4B* *A. thaliana* gene variants respectively. The red numbers represent a measure of support for the node, between 0 and 1 where 1 represents maximal support. The phylogenic model was developed using amino acid sequences and phylogeny.fr tool (Dereeper et al., 2008)..... 62

Figure 13 *In silico* expression patterns of *Nse4A* and *Nse4B* in 10 tissues from 431 individual sequencing samples from the wild-type *A. thaliana* ecotype Col-0 (AT_mRNASeq_ARABI_GL-0 databases <https://genevestigator.com/>). Blue and red bars indicate the relative expression of *Nse4A* and *Nse4B*, respectively..... 63

Figure 14 *In silico* expression patterns of *Nse4A* and *Nse4B* in 10 tissues from 431 individual sequencing samples from the wild-type *A. thaliana* ecotype Col-0 (AT_mRNASeq_ARABI_GL-0 databases <https://genevestigator.com/>). Blue and red bars indicate the relative expression of *Nse4A* and *Nse4B*, respectively. Stages (1-3) indicate early developmental stages of seedling and young rosette; (4-6) developed rosettes, bolting and in young flowers stage; (7-9) mature flowers, silique and seed stage..... 64

Figure 15 Relative expression of the *Nse4A* gene in different tissue types of *A. thaliana*. *Nse4A* expression is present across different tissues, compared to the reference genes *Pp2A* (A) and *Rhip1* (B). The experiment was performed using three technical and biological replicates. 66

Figure 16 Scheme of the *A. thaliana* *Nse4A* and *Nse4B* gene structures (mips.helmholtz-muenchen.de, Version 10; ncbi.nlm.nih.gov; pfam.sanger.ac.uk) and of the expressed truncated transcript of *Nse4A*. Exons are shown as blue boxes. UTRs are visible in grey. The T-DNA insertions (SALK, SAIL and GK lines) and gene specific primers used for genotyping are indicated by arrows. Arabic numbers indicate gene-specific primers used for genotyping. Roman numbers denote primers applied for RT and real-time PCR (Table 5). The transcript of line GK_768H08 with indicated T-DNA insertion (red box) is truncated. 68

Figure 17 PCR genotyping experiment of wild-type and GK-768H08 mutant plants. Gene-specific fragment (GK-768H08-LP + GK-768H08-RP) amplification of a wild-type plant; gene-specific (GK-768H08-LP + GK-768H08-RP) and gene/T-DNA (GK-768H08-LP + GK-LB)

amplification of a heterozygous mutant; and only gene/T-DNA (GK-768H08-LP + GK-LB) amplification of a homozygous T-DNA mutant. 69

Figure 18 RT-PCR-based confirmation of the *nse4A* truncation in the T-DNA mutant line GK-768H08. **(A)** Schemata of gene structure and lengths of transcripts. Primers positions are indicated; the orange box indicates the PCR product of the interstitial gene region; the violet box indicates the PCR product of the central and C-terminal region. **(B)** RT-PCR shows the interstitial region of the *Nse4A* transcript in GK-768H08 and a wild-type plant. **(C)** PCR shows that the PCR product of the C-terminal region of *Nse4A* is missing in line GK-768H08. 71

Figure 19 Full length PCR amplification of the 1.7 kb *Nse4A* promoter and genomic intron-exon sequence of the *Nse4A* gene (*pnse4A::gnse4A*). 72

Figure 20 PCR screening of complemented GK-768H08 mutants using the *nse4A1929F* and *nse4A3953R* primer pair (2024 bp). The numbers indicate individual plants; M indicates the DNA weight marker. **(A)** PCR shows a product for complemented T2 GK-768H08 mutants. **(B)** Control PCR shows a product of wild-type and the lack of amplifications for GK-768H08 mutants. 73

Figure 21 PCR genotyping of T2 mutants from the GK-768H08 x SAIL_296_F02 crossings. P1 – P11 T2 plants display homozygosity for T-DNA in the *Nse4A* and *Nse4B* genes. LP-RP PCR product represents the wild-type (wt) variant of the gene, whereas LB + RP identifies the T-DNA insertion. H₂O: control PCR without template. M: DNA marker. 74

Figure 22 The *nse4A* mutant plants (heterozygous *nse4A* mutant Salk_057130, homozygous *nse4A* mutant GK-768H08 and homozygous *nse4A/nse4B* mutant GK-768H08/SAIL_296_F02) show a reduced growth and branch number compared to wild-type (wt). The wild-type phenotype of GK-768H08 was partially recovered after *pnse4A::gnse4A* complementation. 75

Figure 23 Mitotic defects in *A. thaliana nse4* mutants. **(A)** Somatic wild-type anaphase and examples of chromosome segregation abnormalities (lagging chromosomes and anaphase bridges) in the *nse4A* GK-768H08 and SALK_057130 mutants; **(B)** Frequency of abnormalities (anaphase bridges or lagging chromosomes) in wild-type (wt), *nse4A*, *nse4A/nse4B* double

mutant and *nse4A*-complemented T-DNA lines. The numbers above the columns indicate the number of evaluated mitotic cells. 76

Figure 24 Reduced seed setting and fertility of *nse4* mutants compared to wild-type (wt). (A) Reduced seed number per silique in the *nse4A* and *nse4B* mutants. (B) Shriveled seeds (arrows) from the GK-768H08 mutant. (C) Reduced pollen grain number in an anther of the double mutant GK-768H08/SAIL_296_F02. 77

Figure 25 The mutation of the *Nse4* genes results in reduced fertility. Total pollen number per anther in wild-type (100% - red line), the *nse4A*, *nse4B*, *nse4A/nse4B* mutants and the complemented *nse4A* T-DNA line GK-768H08. The numbers of evaluated pollen grains are indicated above the diagram bars. 78

Figure 26 Mutations in *Nse4A* and *Nse4B* result in meiotic abnormalities. (A) The *nse4A* mutant GK-768H08 shows the fragmentation of the chromosomes at metaphase I and lagging chromosomes at anaphases I and II. The normal behavior of wild-type (wt) chromosomes during meiosis are shown for comparison. Bars = 10 μ m. (B) The frequencies of metaphase I, anaphase I and II abnormalities in wt, the *nse4A* and *nse4B* mutants, the *nse4A/nse4B* double mutant and the complemented *nse4A* line GK-768H08. The number of evaluated cells is shown in Table 14. 80

Figure 27 Chromosomal distribution of 5S and 45S rDNA repeats in wild-type *A. thaliana*. (A) Schematic drawing of the five *A. thaliana* chromosomes showing the localization of 5S and 45S rDNA, (B) Metaphase I chromosomes after FISH with 5S (red) and 45S (green) rDNA probes. 82

Figure 28 FISH-based analysis of metaphase I chromosomes of the *nse4A* line GK-768H08 with 5S (red) and 45S rDNA (green) repeats. (A) Fragmentation of chromosome IV, (B) Fragmentation of chromosome II. 82

Figure 29 The chromosome fragmentation in the *nse4A* mutant GK-768H08 produces predominantly distal acentric fragments. (A) Quantification of chromosome fragments containing telomere and centromere signals in 18 anaphase I cells. (B) Anaphase I cell showing chromosome fragments after FISH with labeled telomeres (red) and centromeres (green). Bar = 5 μ m. 83

Figure 30 Micronuclei in the <i>nse4A</i> mutant GK-768H08. Micronuclei (red arrows) in (A) prophase II and (B) tetrad cells.	84
Figure 31 Comparison of the prophase I stages in wild-type and the <i>nse4A</i> mutant GK-768H08. No abnormalities were observed. Chromosomes were stained with DAPI.	85
Figure 32 The <i>nse4A</i> mutant GK-768H08 shows a wild-type-like distribution of the synaptonmal complex protein ZYP1. Pachytene cells immunostained with anti-ZYP1 (red). Chromatin was counterstained with DAPI (blue).	85
Figure 33 Expression and purification of recombinant NSE4A proteins. Coomassie stained gels after SDS-PAGE electrophoresis. Red arrows indicate recombinant protein NSE4A::6xHIS. (A) Total protein lysate from <i>E. coli</i> cells before and after recombinant protein expression (B) Recombinant protein fraction after Ni-NTA agarose purification.	88
Figure 34 Expression and purification of the recombinant NSE3::6xHIS and SMC5::6xHIS proteins. Coomassie stained gels after SDS-PAGE electrophoresis. Red arrows indicate the recombinant proteins NSE3::6xHIS and SMC5::6xHIS. (A) Total protein lysates from <i>E. coli</i> cells before and after recombinant protein expression. (B) Recombinant protein fractions after Ni-NTA agarose purification.	89
Figure 35 Western blot sensitivity test of the NSE3, NSE4A and SMC5 antibodies against different amounts (1 – 20 ng) of the recombinant proteins (NSE3::6xHIS, NSE4A::6xHIS, SMC5::6xHIS).	90
Figure 36 Structure of the <i>Nse3</i> , <i>Nse4A</i> and <i>Smc5</i> reporter constructs. Black boxes indicate the promoters, blue boxes the genes, orange boxes the fused fluorescent proteins.	91
Figure 37 Nucleus of <i>N. benthamiana</i> showing NSE4A::GFP signals after transient biolistic transformation. BF - bright field illumination, GFP – Green Fluorescent Protein.	91
Figure 38 NSE3::EYFP signals are evident in the nucleus and cytoplasm (in yellow) after transient biolistic transformation of <i>N. benthamiana</i> . White arrow indicates the nucleus.	92

Figure 39 Selection of transgenic T0 *p_{nse4A}::gNse4A::GFP* *A. thaliana* plants expressing BASTA resistance. Within the red circles resistant well developed green seedlings are visible. 92

Figure 40 Genotyping of *A. thaliana* plants containing a *SMC5::EYFP*, *NSE3::EYFP* and *NSE4A::GFP* reporter constructs. Lanes indicate amplified gene fragment. Primers and amplicon size listed in Table 17. GeneRuler 1 kb Plus DNA Ladder used as a DNA size marker..... 93

Figure 41 NSE4A localizes exclusively within the euchromatin of interphase nuclei of *A. thaliana* analyzed by super-resolution microscopy. **(A, C)** Distribution of NSE4A in somatic flower bud and 8C leaf interphase using the NSE4A antibody. **(B)** Distribution of NSE4A::GFP in somatic flower bud interphase nuclei using a GFP antibody. Both anti-NSE4A and NSE4A::GFP specific signals (in green) colocalize with euchromatin, but are absent from heterochromatin (DAPI-intense chromocenters, arrows) and nucleoli (n). The NSE4A labeling visible in the merged image of the 8C nucleus originates from optical slices outside of the nucleolus. 94

Figure 42 The localization of NSE3 and SMC5 in interphase nuclei. Distribution of NSE3 **(A)** and SMC5 **(B)** in somatic flower bud interphase nuclei of wild-type *A. thaliana* analyzed by super-resolution microscopy (SIM). The NSE3 signals are distributed within euchromatin, but were mainly absent in heterochromatic. The SMC5 display euchromatin as well as heterochromatin labeling with strong signal reduction in nucleoli. Arrows indicate heterochromatic chromocenters counterstained with DAPI and (n) indicate nucleoli..... 95

Figure 43 Dynamics of the NSE4A protein during mitosis in the root meristem of *A. thaliana*. GFP signals derived from a genomic construct of NSE4A under the control of the endogenous *Nse4A* promoter were detected by confocal microscopy. **(A)** Global view of an *A. thaliana* root expressing NSE4A::GFP. **(B)** Further enlarged cells undergoing mitosis (in the rectangle). Nuclear NSE4A::GFP signal is present in interphase (0min.), strongly reduced in mitosis (2-10min.) and recovered in telophase (+26min.)..... 96

Figure 44 Maximum intensity projection of a meristematic cell of *A. thaliana* undergoing a mitotic division expressing NSE4A::GFP signals. Time progression is given in minutes..... 97

Figure 45 Detection of NSE4A::GFP signals after anti-GFP immunolabeling of mitotic cells of a transgenic *pnse4A::gNse4A::GFP A. thaliana* plant. Cells were analyzed by super-resolution microscopy (SIM). **(A)** NSE4A::GFP signals (green) in somatic interphase cells colocalize with euchromatin (blue); **(B)** Mitotic metaphase cell without anti-GFP signals (green) at chromosomes (blue). 97

Figure 46 SMC5 is absent during mitosis in the root meristem of *A. thaliana*. A meristematic cell of a SMC5::EYFP transgenic *A. thaliana* plant undergoes a mitotic division (red arrows). Each subfigure represents another stage of mitosis. Time progression is given in minutes. 0 min – Interphase, 3min – mitosis, 27min – telophase, 36min – interphase. 98

Figure 47 Immunolabeling of an *A. thaliana* cell at zygotene using anti-ASY1 (red) and anti-NSE4A (green) antibodies. Chromatin was counterstained by DAPI (blue). 99

Figure 48 Amino acids sequence alignment between NSE4A of *A. thaliana* and putative NSE4A orthologues (XP_009147782 and XP_009144924) of *B. rapa*. (*) identical amino acids, (: or .) similar amino acids, (-) missing amino acids. Alignment performed by Clustal Omega 2.1 (<https://www.ebi.ac.uk/Tools/msa/clustalo/>). 100

Figure 49 Immunolabelling of *B. rapa* prophase I meiocytes using anti-NSE4A (in green), the synaptonemal complex protein ZYP1 (red). The anti-NSE4A colocalizes to ZYP1 (in red) during pachytene. DNA counterstained by DAPI (blue). Bar 10µm. 100

Figure 50 NSE4A::GFP signals are detectable in pollen mother cells of *pnse4A::gNse4A::GFP* transgenic *A. thaliana*. **(A)** Unfixed anther showing NSE4A::GFP signals **(B)** A prophase I cell shows chromatin linked ‘dot-like’ line GFP signals. Chromatin was counterstained with DAPI. 101

Figure 51 Dynamics and localization of NSE4A::GFP signals during meiosis of *pnse4A::gNse4A::GFP* transgenic *A. thaliana* plants. NSE4A::GFP signals are detectable in G2, leptotene, zygotene and pachytene cells. The signals are weak or not visible in condensed metaphase I and anaphase I chromosomes, but recover in prophase II and the tetrads stage. Gray color indicates chromatin counterstained with DAPI, green- anti-GFP. Bars = 10 µm 102

Figure 52 The origin of *Nse4* variants in *A thaliana* explained by the duplication-degradation-complementation model according to Force et al. (1999) and Feder (2007). The *Nse4* common ancestor gene possess two functional modules, required for somatic and embryonic tissue; gene undergoes duplication and gene evolution, in effect two *Nse4* variants were formed *Nse4A* and *Nse4B*. **(A)** *Nse4A* may kept an ancestor gene function (required in different cell types) or underwent subfunctionalization (required for somatic cells), whereas **(B)** *Nse4B* gene kept only part of ancestor gene function required for embryonic tissue. The color boxes indicate gene function modules essential in: red –somatic tissue, blue- embryonic tissue. (Adapted from Feder, 2007). 105

Figure 53 Putative catalytic function of the SMC5/6 complex in somatic cells. SMC5/6 catalytically mediated DSB repair by SUMOylation of the SGS1-TOP3-RMI (STR) complex. SMC5/6 recognize DSB and response in auto SUMOylation, next activated SMC5/6 complex SUMOylate STR complex. Activated STR repair DSB. (Adapted from Bermúdez-López et al. 2010). 108

Figure 54 Putative topological function of the SMC5/6 complex in DNA synthesis and post-synthesis process. SMC5/6 is essential in DNA replication by preventing the formation of replication toxic molecules and sister chromatids intertwining (SCI) (adapted from Jeppsson et al., 2014; Diaz and Pecinka, 2018) 109

Figure 55 Dynamics of NSE4A during mitosis. At interphase NSE4A is present within chromatin. At the entry of mitosis NSE4A becomes released into cytoplasm. The chromosomes contain no or very low amount of NSE4A. At telophase the protein becomes loaded again on chromatin and is evident within euchromatin again in interphase..... 111

Figure 56 Model of meiosis, pollen, embryo and seeds development in *nse4* mutants. **(A)** The *nse4* mutant is partially able to produce viable pollen, fertilize the egg and produce viable seeds. **(B)** On the other hand, the *nse4* mutants display impaired meiosis and fertility, such as unequal division and chromosome damage. This damage results in pollen abortion or abnormal pollen. Abnormal pollen has an unbalanced genetic content, which after fertilization causes embryo lethality and disturbance of seeds formation. 113

Figure 57 Dynamics of NSE4A::GFP during the meiosis of *A. thaliana* meiosis. In G2 and leptotene, NSE4A::GFP displays a strong dispersed chromatin labeling. At zygotene and pachytene, NSE4A::GFP shows ‘line-like’ signals along the chromosome axis. At metaphase I and anaphase I the protein becomes released from the chromosomes and accumulates in the cytoplasm. At prophase II and the tetrad stage NSE4A-signals reappear. 116

Figure 58 ZYP1 and NSE4A colocalize at the synaptonemal complex (SC) of rye. **(A)** Immunolocalization of NSE4A and ZYP1 shows their colocalization at the central region of the SC throughout zygotene Bars = 5µm. **(B)** NSA4A structure between bivalents in diplotene cells. The FISH probe Bilby labels the rye centromeres. Bar = 2µm. **(C)** ZYP1 and NSE4A form ball-like structure embedded in chromatin-free regions during diakinesis; Bar = 1µm. 117

List of Tables

Table 1 List of chemicals and enzymes used in experiments	37
Table 2 List of apparatus used in experiments.....	37
Table 3 List of bacteria strains and vectors used in experiments.....	38
Table 4 List of kits used in experiments	38
Table 5 List of primers used in experiments	39
Table 6 List of antibodies used in the experiments.....	40
Table 7 NSE4 protein sequence similarity of orthologues in different organisms (<i>A. t.</i> – <i>A. thaliana</i> ; <i>S. c.</i> – <i>S. cerevisiae</i> ; <i>E. h.</i> <i>E. histolytica</i> ; <i>D. d.</i> – <i>D. discoideum</i> ; <i>M. m.</i> – <i>M. musculus</i> ; <i>H. s.</i> – <i>H. sapiens</i>). The matrix was generated by the Clustal Omega 2.1 software.	61
Table 8 Primers used in <i>Nse4</i> genes real-time quantitative RT-PCR	65
Table 9 Genes showing high co-expression with <i>nse4A</i> . Scores indicate the level of correlation of expression in different anatomical samples. Gene names and their predicted coded proteins are obtained from databases of https://genevestigator.com . Bold gene names indicate cell division- or chromatin structure-specific genes.	67
Table 10 Primer combinations used for T-DNA line genotyping.....	69
Table 11 Primer combinations used for the analysis of the T-DNA line GK-768H08.....	70
Table 12 Primers combinations used for <i>pnse4A::gNse4A</i> amplification.....	72
Table 13 Primer pair used for the GK-768H08 complementation assay.	73
Table 14 Characterization of <i>A. thaliana nse4A</i> and <i>nse4B</i> T-DNA insertion mutants. Number of – analyzed pollen, seeds, siliques and cells are in parentheses. ** $p < 0.01$; * $p < 0.05$	81
Table 15 Chiasmata number of the <i>nse4A</i> mutant GK-768H08 and wild-type	86

Table 16 Primers used for the amplification of SMC5/6 complex gene fragments. The sequences of restriction sites used for cloning are underlined. 87

Table 17 Primer pair used for the transgenic line genotyping. 93

Abstract

The SMC 5/6 complex along with cohesin and condensin is a member of the structural maintenance of chromosome (SMC) protein family. In yeast and mammals, this complex is engaged in DNA double strand break repair, genome stability, meiotic synapsis and recombination. In plants, the function of SMC5/6 remains enigmatic. Therefore, we analyzed the crucial δ -kleisin component NSE4 of the SMC5/6 complex in the model plant *Arabidopsis thaliana*. We identified and characterized two candidate genes - *Nse4A* and *Nse4B*. The knock-out of the *Nse4A* gene is lethal for the plant. Gene expression analyses demonstrated *Nse4A* expression across different tissue types, whereas *Nse4B* expression was undetectable or limited to generative tissue. This suggests that NSE4A is essential during plant growth in somatic tissues. Functional *nse4A* mutant analyses identified anaphase bridges or lagging chromosomes in mitosis, reduced plant size and fertility. During meiosis the *nse4* mutants displayed abnormalities like lagging or fragmented chromosomes. The complementation of a *nse4A* mutant by a genomic *Nse4A* construct recovered mainly the normal mitotic and meiotic phenotypes. To characterize the dynamics and localization of SMC5/6 complex components, we generated specific antibodies and transgenic fluorescence protein lines for NSE3, NSE4A and SMC5. Thus, we found the presence of these subunits in somatic *A. thaliana* nuclei. Detailed studies using structured illumination microscopy (super-resolution) confirm the localization of NSE3, NSE4A and SMC5 within euchromatin. The analysis of NSE4A::GFP and SMC5::EYFP lines revealed also the labeling of somatic nuclei, but a strong reduction of the chromatin-linked fluorescence signals during mitosis. The analysis of *A. thaliana* plants expressing *nse4A::gNse4A::GFP* revealed a chromatin-specific localization of NSE4A in meiotic G2, prophase I, II and tetrad stage cells. At prophase I, NSE4A creates 'line-like' structures similar to ZYP1, the synaptonemal complex protein. Additional experiments performed on *B. rapa* and *S. cereale* prophase I meiocytes show co-localization with ZYP1. This suggests that NSE4, like in other organisms, might be involved in the synaptonemal complex formation of plants.

Zusammenfassung

Gemeinsam mit cohesin und condensin gehört der SMC5/6-Komplex zur Familie der „Structural Maintenance of Chromosome (SMC)“ Proteine. Bei Hefe und Säugetieren ist dieser Komplex an der DNA-Doppelstrang-Reparatur, der Genomstabilität, sowie an der meiotischen Synapsis und Rekombination beteiligt. Bei Pflanzen sind die Funktionen des SMC5/6-Komplexes nach wie vor weitgehend ungeklärt. Daher untersuchten wir insbesondere die wichtige δ -kleisin Untereinheit NSE4 des SMC5/6 Komplexes bei der Modellpflanze *Arabidopsis thaliana*. Wir identifizierten und charakterisierten zwei Kandidaten-Gene: *Nse4A* and *Nse4B*. Ein „knock-out“ von *Nse4A* ist für die Pflanze letal. Gen-Expressions-Analysen von *Nse4A* zeigten eine Expression in sämtlichen untersuchten Geweben. *Nse4B* hingegen wurde nicht exprimiert, bzw. Transkripte traten nur in generativem Gewebe auf. Das deutet darauf hin, dass NSE4A essentiell in somatischem Gewebe während des Pflanzenwachstums ist. Funktionelle Analysen von *nse4A*-Mutanten zeigten, dass während der Mitose Anaphase-Brücken und „lagging“-Chromosomen auftreten. Zusätzlich wurde eine verminderte Pflanzengröße und Fertilität beobachtet. Im Verlauf der Meiose zeigten die *nse4A*-Mutanten Abnormalitäten, wie fragmentierte und „lagging“-Chromosomen. Die Komplementierung der *nse4A*-Mutante durch ein genomisches *Nse4A*-Konstrukt stellte die normalen mitotischen und meiotischen Phänotypen größtenteils wieder her. Um die Dynamik und Lokalisierung der SMC5/6-Komplex Komponenten zu untersuchen, stellten wir spezifische Antikörper gegen NSE3, NSE4A und SMC5 her. Außerdem produzierten wir transgene Linien, die diese Untereinheiten durch Koppelung an fluoreszenzierende Proteine sichtbar machen. Dadurch identifizierten wir die betreffenden Untereinheiten in somatischen Zellkernen von *A. thaliana*. Detaillierte Untersuchungen durch strukturierte Beleuchtungsmikroskopie (Super-auflösende Mikroskopie) betätigten die Lokalisierung von NSE3, NSE4A und SMC5 im Euchromatin. Die Analyse von NSE4A::GFP und SMC5::EYFP Linien zeigte auch eine Markierung der somatischen Zellkerne. Eine starke Reduzierung der Chromatin-gebundenen Signale erfolgte jedoch während der Mitose. Die Untersuchung von *A. thaliana* Pflanzen, die *pnse4A::gNse4A::GFP* exprimierten, zeigte eine Chromatin-spezifische Lokalisierung von NSE4A in der meiotischen G2 Phase, Prophase I, II und in Zellen des Tetradenstadiums. Während der Prophase I bildet NSE4A linien-artige Strukturen, so ähnlich wie ZYP1, ein Protein des synaptonemalen Komplexes. Zusätzliche Experimente, die an *B. rapa* and *S. cereale* Prophase I Meiozyten durchgeführt wurden, zeigten eine Ko-lokalisierung mit

ZYP1. Das lässt vermuten, dass NSE4, ähnlich wie in anderen Organismen, an der Bildung des synaptonemalen Komplexes beteiligt ist.

Abbreviations

ABC	ATP-binding cassette
ATP	adenosine tri-phosphate
BLAST	Basic Local Alignment Search Tool
bp	base pair
BSA	bovine serum albumin
cDNA	complementary deoxyribonucleic acid
CO	crossing-over
Col-0	Columbia-0
DAPI	4',6-diamidino-2-phenylindole
DSB	double-strand break
dHJ	double Holliday junction
DNA	deoxyribonucleic acid
FISH	Fluorescent <i>in situ</i> hybridization
GFP	green fluorescent protein
H3K9	histone H3 lysine 9
IPTG	isopropyl β -D-1-thiogalactopyranoside
JM	joint molecule(s)
LB medium	Luria-Bertani medium
min	minute(s)
mg	milligram
ml	milliliter

mM	<u>m</u> ilim <u>ol</u>
MMS	<u>m</u> ethyl <u>m</u> ethane <u>s</u> ulfonate
MS medium	<u>M</u> urashige and <u>S</u> koog medium
NaOCl	sodium hypochlorite
nm	<u>n</u> an <u>o</u> meter
PCR	polymerase <u>c</u> hain <u>r</u> eaction
PMC	pollen <u>m</u> other <u>c</u> ell(s)
PTMs	post- <u>t</u> ranscriptional <u>m</u> odifications
RNA	<u>r</u> ibonucleic <u>a</u> cid
rpm	<u>r</u> evolution per <u>m</u> inute
RT-PCR	<u>r</u> everse <u>t</u> ranscription polymerase <u>c</u> hain <u>r</u> eaction
SC	<u>s</u> ynaptonemal <u>c</u> omplex
SDS	<u>s</u> odium <u>d</u> odecyl <u>s</u> ulfate
SMC	<u>s</u> tructural <u>m</u> aintenance of <u>c</u> hromosomes
T-DNA	transferred DNA
WT	<u>w</u> ild type
YFP	yellow <u>f</u> luorescent protein
°C	degree Celsius
µm	micrometer

1. Introduction

1.1 Chromatin organization

The genetic material in eukaryotic cells is organized into macromolecular complexes composed of DNA, RNA and proteins. These components are compacted over 10,000-fold in a form called chromatin and they are located in the nucleus. The cell controls the level of DNA compactness, modulate protein to DNA accessibility and genes expression, which is essential in DNA replication, recombination and repair. The dynamic organization of chromatin has a fundamental role in cell biology processes (Woodcock and Ghosh, 2010).

DNA is highly organized (Figure 1), the most basic DNA “packing unit” is the nucleosome, which is composed of an octamer of the four (H2A, H2B, H3, H4) core, positively charged histone proteins. Due to presence of negatively charged phosphate groups in its sugar backbone, DNA is bound very tightly to the positively charged nucleosomes. Each nucleosome wraps 146 DNA base pairs (bp) and forms a DNA - protein structure of 11 nm diameter. Nucleosomes in chromatin are interlinked by a short (20 - 80 bp) DNA linkers to form beads-on-the-string structures (Olins and Olins, 1974) and build more organized structures such as 30 nm fibers. Fibers can have either a continuous or a discontinuous organization. The continuous fibers have a similar density of nucleosomes, while the discontinuous fibers display a disparate level of nucleosome numbers per fiber length. This causes higher-order structures such as superbeads or clutches (thick chromatin with a high number of nucleosomes). These nucleosome-dense regions can be connected with short and more relaxed fiber structures. It is speculated that these non-condensed linkers can be the regions of interaction with other non-histone structural proteins, like structural maintenance of chromosomes (SMC) complexes (Kuznetsova et al., 2016).

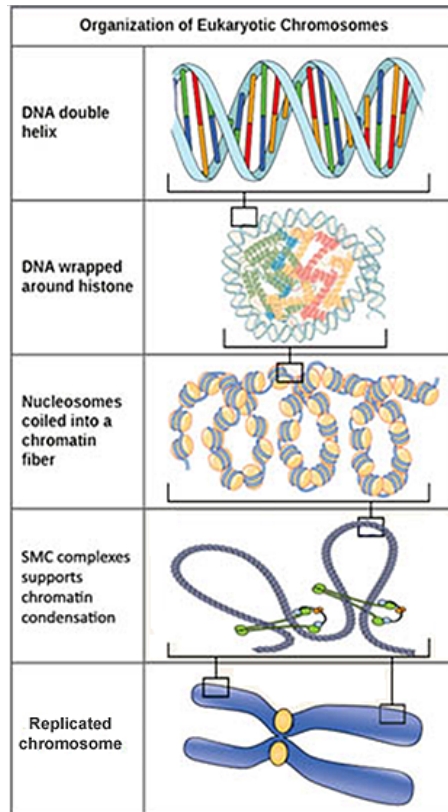


Figure 1 Chromosome organization in eukaryotic organisms (modified from <https://theory.labster.com/dna-packaging/>).

Histone modifications

Chromatin remains structurally loose in interphase cells, allowing access for RNA polymerases and gene expression, but environmental changes demand fast and effective changes of the chromatin state in order to adjust the level of gene transcription. An effective way to manipulate the DNA structural state and transcription are post-transcriptional modifications (PTMs) of histones. For example, modifications such as at histone H3 lysine 9 (H3K9) acetylation provoke the unwrapping of DNA from nucleosomes and thus make chromatin more accessible for transcription mediated by the RNA polymerase. This type of less compacted DNA is called euchromatin. On the other hand, dimethylation of lysine 9 of histone H3 makes chromatin fibers more dense and transcriptionally inactive (heterochromatin) (Bowman et al., 2014).

1.2 Chromatin dynamics in somatic and generative cell divisions

Chromatin becomes more dynamic and condensed during the process of cell division, where a cell divides into two somatic or more generative cells. In that process, DNA becomes condensed and forms chromosomes. Chromosomes are highly compacted chromatin fibers held together by SMC proteins. These protein complexes seem to be involved in the higher-order chromatin organization and dynamics (Verver et al., 2016).

Mitosis

Mitosis is a specialized process where the replicated genetic material from a parental cell is divided into two genetically identical daughter cells. Mitosis has five major phases: interphase, prophase, metaphase, anaphase and telophase (Figure 2). The interphase has three stages: first the gap (G1), which is the growing phase; second the DNA synthesis (S) phase; and finally the second gap (G2). Then, in prophase, DNA is condensed by condensins (SMC complex) and forms chromosomes composed of two sister chromatids held together by cohesin SMC complexes. At metaphase, chromosomes form a metaphase plate, kinetochores and microtubules, and, as part of the mitotic spindle, attach to the centromeres. This spindle machinery allows to separate the sister chromatids during anaphase. Chromatids become decondensed in telophase and two new nuclei are formed (O'Connor, 2008).

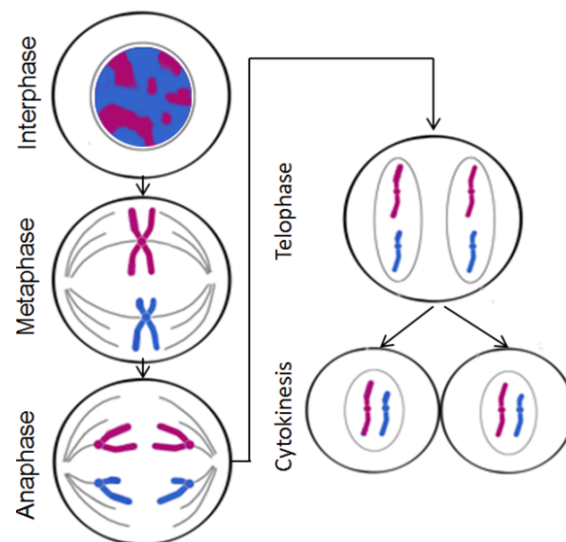


Figure 2 Scheme of mitosis (De Mey et al., 1982).

Meiosis

Meiosis is part of the sexual reproduction process during which DNA material is reduced by half and produces genetically different daughter cells. There are two major stages that can be distinguished in meiosis: meiosis I and meiosis II, representing reductional and equational divisions, respectively (Figure 3).

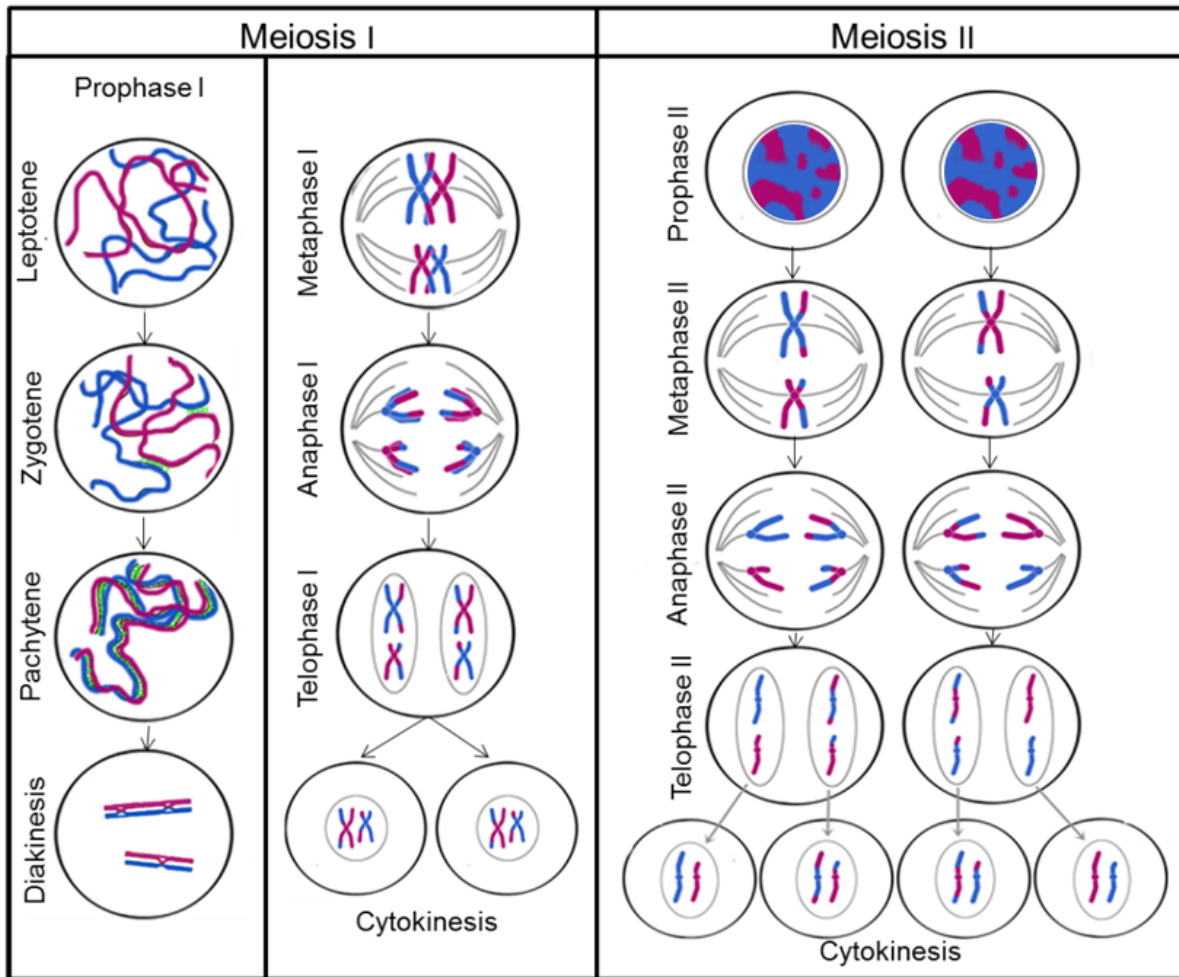


Figure 3 Scheme of meiosis (Lambing et al., 2017).

After DNA replication follows prophase I. Prophase I is the longest meiotic stage, where the chromosomes condense, homologues pair and genetic material becomes exchanged in a process called recombination. The meiotic prophase is divided into five stages: leptotene, zygotene, pachytene, diplotene and diakinesis. In leptotene, the chromatin becomes condensed, and individual chromosomes composed of two sister chromatids become visible under the light

microscope as lines within the nucleus. At zygotene, the homologues start to bind in parallel in the process of synapsis. During pachytene, synapsis takes place, the homologous chromosomes are paired across the entire chromosome and the chromatids are held together by a specialized protein structure called synaptonemal complex (SC). Axial proteins of the SC, such as ZYP1, form a line along the homologous chromosomes. At late pachytene, synapsis ends and the lateral element proteins ASY1 become released from the SC (O'Connor, 2008). The genetic material is exchanged between crossing-over sites of the homologous sister chromatids in a process called recombination.

In diplotene, meanwhile, synaptonemal complex elements depolymerize from chromosomes. Chromosomes become more condensed and the homologues are held together by chiasmata - a point linker between the homologues, however, recent data from rye shows also presence of synaptonemal complex elements (ASY1 and ZYP1) in chiasmata (Hesse et al., submitted). In metaphase I, the homologous chromosomes move to form the metaphase plate to be separated in anaphase I. The divided homologues uncoil in telophase and a new nucleus is formed. In meiosis II, sister chromatids are separated in four stages. Prophase II: the chromatin becomes condensed into chromosomes (composed of two sister chromatids). Metaphase II: the chromosomes form a metaphase plate. Anaphase II: the sister chromatids divide. Finally, the chromosomes are become decondensed in telophase II. As a consequence of meiosis, one diploid cell divides twice to form four haploid, genetically different daughter cells (O'Connor, 2008).

1.3 Structural maintenance of chromosomes (SMC) protein complexes

SMC proteins are one of the most important protein families which are engaged in processes such as chromosome condensation, transcription, DNA repair, homologous recombination and cell division. Their conserved function from archaea to mammals is required to organize chromatin and chromosomes.

SMC proteins were first identified in *Escherichia coli* (Niki et al., 1992) The first eukaryotic orthologue was found in budding yeast and was named SMC1 (Strunnikov et al., 1993). The characteristic feature of this highly conserved protein is its unique structure. SMC proteins have an ATP-binding cassette (ABC) located in the C- and N-terminus called *walker A* and *walker B*, respectively. Walker themes are interconnected by a long coiled-coil structure and consequently

form a protein with a hinge domain at one terminus and an ATPase domain at the other. The hinge domain is a dimerization point with other SMC subunits; two dimerized SMC subunits form a heterodimeric V-shaped structure. ATPase domains from each SMC subunit bind with the kleisin bridge protein through ATP-dependent dimerization. These two SMCs and one kleisin form together a ring-shaped SMC complex (Figure 4) (Haering et al., 2002). To the SMC ring complex additional proteins may be attached. These supporting proteins have different functions influencing the dynamics and the functions of the complexes, like DNA binding or catalytic support (Jeppsson et al., 2014).

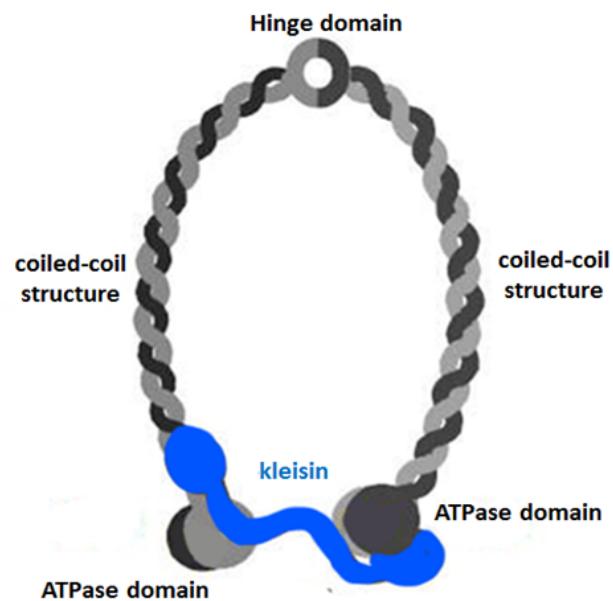


Figure 4 Schematic draft of SMC ring structure (Nasmyth and Haering, 2005)

In eukaryotes, there are three major SMC complexes: cohesin, condensin and the SMC5/6 complex. These complexes have a typical heterodimer ring structures and topologically embrace the chromosomes (Kanno et al., 2015; Wilhelm et al., 2015), which seems to be one of their most crucial functions. Alternatively, a hold-and-release model has been proposed for cohesin (Xu et al., 2018).

The SMC complexes most studied so far are cohesins and condensins. Cohesins realize inter-chromatin links for sister chromatid cohesion during mitosis and meiosis (Jeppsson et al., 2014).

Condensins contribute to chromosome assembly and segregation during cell division (Jeppsson et al., 2014). The third and still most enigmatic complex is SMC5/6.

1.4 SMC5/6 structure

The SMC5/6 complex is composed of three major SMC subunits: SMC5, SMC6 and one δ -kleisin bridge protein, the non-SMC element 4 (NSE4). NSE4 connects two SMC subunits and together they form the core ring of the SMC5/6 complex. In addition to the core proteins, the complex contains further NSE subunits (Figure 5). NSE1 is an ubiquitin ligase-like protein, while the NSE2 (also called MMS21) is a catalytically active E3 SUMO ligase. The NSE3 alpha-helix is essential for the SMC5/6 complex, as it triggers DNA binding. There are two additional NSE subunits - NSE5 and NSE6. In budding yeast they are associated with the hinge domain responsible for the complex stabilization (Verver et al., 2016).

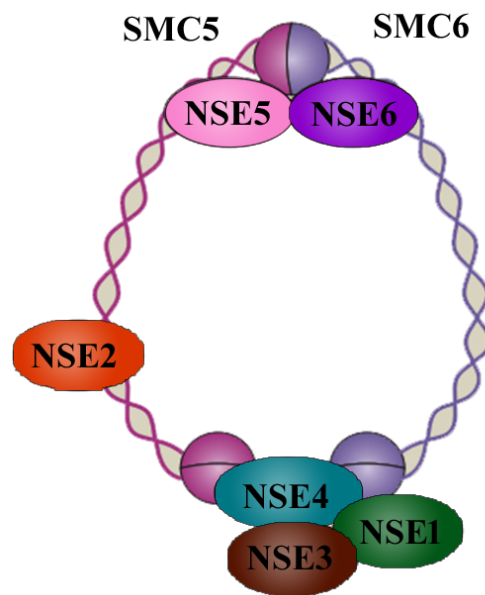


Figure 5 Model of the SMC5/6 complex (modified from Jeppsson et al., 2014)

1.5 SMC5/6 localization

Somatic cells and mitosis

The studies in human, mice, yeast and plants using fluorescently tagged proteins and staining with antibodies demonstrated a disperse distribution of the SMC5/6 subunits within the

chromatin of interphase cell nuclei. In humans, the SMC5 signals were detected in interphase nuclei and at the entry of mitosis. When the cell cycle progresses, the signals dissociate from the mitotic chromosomes, to be recovered in the G1 phase (Gallego-Paeza et al., 2014). On the other hand, in mice and yeast, SMC6 displays the localization within mitotic chromosomes with an enrichment at centromeres (Gomez et al., 2013; Young-Gonzales et al., 2012). In plants, transiently transformed *N. benthamiana* leaves using *A. thaliana* NSE1 and NSE3 fluorescent tagged proteins showed signals within the nucleus (Li et al., 2017).

Meiosis

A number of localization studies demonstrated the colocalization of SMC5/6 subunits with synaptonemal complex proteins during prophase I (Gomez et al., 2013; Verver et al., 2016). On the other hand, there is not much evidence regarding the localization and dynamics of SMC5/6 subunits in subsequent meiotic stages. Depending on the species and type of study the distribution of SMC5/6 was observed differently.

Studies on human spermatocytes demonstrated the localization of SMC5 within chromatin from zygotene until diplotene. In zygotene, where synapsis begins, SMC5 signals are dispersed along the chromosomes. The signals become more linear with the progression of synapsis. At pachytene, SMC5 forms a continuous line colocalizing with the synaptonemal complex axis and the cohesin subunit SA-3 (STAG3, a component of the synaptonemal complex assembly). In later meiotic stages, the signals disappeared (Verver et al., 2014).

In mouse spermatocytes SMC5 and SMC6 were found in prophase I. These subunits were detected from early zygotene until late diplotene. The SMC5 and SMC6 signals colocalized with the synaptonemal complex protein SYCP3 (synaptonemal complex protein 3). Interestingly, in contrast to human, SMC5 and SMC6 were still detectable after prophase I. In diplotene, both subunits were detected in the pericentromeric regions (Rattner et al., 1996; Gomez et al., 2013).

In *C. elegans*, fluorescent reporter protein tagged SMC6 is present within the chromatin of generative germ cells. SMC6 signals form lines along the chromosome axes from early prophase I until diakinesis (Bickel et al., 2010).

In yeast, SMC5 and SMC6 are present in the nucleus from the outset of meiosis. As meiosis progresses, both signals form continuous foci within the chromosome axes and they are additionally colocalized with the synaptonemal complex protein ZYP1 (Copsay et al., 2013; Farmer et al., 2011). Controversial is the distribution of SMC5/6 after prophase I. Some studies report that SMC6 is localized within chromatin during the entire meiosis process (Xavier et al., 2013), while other studies point to the absence of SMC5 and SMC6 proteins after prophase I (Copsay et al., 2013).

Chromatin immunoprecipitation studies using prophase I yeast cells and SMC6 antibodies demonstrate an enrichment of SMC6 in the pericentromere, along with cohesin and RAD51 (an indicator of double strand breaks (DSB)) DNA binding sites (Copsay et al., 2013; Xavier et al., 2013).

1.6 SMC5/6 function

SMC5/6 was first characterized as a DNA repair complex, but recent studies show that the SMC5/6 complex is involved in several other processes related to genome stability, DNA replication, homologous recombination, proper mitosis and meiosis (reviewed in Verver et al., 2016).

SMC5/6 and joint molecules

Downregulation of SMC5/6 genes influences the stability of genomes in all species investigated so far. In yeast, human and plant cells, SMC5/6 inhibition results in mitotic and meiotic defects such as lagging chromosomes and anaphase bridges (Copsay et al., 2013; Galego-Peaz et al., 2014; Li et al., 2017).

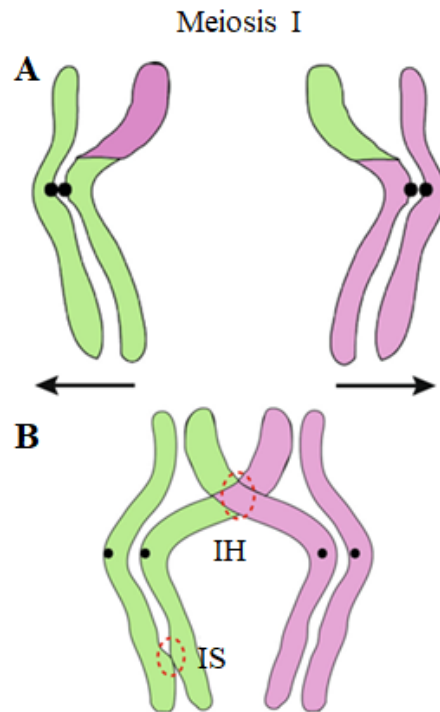


Figure 6 Proposed meiotic function of the SMC5/6 complex. (A) In presence of functional SMC5/6 complexes accurate chromosome segregation occurs. (B) Lack or down-regulation of SMC5/6 function results in the accumulation of joint molecules including inter-homolog (IH) and inter-sister (IS) joint molecules (Verver et al., 2016).

Recent studies on joint molecules (JM) suggest that these molecules are a product of unresolved double Holliday junction (dHJ) intermediates. dHJ occur as a result of DNA repair after the collapse of the replication fork in the S phase, and after crossing-over (CO) formation during meiotic recombination (Figure 6). Studies in different species demonstrate SMC5/6 knock-out and knock-down effects on the formation of joint molecules.

In yeast, NSE2 is required for auto-SUMOylation of the SMC5/6 complex. Auto-SUMOylation is essential for DNA binding and activation of TOP3 and SGS1 in the STR (STR is a complex of SGS1, TOP3 and RMI1 proteins) complex, which is crucial for 5' to 3' DNA resection and resolving/dissolving of dHJ intermediates (Bermudez-Lopez et al., 2016).

Other studies involving humans and yeast show that SUMOylation of the cohesin subunit SCC1 requires the engagement of the SMC5/6 complex. The α -kleisin SCC1 is a major component of the cohesin ring and the docking site for support proteins such as PDS5 and SCC3 (Hearing et al., 2002). SUMOylation of SCC1 counteracts the release of cohesin from chromosomes and

interferes with their dynamics. In higher organisms cohesins are responsible for DNA repair, mitotic and meiotic spindle attachment, and sister chromatid cohesion (Jeppsson et al., 2014). The interruption of cohesion's function can lead to the formation of joint molecules.

Homologous chromosome pairing

Several independent studies in a number of organisms demonstrated the localization of SMC5/6 complexes in chromosome axes during prophase I (Gomez et al., 2013; Verver et al., 2014; 2016). Unfortunately, the role of SMC5/6 in synapsis remains enigmatic. In mice, the colocalization of SMC6 and SYCP3 (Synaptonemal Complex Protein 3) was observed starting from zygotene until late pachytene. Studies in mutants prove that the loading of SMC6 into the synaptonemal complex (SC) depends on SYCP1 (transverse filament of synaptonemal complex protein), but it is independent of REC8 (meiosis-specific homolog of the α -kleisin SCC1) and the SMC1 β cohesin subunits (Gomez et al., 2013). This suggests that the SMC5/6 complex embrace of homologous chromosomes or support the SC machinery. In both cases SMC5/6 functions independently of cohesin (Gomez et al., 2013). Another explanation of the role of SMC5/6 in SC formation and synapsis is the SUMOylation activity of NSE2. Studies in budding yeast show the need for SUMOylation of the SC for proper chromosome synapsis (Voelkel-Meiman et al., 2013; De Carvalho and Colaiacovo, 2006).

Meiotic recombination

SMC5/6 complexes antagonizes the formation of joint molecules by supporting the resolution of dHJ. This type of recombination occurs during the CO process. In budding yeast, SMC5/6 accumulates in recombination hot-spots and antagonizes the formation of JM by destabilizing single-end invasion. This prevents the formation of improper recombination intermediates (Copsey et al., 2013; Verver et al., 2016). Together with the endonucleases MUS81 and STR, the SMC5/6 complex promotes the normal formation and resolution of dHJ during the CO process (Bermudez-Lopez et al., 2016).

In *C. elegans*, mutations of SMC5 and SMC6 show meiotic chromosome dysmorphia and chromosome fragmentation. A similar phenotype was observed in *mus81* mutant (MUS81 is essential for meiotic homologous recombination), which indicates the supportive role of SMC5/6

complexes in resolving dHJ intermediates. Furthermore, *smc5* and *smc6* mutants demonstrate abnormal accumulation of SPO11-dependent homologous recombination intermediates (marked by RAD51 protein), which potentially indicate blocked or delayed formation of dHJ. This could be affected by dysfunctional single-end invasion in dHJ stabilization (Bickel et al., 2010; Verver et al., 2016).

1.7 The SMC5/6 complex of *Arabidopsis thaliana*

Knowledge about the plant SMC5/6 complexes is still very limited, and most of the studies have been performed on the model plant *A. thaliana*. The current model of the *A. thaliana* SMC5/6 complex (Figure 7) assumes the existence of SMC5, two variants of SMC6, SMC6A and SMC6B, NSE1, NSE2, NSE3, and two variants of the NSE4 δ -kleisin, NSE4A and NSE4B (Schubert, 2009). There is also evidence for the existence of NSE5 and NSE6 orthologues in *Arabidopsis* known as ASAP1 and SNI1, respectively (Yan et al., 2013).

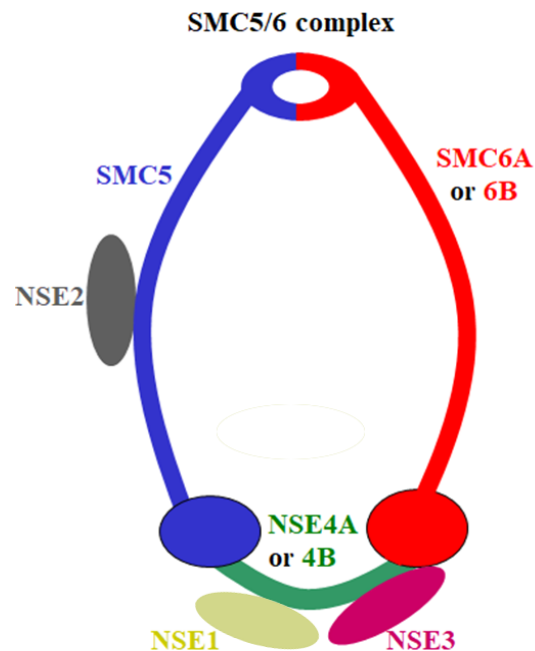


Figure 7 Model of the *A. thaliana* SMC5/6 complex (Schubert, 2009)

The transcripts of the SMC5/6 genes are present across different tissues and developmental stages. Only NSE4B is very seldom or undetectable (Watanabe et al., 2009). The recent data indicate the involvement of SMC5/6 complex components in DNA repair, somatic homologous

recombination, embryogenesis, plant development, as well as meiosis (Jeppsson et al., 2014; Verver et al., 2016).

DNA repair and homologous recombination

The first attempts to characterize one of the subunits of SMC5/6 SMC6B date back to 1999. (Mengiste et al., 1999) demonstrated hypersensitivity of *smc6B* mutants after a DNA-damaging treatment. On the other hand overexpression of SMC6 increased intrachromosomal recombination (Hanin et al., 2000).

Interestingly, later studies confirmed the relationship between DNA-damaging treatment and homologous recombination for other SMC5/6 subunits. *nse2* mutants exhibit an increased DSB number after treatment with the toxic agent methyl methanesulfonate (MMS) (Xu et al., 2013). SMC5, SMC6A and SMC6B are essential for sister chromatid alignment and homologous recombination after DNA breakage. Furthermore, SMC6B is important for DNA repair induced by the non-methylable cytidine analog – Zebularine (Liu et al., 2014). NSE6 (SNI1) is engaged in DNA DSB response (Yan et al., 2013).

The current data from different laboratories support the hypothesis that the SMC5/6 complex is required for effective homologous recombination (HR) repair and can be used to manipulate intrachromosomal recombination.

Plant development

The SMC5/6 complex has, beside its function in genome stability, also a function in plant development and embryogenesis. NSE1 and NSE3 are essential for early embryogenesis and post-embryonic development. *nse1* and *nse3* mutants display anaphase bridges and lagging chromosomes during mitotic anaphase (Li et al., 2017). *Nse1* and *Smc5* genes were originally identified as embryo defective genes *Nse1* (EMBI1379) and *Smc5* (EMBI2782) (Tzafrir et al., 2004). *nse2* has dwarf phenotype, display impaired embryogenesis and root development (Liu et al., 2014; Xu et al., 2013). The expression of a *pNse2::GUS* construct is detectable in anthers, leaf vein and hypocotyl *A. thaliana* cells (Ishida et al., 2012). A recent study demonstrated a regulatory role of NSE2 in the floral repressor of FLC (flowering locus C) via its SUMO E3 ligase activity, and *nse2* mutant displayed early flowering (Kwak et al., 2016). In addition,

Arabidopsis Nse2 deficient plants show an improved drought tolerance; whereas the constitutive expression of *Nse2* reduced drought tolerance (Zhang et al., 2013).

Meiosis

Mutants of the SMC5/6 complex subunits display a number of meiosis-related problems. *nse1* and *nse3* mutants show aborted ovules and sterile seeds (Li et al., 2017). *nse2* mutant displays semi-sterility, reduced siliques length and seed settings. At microscopic level, *nse2* revealed abnormalities in meiosis from diakinesis until tetrad stage, such as chromosome fragmentation and anaphase bridges. Furthermore, these mutants exhibit a high overexpression of recombination-related genes like *Rad51* and *Spo11-1* (Ishida et al., 2012; Liu et al., 2014). Recent knowledge about the SMC5/6 complex in plants, like in other organisms, suggests that this complex is essential for proper development, recombination and meiosis.

2. Materials

Table 1 List of chemicals and enzymes used in experiments

Name	Distributor
Ampicillin	Duchefa Biochemie
Bradford	Bio-Rad
Chloramphenicol	Duchefa Biochemie
Coomassie Brilliant Blue R-250	Serva
DNA Gel 6X Loading Dye	Thermo Fisher Scientific
DNA GeneRuler™ 1 kb Ladder	Thermo Fisher Scientific
DNA Polymerase KOD Xtreme™ Hot Start	Merck
DNA Polymerase GoTaq®	Promega
dNTPs	Thermo Fisher Scientific
Formaldehyde	Sigma-Aldrich
Freund Adjuvant	BD
HDGreen Plus DNA Stain	Elchrom Scientific
IPTG	Sigma-Aldrich
Kanamycin	Duchefa Biochemie
Ligase T4	Thermo Fisher Scientific
Lysozyme	Carl Roth
Milk (powdered)	Salifer
Phosphatase (sap)	Thermo Fisher Scientific
Protino® Ni-NTA Agarose	MACHEREY-NAGEL GmbH
Restriction enzymes	Thermo Fisher Scientific
Rifampicylin	Duchefa Biochemie
Silvet 77	Helena Chemical
Streptomycine	Duchefa Biochemie
Tris	Carl Roth
Triton X-100	Serva
TRIzol	Thermo Fisher Scientific
Tween 20	Serva

Table 2 List of apparatus used in experiments

Name	Distributor
Alpha Imager HP System Automated Gel Imaging	Protein simple
Centrifuge BIOFUGE® FRESCO	Heraeus
Confocal microscopy LSM780	Carl Zeiss

Elektrophorese System Mupid ONE	Eurogentec
Mastercycler Nexus PCR Machine	Eppendorf
Mini Electrophoresis Systems (Bio-Rad)	Bio-Rad
MyCycler™ Thermal Cycler System	Bio-Rad
NanoDrop Microvolume Spectrophotometers	Thermo Fisher Scientific
Odyssey fluorescence scanner	Li-Cor
PDS-1000/He Hepta	Bio-Rad
Semi-Dry and Rapid Blotting Systems	Bio-Rad
SMZ1500 microscope	Nikon
Fluorescence microscope BX61	Olympus

Table 3 List of bacteria strains and vectors used in experiments

Cells and Vectors	Function	Resistance
<i>A. tumefaciens</i> GV3101	<i>N. benthamiana</i> and <i>A. thaliana</i> transformation	Rifampicin
<i>E. coli</i> BL21(<i>pLysS</i>)	High yield recombinant protein expression bacteria strain	-
<i>E. coli</i> DH5 α	Stable bacteria strain	-
pENTR	Entry clone for Gateway cloning	Kanamycin
pJET1.2	Poly-A smart cloning system; vector for sequencing	Ampicilin
pET21a	Recombinant protein expression vector; contains 6xHis (C-term)	Ampicilin
pBWG	Binary vector; pro., no tag	Spectinomycin, BASTA
pGWB504	Binary vector; 35S pro, C-EYFP	Spectinomycin, BASTA
pGWB505	Binary vector; 35S pro, N-EYFP	Spectinomycin, BASTA
pGWB604	Binary vector; no pro., C-GFP	Spectinomycin, BASTA

Table 4 List of kits used in experiments

Name of KIT	Distributer
RevertAid RT Reverse Transcription Kit	Thermo Fisher Scientific
SYBR™ Green PCR Master Mix	Thermo Fisher Scientific

CloneJET PCR Cloning Kit	Thermo Fisher Scientific
Gateway™ BP Clonase™ II Enzyme mix	Thermo Fisher Scientific
Invisorb® Spin Plasmid Mini	Stratec
TURBO DNA-free™ Kit	Ambion
Nick Translation Atto488 NT Labeling Kit	Jena Bioscience

Table 5 List of primers used in experiments

Primers used for genotyping			
Gene	T-DNA insertion line	Primer	Sequences (5' - 3')
AT1G51130 (<i>Nse4A</i>)	GK-768H08	1	GTGGTTCCCGAGGAAGTAAAC
		2	CAGCTTGAGAATTTGGTGCTC
	Sail-71-A08	3	AAAATCCCCAAATTCAACCTG
		4	TACCTCATCTGGACGAACACC
	Salk-057130	5	AAACACCACTGATCGATCAGG
		6	AAAATCCCCAAATTCAACCTG
AT3G20760 (<i>Nse4B</i>)	GK-175D11	7	TGCTATTCCAGAAATGTTGCC
		8	CAGAAAACGTACAAAGCCTGG
	Sail-296F02	9	TTTGTACGTTTTCTGTTGCC
		10	GTTTCACCTTTTTCTTTCCG
	Salk LB		ATTTTGCCGATTTTCGGAAC
	Sail LB		GCCTTTTCAGAAATGGATAAATAGCCTTGCTT CC
	GABI LB		ATAATAACGCTGCGGACATCTACATTTT
Real-time quantitative PCR primers used to amplify transcripts			
Gene	Primer	Sequences (5' - 3')	
AT1G51130 (<i>Nse4A</i>)	I	CTTGCACCAACAAGTTCGGA	
	II	GCAGACTGAGACTTCACCGA	
	III	TGGATCCTTATGAGGAAGACGGTGAAGC	
	IV	TGATTGTGAATCATCTACCTGGTTA	
	V	CGCCCTCTTTGTCAGGAGTA	
AT3G20760 (<i>Nse4B</i>)	VI	TGCACCAGAAAGTTCGGAAG	
	VII	AGCTGATTGCGATTTACCCG	
AT1G13320 <i>Pp2A</i>	PP2A_F	TAACGTGGCCAAAATGAT GC	
	PP2A_R	GTTCTCCACAACCGCTTGGT	
AT4G26410 <i>Rhip1</i>	RHIP1_F	GAGCTGAAGTGGCTTCCATGAC	
	RHIP1_R	GGTCCGACATACCCATGATCC	
Primers used for gene cloning and the generation of recombinant proteins			
NSE4A (cloning)	Nse4A_Start_F	TGGATCCTTATGAGGAAGACGGTGAAGC	
	NSE4A_StopMiss	AACTCGAGGCAGAGGTGAGTCTCCGCTTACA T	
NSE3 (cloning)	Nse3_Start_F	TGGATCCTT ATGGCCGACGAAGAAGATT	

	Nse3_ StopMiss	AACTCGAGGCATCATTAAAGCTCTACAACCTGC TACATC
SMC5 (cloning)	Smc5_Start_F	TTGCGGCCGCATGTCTGAACGTCGTGCTAAG
	Smc5_ StopMiss	TTGCGGCCGC GCGGAACATTGACTAGCTTCG GTTC
NSE4A (recombinant protein)	AtNSE4a_AB_For	TGGATCCCCTCAGGAGGAAGAACAAGG
	AtNSE4a_AB_rev	AACTCGAGCATGGCGAAATGAGAACCAC
NSE3 (recombinant protein)	AtNSE3_AB_For	TGAATTCGAAGATTCTCTCTCAATTCGAT
	AtNSE3_AB_rev	AACTCGAGATCATTAAAGCTCTACAACCTGCTA CATC
SMC5 (recombinant protein)	AtSMC5_AB_For	TGAATTCTTGCCTGGGAATATAATCGAAA
	AtSMC5_AB_rev	AACTCGAGCTGATTCAGCGTCTCTCCATTT

Table 6 List of antibodies used in the experiments

Primary antibody			
Name	Animal	Application and antibody dilution	
Anti-AtNSE3	Rabbit	Immunocytogenetics 1:250	
Anti-AtNSE4A	Rabbit	Immunocytogenetics 1:250	
Anti-AtSMC5	Rabbit	Immunocytogenetics 1:250	
Anti-ZYP1 (Higgins et al. 2005)	Rat	Immunocytogenetics 1:1000	
Anti-GFP (sc-9996 - Santa Cruz Biotechnology)	Mouse	Immunocytogenetics 1:100	
Secondary antibody			
Name	Animal	Antibody dilution	Fluorophore
Donkey anti-rabbit (711545152 -Dianova)	Donkey	1:500	Alexa Fluor 488
Goat anti-rat (ab98383 – Abcam)	Goat	1:600	DyLight 594
Goat anti-mouse (115545062 - Dianova)	Goat	1:500	Alexa Fluor 488

3. Methods

3.1 Plant materials and growth conditions

3.1.1 *Arabidopsis thaliana*

A. thaliana SALK, SAIL, and GABI KAT T-DNA insertion lines were obtained from the Nottingham Arabidopsis Stock Center (NASCC) (<http://arabidopsis.info/BasicForm>). Seeds were planted into the soil and underwent an overnight vernalization at 4°C. Afterwards plants were transferred to the growth chamber. Plants were initially grown under short-day condition (8 hours photoperiod, 22°C/18°C day/night temperature). After one month plants were transferred to long-day light period chamber (16 hours photoperiod, 22°C/18°C day/night temperature).

Preparation of *A. thaliana* plants for live imaging using a confocal microscope

Freshly sterilized NSE4A::GFP seeds were planted on 1.5 ml ½ MS medium in X-Well Tissue Culture Chambers (Sarstedt) and grown in a long-day light period chamber. After one week seedlings roots were close to bottom of the tissue culture chamber, ready for confocal microscopy.

3.1.2 *Brassica rapa*

B. rapa seeds were planted into the soil and transferred to a long-day light period chamber (16 hours photoperiod, 22°C/18°C day/night temperature). One month-old flowering plants were harvested; mature flower buds collected and freshly used for immunolocalization experiments.

3.1.3 *Nicotiana benthamiana*

N. benthamiana plants used, for transient transformation, were grown in a temperature chamber 22°C/18°C day/night and a photoperiod of 16 hours. Leaves of four week old plants were used for transient transformation.

3.1.4 Surface sterilization of *A. thaliana* seeds

Dry *A. thaliana* seeds were placed into an Eppendorf tube containing 70% ethanol and incubated for 10 min with rotation. After, ethanol was discarded and seeds were treated two times for 5 min with 4% NaOCl in H₂O with rotation. Seeds were washed 3 times with ddH₂O. Prepared seeds

were suspended in 1% agarose in H₂O and planted on ½ MS plates containing the desired selection marker (selection markers listed in Table 3).

½ MS plates (pH=5.7)	
Murashige and Skoog (MS)	2.16 g
Phytoblend agar plus	8 g
MS modified vitamins stock (1000x)	2 ml
ddH₂O	1000 ml

3.1.5 Plant crossings

To obtain double homozygotes mutants, *nse4A* mutants (GK-768H08) were crossed with *nse4B* mutant. Therefore siliques were removed from the mother plant. Under the microscope too young and too old flower buds were cut, proper sized flower buds were opened using forceps; anthers, sepals and petals leaves were removed. Emasculated stigmas from mother plants were pollinated by tapping mature yellow anthers from the father/donor plant. Pollinated inflorescences were marked. Mature hybrid seeds were harvested 15 - 25 days after pollination.

3.2 Genetic material extraction

3.2.1 Isolation of plant genomic DNA

Approximately 200 mg of rosette leaves were frozen in liquid nitrogen and mechanically ground with 5 mm metallic balls (50 s, 30 Hz). Grinded leaves were incubated for 10 min at 65°C in DNA extraction buffer with 0.5 µg/µl RNase. After incubation, 0.6 ml isoamylalcohol : chloroform (1 : 24) solution was added, probes were mixed and centrifuged for 5 min, 14,000 rpm at room temperature. The upper phase was transferred into 0.7 ml isopropanol and mixed. Solution was centrifuged and pellet was washed with 0.3 ml of 70% ethanol and resuspended in 30 µl ddH₂O. Quality of the DNA was checked by agarose gel electrophoresis. Concentration was measured using a NanoDrop apparatus (section 3.4.1). DNA samples were stored in -20°C.

DNA extraction buffer (pH=8)

NaCl	700 mM
Tris-HCl	100 mM
EDTA	0.05 mM
RNase (10 U/ μ l)	2.5 μ l
Total volume	100 ml

3.2.2 Isolation of plant RNA

Total RNA was isolated from approximately 200 mg seedlings, three and six weeks old rosette leaves, flower buds, and roots using the TRIzol method (Chomczynski and Mackey, 1995). Extracted RNA was digested with the TURBO DNA-free™ Kit (Ambion) following producer's instruction. Reactions were stopped using an inhibitor (kit included). RNA concentration was measured using a NanoDrop apparatus (section 3.4.1) and immediately used for reverse transcription reaction (section 3.7).

3.2.3 Plasmid extraction from *E. coli* cells

Overnight bacteria culture containing high yield copy plasmid was used. Extraction was performed using the Invisorb® Spin Plasmid Mini (Stratec) kit according to the manufacture's manual. Plasmid DNA was resuspended in ddH₂O. Quality of the plasmid DNA was checked using agarose gel electrophoresis (section 3.14), concentration was measured using a NanoDrop (section 3.4.1). DNA samples were stored at -20°C.

3.2.4 Preparation of DNA for sequencing

PCR amplified fragments were cloned into the vector pJET 1.2 using the CloneJET PCR cloning kit (Thermo Fisher Scientific). Constructs were transformed into DH5 α *E. coli* (section 3.6.1), and isolated using a plasmid isolation method (section 3.2.1). Plasmid inserts were sequenced using the dideoxynucleotide chain-termination method (Sanger et al., 1977). Therefore, 5 μ l purified plasmid DNA (~200 ng) in ddH₂O mixed with 1 μ l of 5 μ mol primer were delivered to the Sequencing Service of the IPK Gatersleben. Sequences were *in silico* assembled and verified using the software Sequencher 5.2.3.

3.3 Plant genotyping

Genomic DNA of the *A. thaliana* T-DNA insertion lines were isolated (section 3.2.1) and used in a PCR-based plant zygosity screening. Three types of primers were used: LP, RP (gene specific primers) and LB (left border of T-DNA insertion). Two PCR reactions were performed. First reaction, product for LP and RP primers indicates the wild type allele (no T-DNA insertion). Second reaction including LB (left border of T-DNA) and RP primers combination gives a product indicating a T-DNA insertion (Figure 8). Dependent on the gene and T-DNA insertion, the size of the PCR products differs. The primers used for genotyping are listed in Table 5.

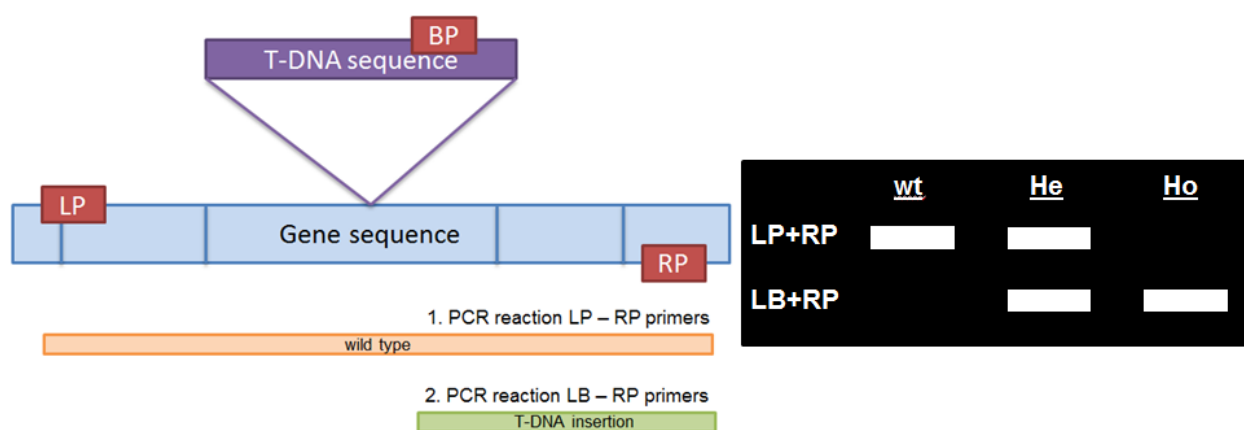


Figure 8 Schemata of the T-DNA genotyping experiment - localization of LP, RP and LB primers with PCR reaction products; wild type (wt) has unchanged genomic DNA (LP+RP); heterozygote (He) possesses one T-DNA insertion (LB+RP) and one unchanged gene copy (LP+RP), homozygote (Ho) has T-DNA insertion (LB+RP), in both gene copies. Adapted from <http://signal.salk.edu/tdnaprimers.2.html>

3.4 Determination of the DNA, RNA and protein concentration

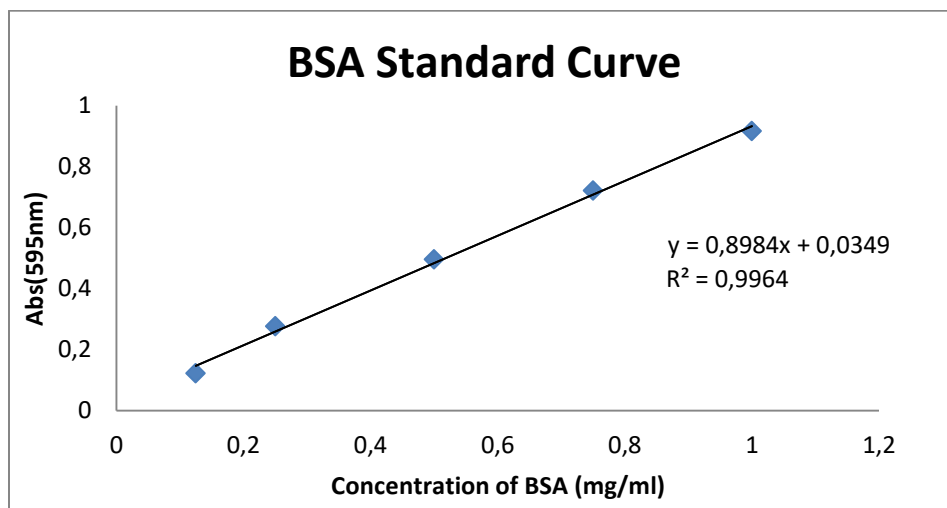
3.4.1 DNA and RNA concentration

Nucleic acid concentration was determined by optical absorption of the samples using a NanoDrop (Thermo Fisher Scientific) microfluidic spectrophotometer apparatus. Absorption of DNA and RNA was determined using a wavelength of 260 nm (A₂₆₀). Quality/purity of the samples was established by OD₂₆₀/OD₂₈₀ ratio; where pure DNA has ~1.8, RNA~ 2.0 OD₂₆₀/OD₂₈₀ ratio. 2 µl of solvent (ddH₂O) was placed at clean lower measurement pedestal, apparatus was blanked. The pedestal was wiped with lint-free laboratory wipe, the 2 µl of sample

was placed and A260 and OD₂₆₀/OD₂₈₀ ratio was measured. To obtain an accurate result three independent measurements for one sample were performed.

3.4.2 Protein concentration

A colorimetric protein assay, based on the Bradford method was used to determine the protein concentration (Bradford, 1976). 1 ml of Bradford (Bio-Rad) reagent were placed into a 1.5 ml Eppendorf tube and mixed with 50 µl of sample for 5 min. Solution was transferred into an absorbance measurement cuvette. Concentration was determined using a formula indicated in figure 9. Formula was created using a BSA standard curve.



$$C\left[\frac{mg}{ml}\right] = \frac{Abs(595nm) - 0.0349}{0.8984}$$

Figure 9 BSA standard curve and concentration formula

3.5 DNA restriction, dephosphorylation and ligation

DNA enzymatic restriction, vector dephosphorylation and vector-insert ligation were required for molecular cloning.

3.5.1 DNA restriction

DNA cleavage was performed using restriction enzymes and buffers set recommended by manufacturer (Thermo Fisher Scientific). Enzymes were deactivated after reaction using the

recommended deactivation temperature. 0.5 – 1 µg plasmid DNA were enzymatically digested for 2 - 3 hour at 37°C following reaction. Cleavage products were analyzed using agarose gel electrophoresis.

DNA restriction reaction

DNA	0.5-1 µg
Restriction buffer (10x)	2 µl
Restriction enzymes	0.5-2 U
ddH₂O	to 20 µl

3.5.2 Plasmid dephosphorylation

To prevent self-ligation, digested plasmids were dephosphorylated using the shrimp alkaline phosphatase (SAP) (Thermo Fisher Scientific) enzyme. 0.1 - 1 µg plasmid DNA, 1 U SAP and SAP buffer in 20 µl of total reaction was incubated for 60 min at 37°C. Reaction was terminated using temperature deactivation – 15 min at 65°C. Dephosphorylated products were used in plasmid – insert ligations.

Plasmid dephosphorylation reaction

Plasmid DNA	0.1 - 1 µg
SAP buffer (10x)	2 µl
SAP (1 U/µl)	1 µl
ddH₂O	to 20 µl

3.5.3 Plasmid insert ligation

Digested and dephosphorylated plasmids were ligated with appropriate DNA inserts using the T4 ligase (Thermo Fisher Scientific). 20 - 100 ng of linear plasmid DNA was mixed 1:3 of molar ratio with DNA insert, buffer and enzyme in a total volume of 20 µl. Incubation was performed at 4°C overnight or 1 hour in room temperature. 1 µl of the reaction were used to bacteria transformation (section 3.6).

Plasmid – insert ligation reaction

Digested plasmid DNA	20 - 100 ng
Insert DNA	1 : 3 molar ratio over plasmid
T4 Ligase buffer (10x)	2 µl
T4 DNA Ligase	1 U
ddH₂O	to 20 µl

3.6 Bacteria transformation and selection

For cloning and expression of recombinant protein *E. coli* was used. For plant transformation the bacteria *A. tumefaciens* was used. Bacteria strains (listed in Table 3) were transformed using the heat shock or electro-transformation method.

3.6.1 Heat shock transformation of *E. coli* DH5 α and BL21 (pLysS) strains

50 µl of competent *E. coli* cells were incubated on ice with 1 µl of ligation mixture (section 3.5.3) for 20 min. After incubation, cells were transferred into a water bath of 42°C and incubated for 45 s. Next, treated cells were placed on ice for 1 min, suspended in 1 ml S.O.C medium and incubated for 1.5 h at 37°C with 250 rpm shaking. After incubation cells were plated on LB plates containing selective antibiotics (ampicillin 50mg/l, kanamycin 50mg/l or spectinomycin 100mg/l). Plates were incubated overnight at 37°C; colonies were checked using PCR screening.

S.O.C medium		LB plates	
Tryptone	2 %	Tryptone	5.0 g
Yeast extract	0.5 %	Yeast extract	2.5 g
NaCl	10 mM	NaCl	5.0 g
Glucose	20 mM	Agar	7.5 g
MgCl ₂	10 mM	H₂O	to 500 ml
MgSO ₄	10 mM		
KCl	2.5 mM		
Total volume	50 ml		

3.6.2 Electroporation of *A. tumefaciens*

50 μ l of ice cold *A. tumefaciens* (GV3101) cell suspension was mixed with 1 μ l of ligation reaction (section 3.5.3). Mixture was placed on ice for 30 min and transferred into a electroporation cuvette. Bacteria were electroporated ($U = 2.5$ kV; $C = 25$ μ F; $R < 200$ Ω ; time pulse = 5 ms) and resuspended in 1 ml of S.O.C medium. Bacteria were incubated for 1.5 h at 28°C and plated onto YEB plates with 50 mg/l rifampicin, 50 mg/l kanamycin and incubated for 2 days at 28°C. Colonies were PCR screened for the presence of the desired constructs.

YEB plates

Beef extract	2.5 g
Yeast extract	0.5 g
Peptone	2.5 g
Sucrose	2.5 g
MgCl ₂	0.25 g
Kanamycin	25 mg
ddH₂O	to 500 ml

3.7 Reverse transcription-PCR (RT-PCR)

Reverse transcription was performed using the RevertAid Reverse Transcriptase kit (Thermo Fisher Scientific). A minimum of 200 ng RNA and random hexamers primers were used following the producer manual instruction.

3.8 Gene expression analysis by quantitative real time PCR

Real time quantitative PCR was performed using a Quant Studio 5 flex apparatus (Quant Studio™ Real-Time PCR Software v1.1) and a SYBR™ Green PCR master mix (Thermo Fisher Scientific). cDNA was prepared using reverse transcription-PCR (RT-PCR) (section 3.7). 0.5 μ l of cDNA was used for each reaction with three replicates. Three independent biological repetitions for each tissue type or developmental stage were used. The genes *AtRhip1* (AT4G26410) and *AtPp2A* (AT1G13320) were used as a reference. Following PCR program were used for reaction: 5 min. 95°C initial denaturation, then 40 cycles with 95°C, 15s (denaturation) and 60°C, 30 s (hybridization and elongation). Calculations were based on the

reference gene and the gene of interest CT values. Primers used in experiments are listed in Table 5.

Real-time qPCR reaction	
SYBR™ Green mix	5 µl
Primer F (10 mM)	0.6 µl
Primer R (10 mM)	0.6 µl
cDNA	0.5 µl
ddH₂O	to 10 µl

3.9 Plant transformation and selection

Two types of plant transformation methods were performed. Stable *A. tumefaciens* mediated transformation of *A. thaliana* (floral dipping) and transient biolistic transformation of *N. benthamiana* (gene gun).

3.9.1 Floral dipping of *A. thaliana*

Inflorescences of *A. thaliana* were submerged in transforming solution for 45 s. Afterwards, plants were protected from light and horizontally stored over night at room temperature. Next day, plants were transferred to the long day light condition (section 3.1.1) and grown in normal position until seed harvest. Collected seeds were selected by ½ MS plates containing 16 µg/ml PPT. Positively selected seedlings were transferred to the soil and genotyped (section 3.3) for the presence of the construct.

Transforming solution	
<i>A. tumefaciens</i>	Pellet from 800 ml culture
Sucrose	40 g
Silvet L-77	800 µl
H₂O	Up to 800 ml

3.9.2 Transient transformation of *N. benthamiana*

10 µl of 500-1000 ng plasmid DNA was slowly vortexed with 3 mg of 1.0 µm diameter gold micro particles (Bio-Rad), 25 µL 25 mM CaCl₂ and 10 µL 0.1 M spermidine. Afterwards the suspension was centrifuged; pellet was washed two times with 75% and 100% ethanol.

Suspension were centrifuged and pellet was resuspended in 60 µl of absolute EtOH and used in experiments.

Leaves of four week old *N. benthamiana* plants (section 3.1.3) were harvested and transferred on transforming plates containing 4.3 % Murashige and Skoog (MS) medium, 2 % sucrose, 400 mg/l ticarcillin and 0.8% agar. Leaves were bombarded with ~1 - 3 µl of plasmid DNA-coated gold particle suspension using the PDS-1000/He Hepta device equipped with a 1100 psi rupture disc (Bio-Rad). Bombarded leaves were stored in the dark for 24 h at RT. Transformed leaves of *N. benthamiana* were analyzed with a Zeiss LSM780 confocal laser microscope (Carl Zeiss).

3.10 Production of recombinant proteins

Recombinant proteins were expressed in *E. coli* and used as an antigen for rabbit immunization to produce anti-NSE3, -NSE4A and SMC5 antibodies.

3.10.1 Recombinant proteins expression

Nse3 (13-237 bp), *Nse4A* (146-867 bp) and *Smc5* (19-209 bp) gene fragments were PCR amplified, sequenced and cloned into the 6xHis tag expression vector pET23a (Novagen). Expression construct was used for BL21 *E. coli* transformation (section 3.6.1). The recombinant protein was expressed after IPTG induction and purified using Ni-NTA agarose (Protino) affinity chromatography column. Therefore, positive verified colonies were transferred into 20 ml of LB medium containing 50 mg/l ampicillin. Culture was incubated overnight with 180 rpm mixing at 37°C. Next day, the starter culture was used to inoculate a 1000 ml LB culture. Culture was shaken 180 rpm at 37°C until an optical density of 0.6 (OD₆₀₀) was reached. Then, β-D-1-thiogalactopyranoside (IPTG) was added to a final concentration of 1 mM. An induced culture was incubated for 3 h and centrifuged at 6000 rpm for 40 min at 4°C. The pellet was stored at -20°C.

3.10.2 Extraction of recombinant proteins

After protein expression in *E. coli*, the recombinant proteins were released from bacterial cells using chemical (lysozyme) and mechanical (sonification) lysis. The frozen bacterial pellet (section 3.10.1) was thawed on ice and resuspended in 50 ml of isolation buffer containing

1mg/ml lysozyme and mixed on ice for 30 min. Afterwards, the incubation mixture was sonicated on ice using 10x 15 s burst with 10 s cooling pause between each burst. Next, 5 µg/ml DNase I was added, and the solution was mixed on ice for 15 min. After DNase treatment the lysate was centrifuged, 10,000 rpm at 4°C for 30 min. The supernatant was discarded and the remaining pellet was washed two times with 40 ml NPI-10, resuspended in 10 ml NPI-10 buffer and stirred on ice for 60 min. Finally, the pellet was centrifuged at room temperature and 10000 rpm for 20 min.

Isolation buffer		NPI-10	
NaCl	300 mM	NaCl	300 mM
NaH ₂ PO ₄	50 mM	NaH ₂ PO ₄	50 mM
		Imidazole	10 mM

3.10.3 Purification of recombinant proteins

The released recombinant proteins after lysis have to be purified from other components of the bacteria culture. The purification was based on the affinity between the negatively charged 6x histidine tag, which is localized at the amino acid terminus of the recombinant protein, and positively charged nickel ions attached to agarose beads.

Therefore, 2 ml of Protino® Ni-NTA Agarose (Protino) was washed twice with 10 ml DNPI-10, and then added to solubilized protein supernatant (section 3.10.2). The mixture was mixed gently for 60 min, then centrifuged at 300 rpm for 5 min, and washed twice with 10 ml DNPI-25. The suspension of recombinant protein and agarose was mixed with 1 ml of DNPI-250 for 2 min at room temperature to elute the polyhistidine-tagged proteins from the nickel ions attached to the agarose beads. The mixture was centrifuged at 300 rpm for 5 min, and supernatant was saved. These steps were repeated 5 times. The concentration of isolated recombinant proteins was checked using the Bradford method (section 3.4.2)

Wash buffer DNPI-25		Elution buffer DNPI-250	
NaCl	300 mM	NaCl	300 mM
NaH ₂ PO ₄	50 mM	NaH ₂ PO ₄	50 mM
Imidazole	25 mM	Imidazole	250 mM
Urea	8 M	Urea	8 M

3.10.4 Recombinant protein dialysis

Dialysis was performed to remove redundant chemicals like urea and imidazole included in the elution DNPI-250 buffer. Highly concentrated (~5 mg/ml) recombinant protein solution purified using Ni-NTA agarose affinity chromatography (section 3.10.3) was placed into a dialysis membrane tube Spectra/Por[®] 2 (Spectrum Labs) with a molecular weight cut-off 12000 - 14000 Da. Dialysis was performed in a 2 l beaker at 4°C. Dialysis solutions were replaced every 2 h; new solution had a reduced amount of urea. Last dialysis was performed overnight. Dialyzed recombinant protein solution was centrifuged 8000 rpm for 10 min at 4°C, supernatant was transferred into new Eppendorf tubes. The final concentration of the proteins was measured using the Bradford method (section 3.4.2)

Dialysis buffer

NaCl	137 mM
KCl	2.7 mM
Na ₂ HPO ₄	1.42 mM
KH ₂ PO ₄	0.24 mM
Urea*	6 M, 4 M, 2 M, 1 M, 0.5 M

**Concentration of urea decreases after each step of changing of buffer in dialysis process*

3.11 Antibody production

Polyclonal rabbit NSE3, NSE4A and SMC5 antibodies were produced and purified in collaboration with Prof. Udo Conrad (research group Phytoantibodies, IPK Gatersleben). Antibodies were purified using ammonium sulfate precipitation (section 3.10.3) and validated against the anti-gene (NSE3-6xHis NSE4A-6xHis and SMC5-6xHis) using Western-blot (section 3.13). After verification antibodies were stored at -20°C and used for further studies.

3.12 Polyacrylamide gel electrophoresis (PAGE)

SDS-PAGE system was used for electric field separation of denaturated proteins in the presence of SDS and β-mercaptoethanol. Extracted, solubilized protein (section 3.10.4) samples were mixed 1:1 with Laemmli buffer (2x) followed by boiling for 5 min. Samples were separated

using 12 % SDS-PAGE two phase gels at 100 mV, 200 mA by 2 h. SDS gels were stained using Coomassie Brilliant Blue R-250 or proceeded in Western blot experiments.

Laemmli buffer (2x)

Tris-HCl (pH=6.8)	65.8 mM
Glycerol	26.3 %
SDS	2.1 %
Bromophenol blue	0.02 %

3.13 Western blot analysis

For checking of the specificity of antibody to antigens and detection of protein Western-blot analysis was performed. After SDS-PAGE electrophoresis (section 3.12) polyacrylamide gels were transferred to nitrocellulose Immobilon-FL PVDF, 0.45 µm membranes (Millipore) using 108 mA, 5 V volt and 2 h electrical transfer. Afterwards membranes were blocked in TBST with 3% dry milk for 30 min. Blocked membranes were placed into a TBST solution with diluted antibodies (Table 6) and incubated over-night at 4°C with shaking. Next day membranes were washed 3 times 50 ml TBST for 5 min and incubated with secondary antibodies suspended in TBST (secondary antibodies concentration listed in Table 6). After incubation membranes were washed 3 times in 50 ml TBST for 5 min and analyzed using the Odyssey fluorescence scanner (Li-Cor).

TBST buffer (pH=7.6)

Tris	50 mM
NaCl	150 mM
Tween 20	0.1 %

3.14 DNA gel electrophoresis

100 ml of 0.5 x TBE buffer was mixed with 0.5 - 1.5 g of UltraPure™ Agarose (Thermo Fisher Scientific) and heated in a microwave until complete agarose melting. Mixture was cooled in the water bath and 5 µl of the DNA dye HDGreen® Plus (Intas Science Imaging) was added. Mixture was placed into the gel form for polymerization.

DNA samples were mixed with 6x Loading Dye (Thermo Fisher Scientific) and gel separated together with a GeneRuler™ 1 kb DNA Ladder (Thermo Fisher Scientific). Electrophoresis was

performed for 45 min under 100 mV using a Mini Electrophoresis Systems (Bio-Rad). Afterwards, the gel was evaluated and documented using an AlphaImager HP System Automated Gel Imaging (Protein simple).

3.15 Microscopy

Prepared slides were evaluated by light microscopy (SMZ1500, Nikon), fluorescence microscopy (Olympus BX61), structured illumination microscopy (SIM, Zeiss ELYRA PS.1, Carl Zeiss GmbH) and/or confocal laser microscopy (LSM 780, Carl Zeiss). Images were taken separately for each of the fluorophores using the appropriate filter sets. Images were processed and merged applying the software Photoshop CS5 (Adobe).

3.15.1 Alexander staining of pollen

Flower buds in stage 12 (Smyth et al., 1990) were collected, fixed in Carnoy's fixative for 3 days at RT. Fixed buds were placed on a microscope slide and six anthers were isolated. Fixation buffer was carefully removed and 2 - 3 drops of staining solution was immediately applied. Slide was quickly heated up to 60°C for 1.5 min using a heat block. Anthers were fixed using cover glass. Prepared slide was ready to analyze the viability and number of pollen. Undamaged anthers were used for pollen per anther counting, afterwards anthers were squashed, and released pollen grains were evaluated into two classes – viable (pink round grains) and aborted (gray/green abnormal shape grains) pollen. Anthers and pollen grains were evaluated using a Nikon SMZ1500 microscope. Pictures were taken using a Nikon SMZ1500 light microscope equipped with a camera and NIS-Elements AR 3.0 software.

Carnoy's fixative solution		Alexander staining solution	
Ethanol	300 ml	Ethanol (95%)	10 ml
Chloroform	150 ml	Malachite green	1 ml
Acetic acid	50 ml	Glycerol	25 ml
Total	500 ml	Acid fuchsin (1%)	5 ml
		Orange G (1%)	0.5 ml
		Glacial acid	4 ml
		ddH₂O	Up to 100 ml

3.15.2 Clearing of siliques

Green mature siliques were collected and mounted in ethanol : acetic acid (9:1) solution overnight at room temperature. Next day, solution was washed with 70% and 90% ethanol for 60 minutes each and replaced by chloral hydrate : glycerol : water (8 : 1 : 3) solution, and stored at 4°C until documentation. Fixed siliques were transferred in a Petri dish with filter paper and photographed using a Nikon SMZ1500 light microscope equipped with a camera and NIS-Elements AR 3.0 software.

3.15.3 Seed setting analysis

Mature dry siliques were collected to evaluate the setting and quality of seeds. The length of siliques was measured; seeds were dissected and transferred in a Petri dish with wet filter paper. The number of seeds per siliques was counted and the seeds were classified into two classes: normal (wild type-like) and shriveled (dry, dark and flat). Seeds were photographed using a Nikon SMZ1500 light binocular microscope equipped with a camera and NIS-Elements AR 3.0 software.

3.15.4 Meiosis slide preparation

Fixation of flower buds and slide preparation were carried out according to Armstrong (2013). Flower buds fixed in Carnoy's solution were washed two times with ethanol : acetic acid solution (3 : 1) and three times by citrate buffer (10 mM, pH 4.5). Prepared flower buds were digested with an enzyme mixture for 2 h at 37°C. Enzymatic reaction was stopped using ice cold citrate buffer. Single flower bud was transferred to microscopic slide and macerate with a needle. 10 µl of 60% acetic acid were added and the slide was placed on a heating block for 1 min at 42°C. Afterwards, additional 10 µl of 60% acetic acid were added before washing with 150 µl of ice cold 3 : 1 fixative solution. Slide was air dried for 10 min at room temperature.

Enzyme mixture solution

Cellulase	30 µg
Cytohelicase	30 µg
Pectolyase	30 µg
Citrate buffer (10 mM pH=4)	Up to 10 ml

3.15.5 Fluorescent *in situ* hybridization (FISH)

Fluorescent *in situ* hybridization (FISH) was carried out according to Sánchez-Morán et al. (2001). DNA probes used in experiment: 5S, 45S rDNA (Gerlach and Bedbrook, 1979) were used to identify the chromosomes of *A. thaliana*. pAL1 (Martínez-Zapater et al., 1986) and telomere (Richards and Ausubel, 1988) probes were used as centromeric and telomeric probes, respectively. DNA probes were labeled with either Texas Red-12-dUTP (Invitrogen) or Alexa Fluor 488-5-dUTP (Invitrogen), using a nick translation Atto488 NT Labeling Kit (Jena Bioscience) following producer's instruction. Size of the nick translation products was checked by DNA gel electrophoresis (section 3.14).

Meiotic slide was washed twice with 2x SCC buffer. Afterwards slide was treated with 45% acetic acid for 10 min at room temperature and two times with 2x SCC buffer. Slide was treated with 0.1% pepsin for 10 min at 37°C and again washed two times with 2x SCC buffer. Next, specimen was fixed for 10 min at room temperature using 4% paraformaldehyde in 2x SCC buffer and washed four times in 2x SCC buffer. Slide was dehydrated 2 min in 70%, 90%, 100% ethanol subsequently and dried at room temperature.

20 µl of hybridization buffer was per slide. A coverslip was applied and fixed with fixogum (Marabu). Slide was desaturated for 2 min at 80°C on a hot plate and incubated in a moist chamber at 37°C overnight. Next day, the coverslip was removed and slide was incubated in a water bath with 2x SCC for 20 min at 55°C. Afterwards slide was dehydrated for 2 min in 70%, 90%, 100% ethanol subsequently, air dried in the dark and counterstained with DAPI. Slides were evaluated using a fluorescence microscope BX61 (Olympus).

2x SCC buffer (pH=7)		Hybridization buffer		4x Buffer stock	
NaCl	8.8 g	Deionized formamide	10 µl	20xSCC	80 µl
Trisodium Citrate	4.4 g	4x buffer stock	5 µl	1M Tris-HCl, pH= 8	8 µl
H₂O	500 ml	DNA probe	3 µl	0.5 M EDTA	1.6 µl
		H₂O	2 µl	Salmon sperm DNA (10 µg/µl)	11.2 µl
				ddH₂O	99.2 µl

3.15.6 Indirect immunostaining

Immunolabeling of pollen mother cells (PMC) was performed according to Chelysheva et al. (2013). Anti-AtNSE4A (rabbit; 1:250) and anti-Zyp1 (rat; 1:1000) (Higgins et al., 2005), were used as primary antibodies. Goat anti-rabbit-Alexa Fluor[®] 488 and goat anti-rat-Dylight[®] 594 were used as a secondary antibodies. Slides were analyzed under a fluorescent or SIM microscope.

Preparation of pollen mother cells

Five to ten *A. thaliana* flower buds of approximate length of 0.2 - 0.4 mm were collected. Anthers were separated from buds, placed into 10 µl digestion medium and incubated 5 min at 37°C. Afterwards anthers were macerated using a needle to release meiocytes and incubated for 7 min at 37°C with 10 µl digestion medium. After incubation, 10 µl of 1% Lipsol[®] detergent were added and mixed for 2 min using a needle. Next, 40 µl of ice cold 4% paraformaldehyde in H₂O (pH=8.0) was added and the solution was spread around the slide using a needle. Slides with meiocytes were dried for 2 – 3 h at room temperature.

Digestion medium	
Cytolhelicase	0.1 g
Polyvinylpyrrolidone	0.25 g
Sucrose	0.375 g
ddH₂O	25 ml

Immunostaining

Dried slides were washed 3 times for 5 min with 1% Triton X-100 in PBS and blocked with 1% BSA in 1x PBS for 30 min at room temperature. Primary antibodies were diluted (antibody list and recommended dilution in section Table 6) in 1x PBS and applied on the slides. To prevent evaporation, the slides were covered by parafilm. Prepared slides were incubated at 4°C overnight in a humid chamber. Next day slides were washed 3 times, 5 min. with 1% Triton X-100 in 1x PBS. Secondary antibodies (secondary antibody dilution in Table 6) were applied and incubated for 1 h at 37°C in the dark. After, slides were washed 3 times in 1x PBS. After short

drying of slides, application of antifade containing DAPI and coverslip mounting the slides were ready for microscopic analysis.

3.16 Counting of chiasmata

Chiasmata counts were performed by Prof. J. L. Santos from UCM (Madrid, Spain) as described in Sánchez-Morán et al. (2001). FISH 5S and 45S rDNA probes were used as a reference in chromosome identification.

4. Results

The NSE4 protein is the ‘bridge’ component of the SMC5/6 complex ring and the attaching site for other non-SMC proteins. This protein is essential for the complex formation and function. The key role of NSE4 makes this protein an interesting object for further studies.

In our studies, we decided to investigate *Nse4* in the model plant *A. thaliana*, evaluate *nse4* mutant plants, check the role and function of *Nse4* in plant development and mitotic and meiotic division. Furthermore, we generated specific anti-NSE4 antibodies and a NSE4::GFP transgenic line to track the NSE4 protein dynamics and localization. To investigate the dynamics of the SMC5/6 complex in detail, we generated antibodies and transgenic lines also for the SMC5/6 subunits NSE3 and SMC5. The obtained results are described below.

4.1 Characteristics of *A. thaliana* *Nse4* genes

4.1.1 *A. thaliana* encodes two *Nse4* gene variants

The Basic Local Alignment Search Tool (BLASTX) was used to identify the *A. thaliana* *Nse4* orthologues of the *Homo sapiens* *Hnsmc4A* (FLJ20003) and *Hnsmc4B* (AAH27612) (known also as EID3) (Bavner et al., 2005) and *Saccharomyces cerevisiae* *Nse4* (YDL105W) (Hu et al., 2005) genes. The analysis identified two *Nse4*-like variants, denominated as: *Nse4A* (AT1G51130) and *Nse4B* (AT3G20760) (Schubert, 2009) (Figure 10).

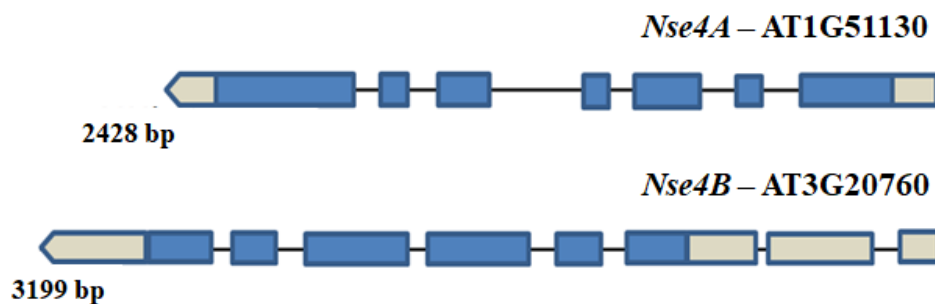


Figure 10 Gene models of *A. thaliana* *Nse4A* and *Nse4B*. Exons are shown as blue boxes, introns as lines. UTRs are shown in grey.

The genomic sequence of *Nse4A* is 2428 bp long, contains seven exons, six introns and is encoded by chromosome I of *A. thaliana*. The second variant, *Nse4B*, is 3199 bp long, harbors

six exons, seven introns and is encoded by chromosome 3. Both NSE4 proteins show an almost similar amino acid sequence length (NSE4A– 403 amino acids, NSE4B– 383 amino acids).

The NSE4A and NSE4B proteins have a 68% amino acid alignment identity and contain a conserved NSE4-C domain located at the C-terminus (Figure 11).

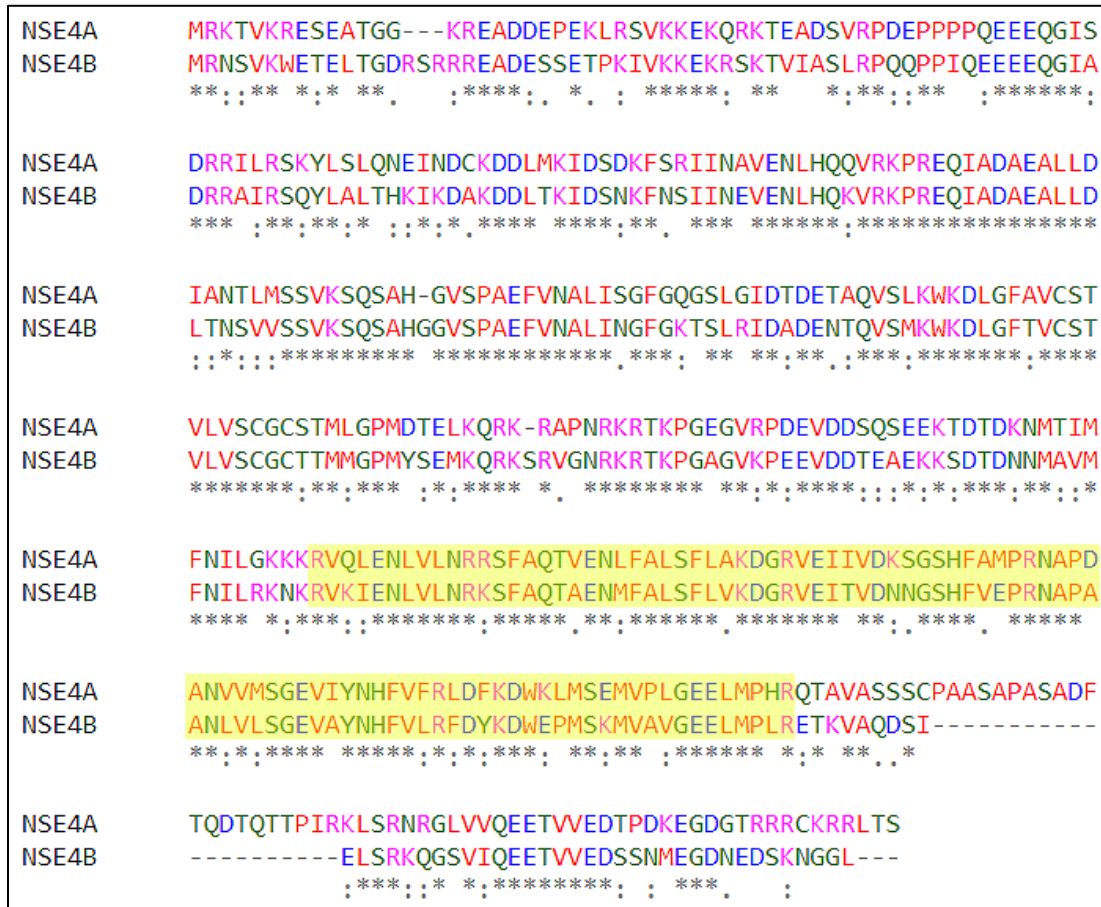


Figure 11 Amino acids sequence alignment between full length NSE4A and NSE4B of *A. thaliana*. (*) identical amino acids, (: and .) similar amino acids, (-) missing amino acids. The yellow box marks the NSE4-C domain. The alignment was performed by the Clustal Omega 2.1 software (<https://www.ebi.ac.uk/Tools/msa/clustalo/>).

The C-terminal domain has a hydrophobic sequence which is conserved in non-plant organisms, such as *Saccharomyces cerevisiae*, *Entamoeba histolytica*, *Dictyostelium discoideum*, *Arabidopsis thaliana*, *Mus musculus* and *Homo sapiens*, and is involved in SMC5 binding (Palecek et al., 2006). Furthermore, both NSE4A and NSE4B proteins display homology to the NSE4 orthologues of *S. cerevisiae*, *E. histolytica*, *D. discoideum*, *M. musculus* and *H. sapiens* (Table 7).

Table 7 NSE4 protein sequence similarity of orthologues in different organisms (A. t. – *A. thaliana*; S- c. – *S. cerevisiae*; E. h. *E. histolytica*; D. d. – *D. discoideum*; M. m. – *M. musculus*; H. s. – *H. sapiens*). The matrix was generated by the Clustal Omega 2.1 software.

	A. t. (A)	A. t. (B)	S. c.	E.h.	D. d.	M. m. (A)	H. s. (A)	M. m. (B)	H. s. (B)
A. t. (NSE4A)	100%	67.7%	17.6%	21.6%	23.5	21.5%	20.1%	21.0%	18.2%
A. t. (NSE4B)		100%	16.7%	22.1%	20.6	20.7%	21.4%	20.1%	18.1%
S. c.			100%	18.3%	18.7	23.6%	23.6%	21.2%	21.7%
E. h.				100%	21.2%	21.7%	21.7%	24.0%	18.7%
D. d.					100%	25.3%	24.7%	22.8%	19.5%
M. m. (NSE4A)						100%	88.2%	48.6%	43.6%
H. s. (HNSMC4A)							100%	47.8%	43.1%
M. m. (NSE4B)								100%	64.6%
H. s. (HNSMC4B)									100%

The protein length of *A. thaliana* NSE4A and NSE4B is similar with the NSE4 proteins of *S. cerevisiae* (402 amino acids), *M. musculus* (381 amino acids for NSE4A and 375 for NSE4B), *H. sapiens* HNSMCE4A (385 amino acids) orthologues, but longer than the *H. sapiens* HNSMCE4B (333 amino acids).

In the analyzed non-plant organisms, lower organisms like *S. cerevisiae*, *E. histolytica* and *D. discoideum* display only one putative *Nse4* gene orthologue. Similar to *A. thaliana*, higher organisms, such as *M. musculus* and *H. sapiens* display two *nse4* gene variants in their genomes with differences in amino-acid sequence and length. Two homologues may have different expression patterns, e.g. in humans *Hnsmc4A* (*Nse4A*) is expressed across different tissue types, while *Hnsmc4B* (*Nse4B*) is expressed only in testis (Bavner et al., 2005). Different expression may indicate different functions of both NSE4A and NSE4B proteins.

In order to analyze whether besides *A. thaliana* also other plant species encode two variants of *Nse4*, a BLASTX analysis was conducted. The analysis indicates a number of putative *Nse4A* and *Nse4B* orthologues in *Plantae* (Figure 12).

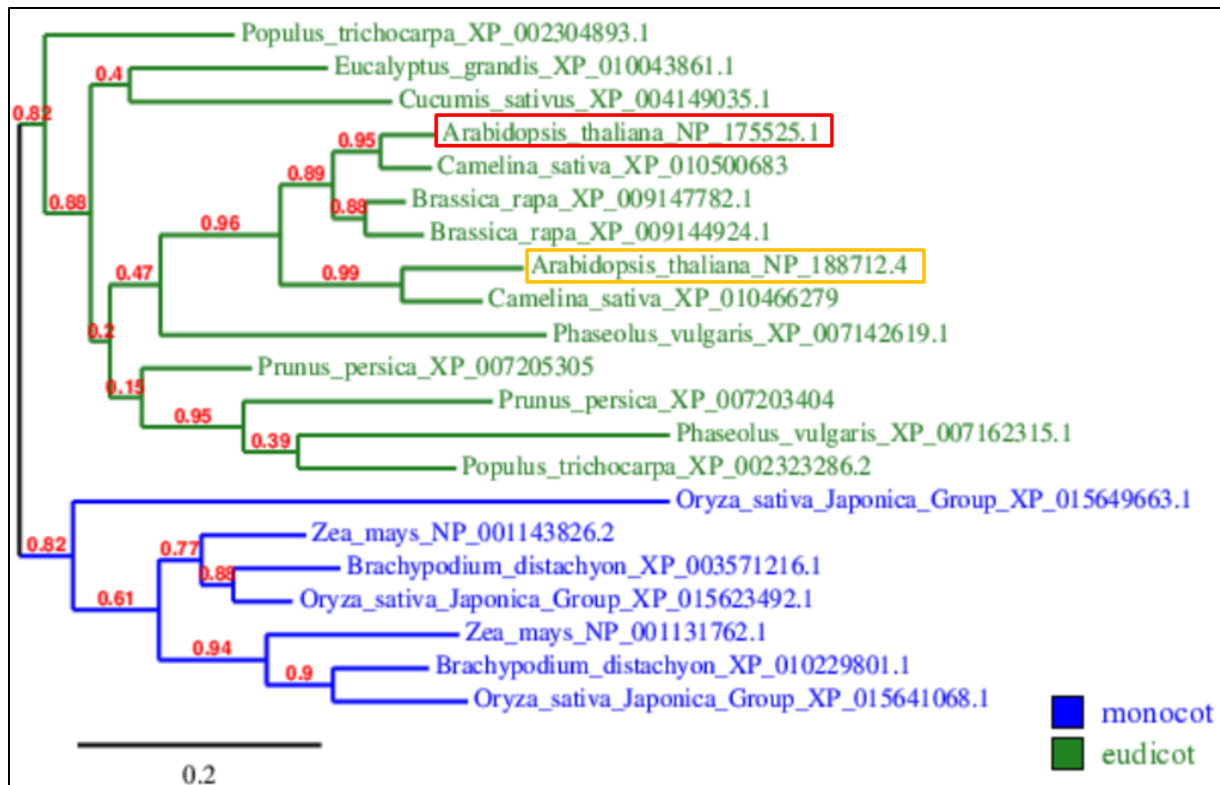


Figure 12 The phylogenetic relationships of the putative *Nse4* orthologues in plants. Red and green boxes indicate the *Nse4A* and *Nse4B* *A. thaliana* gene variants respectively. The red numbers represent a measure of support for the node, between 0 and 1 where 1 represents maximal support. The phylogenetic model was developed using amino acid sequences and phylogeny.fr tool (Dereeper et al., 2008).

All of the eleven investigated monocot and eudicot plant species have one or more putative *Nse4* genes. The orthologues differ in size (from 243 aa in *Phaseolus vulgaris* up to 475 aa in *Eucalyptus grandis*). Nevertheless, all of them display a conserved NSE4-C terminal domain in their sequence. Nine of the eleven analyzed genomes encode at least two hypothetical *Nse4* variants. Only in *E. grandis* and *Cucumis sativus* the BLAST analysis revealed only one *Nse4* gene.

The screening of plant genomes points to the presence of *Arabidopsis Nse4A* and *Nse4B* gene orthologues in monocot and eudicot plant species. The investigated plants, similar as in *A. thaliana*, display mostly two *Nse4* gene copies, but most of the *Nse4* orthologues are similar to the *Nse4A* isoforms. Plant species with only one *Nse4A* gene copy also show a higher similarity to the *Arabidopsis Nse4A* gene. The dominant presence of the *Nse4A* orthologue in plant genomes suggests that the *Nse4A* variant appeared first and has undergone gene duplication.

4.1.2 Transcription activity differs between *A. thaliana* *Nse4A* and *Nse4B*

To determine the specific expression level and dynamics of both *Nse4* genes, *in silico* analysis and quantitative real-time RT-PCR were performed.

In silico RNA-seq analysis

To investigate the expression pattern of *Nse4* genes, the *A. thaliana* database of the Genevestigator website (<https://genevestigator.com>) was used first. Based on 431 RNA sequencing experiments of wild-type *A. thaliana* it was found, that *Nse4A* is strongly transcribed in the radicle root tip, while a medium level of expression appeared in pistil, embryo, endosperm, flower, hypocotyl, inflorescence and root tissue. The weakest expression of *Nse4A* was found in seedling and rosette leaf tissues (Figure 13).

The expression of *Nse4B* is very low or undetectable across all tested tissue types, except in embryo and endosperm. The highest activity was found in endosperm whereas in embryonic tissue the expression is three up to seven times less than in endosperm (Figure 13).

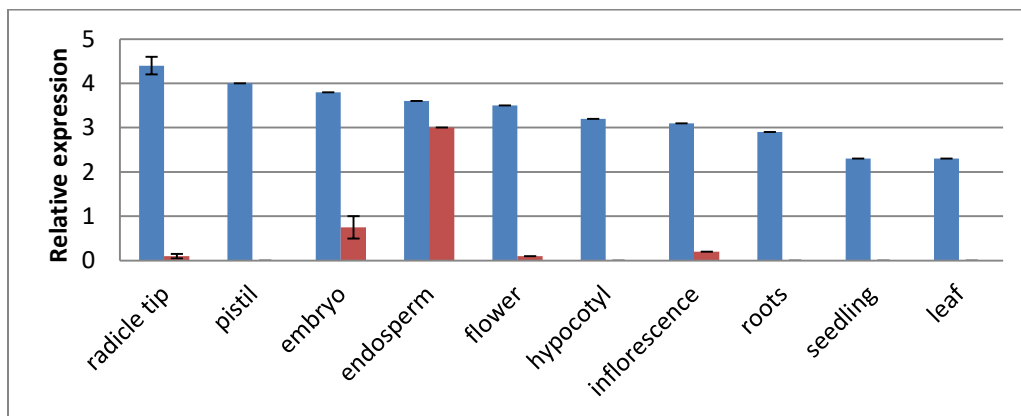


Figure 13 *In silico* expression patterns of *Nse4A* and *Nse4B* in 10 tissues from 431 individual sequencing samples from the wild-type *A. thaliana* ecotype Col-0 (AT_mRNASeq_ARABI_GL-0 databases <https://genevestigator.com/>). Blue and red bars indicate the relative expression of *Nse4A* and *Nse4B*, respectively.

In order to analyze whether *Nse4* and other SMC5/6 subunit genes display a coordinated expression during ontogenesis, an analysis using the Genevestigator website was conducted. Similar expression patterns as *Nse4A* were found for the other SMC5/6 complex genes *Nse1*,

Nse2, *Nse3*, *Smc5*, *Smc6A* and *Smc6B* at different developmental stages of *A. thaliana*. These genes display a relatively high expression during germination (stage 1-3), and the early developmental stages such as the seedling and young rosette stages 2 and 3. The expression was lower in developed rosettes, during bolting and in young flowers (stages 4-6), but elevated in developed flowers, siliques and mature siliques (stages 7-8). The exception is *Nse4B*, which is very weak expressed across all developmental stages, besides stage 8 - where the development of embryos and siliques appears (Figure 14).

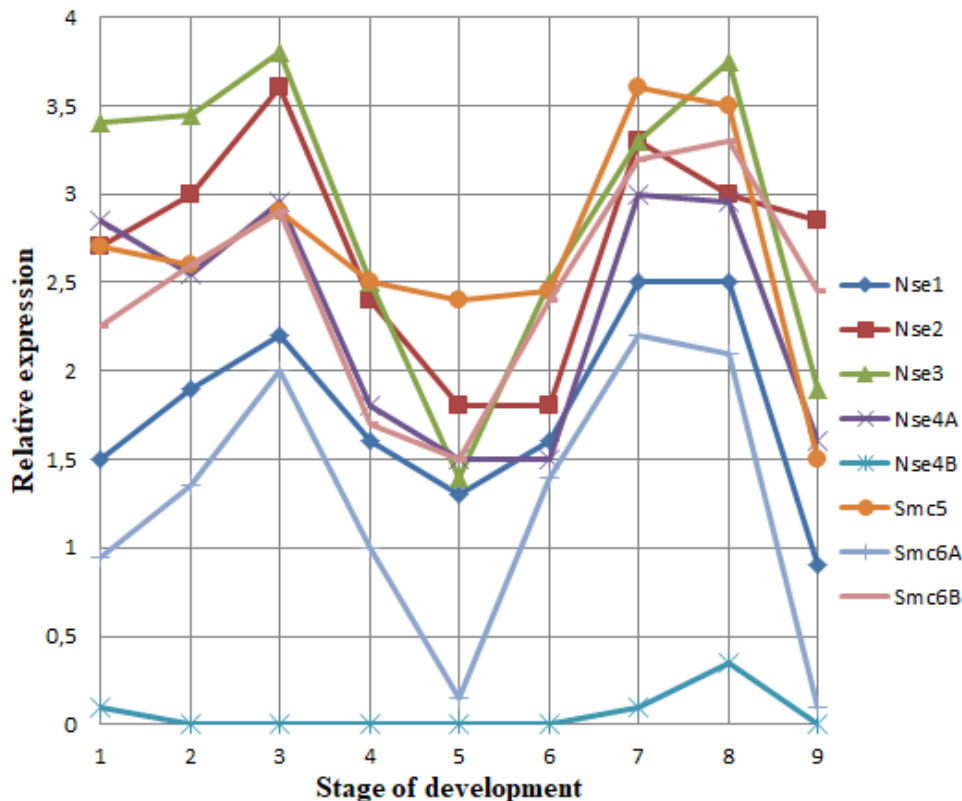


Figure 14 *In silico* expression patterns of *Nse4A* and *Nse4B* in 10 tissues from 431 individual sequencing samples from the wild-type *A. thaliana* ecotype Col-0 (AT_mRNASeq_ARABI_GL-0 databases <https://genevestigator.com/>). Blue and red bars indicate the relative expression of *Nse4A* and *Nse4B*, respectively. Stages (1-3) indicate early developmental stages of seedling and young rosette; (4-6) developed rosettes, bolting and in young flowers stage; (7-9) mature flowers, silique and seed stage.

Based on the obtained *in silico* data, it can be concluded that the *A. thaliana* *Nse4A* gene is expressed across different tissue types and plant developmental stages. In contrast the expression of *Nse4B* is limited to embryo and endosperm tissues in developing siliques. *Nse4A* displays a

similar pattern as the other SMC5/6 complex subunits and shows always a higher expression than *Nse4B*. Taken together, the obtained results suggest that *Nse4A* is the major δ -kleisin gene of the SMC5/6 complex in somatic and generative cells. However, it seems that *Nse4B* may have an important function in embryo and endosperm cells where it is expressed.

Confirmation of the *in silico* expression data by quantitative real-time RT-PCR

After *in silico* analysis, the tissue-specific expression dynamics of both *Nse4* genes was determined by quantitative real-time RT-PCR. In this experiment, RNA from different anatomical plant parts (young and old rosette leaves, flower buds, roots) and developmental stages (seedlings) were isolated and used for cDNA preparation. Primer pairs nse4A-290F and nse4A-392R for *Nse4A* and nse4B-302F and nse4B-403R for the *Nse4B* gene were used (Table 8).

Table 8 Primers used in *Nse4* genes real-time quantitative RT-PCR

Gene	Primer name	Sequence	Location	Product size
<i>Nse4A</i> (AT1G51130)	nse4A-290F	CTTGCACCAACAAGTTCGGA	exon II	102
	nse4A-392R	GCAGACTGAGACTTCACCGA	exon III	
<i>Nse4B</i> (AT3G20760)	nse4B-302F	TGCACCAGAAAGTTCGGAAG	exon II	101
	nse4B-403R	AGCTGATTGCGATTTACCG	exon III	

The housekeeping genes *Pp2A* (AT1G13320) and *Rhip1* (AT4G26410) were used as a reference (Czechowski et al., 2004) (Table 2). The relative expression was calculated using the delta CT value (Schmittgen and Livak, 2008).

The *Nse4A* gene shows expression in seedlings, young and old rosette leaves, flower buds and roots (Figure 15). The expression in roots and flower buds is up to five times higher than in seedlings, young or old leaves compared to the expression of the reference genes *Pp2A* and *Rhip1*. *Nse4B* transcripts were undetectable in the investigated tissues.

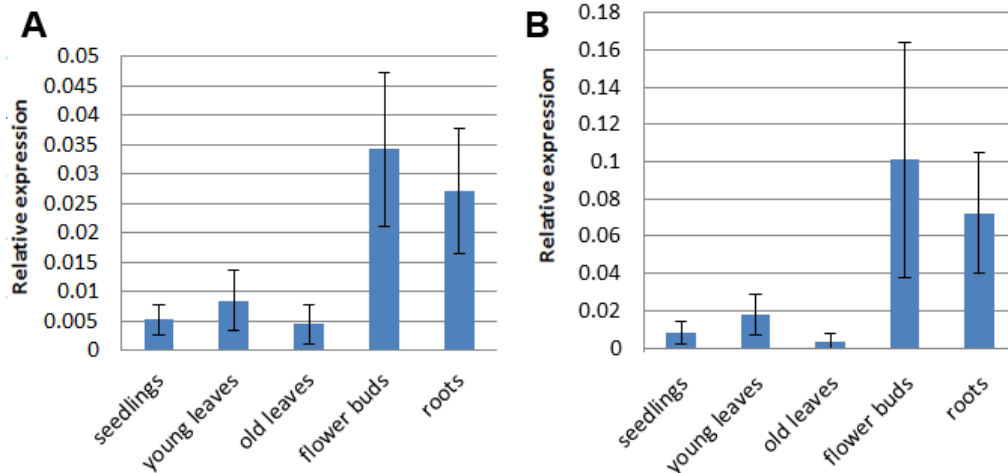


Figure 15 Relative expression of the *Nse4A* gene in different tissue types of *A. thaliana*. *Nse4A* expression is present across different tissues, compared to the reference genes *Pp2A* (A) and *Rhip1* (B). The experiment was performed using three technical and biological replicates.

In summary, two independent methods, *in-silico* RNAseq and quantitative real-time RT-PCR show a differential expression of *Nse4A* and *Nse4B* genes across different tissue types and plant developmental stages. The expression of *Nse4A* is elevated in flowers and roots and weaker in leaves and seedlings tissues. The expression of *Nse4B* gene is very weak in all tissues except in embryo and endosperm tissue (*in-silico* RNAseq) or undetectable (quantitative real-time RT-PCR). The co-expression analysis shows that all other SMC5/6 complex genes display a similar expression pattern in different developmental stages of *A. thaliana* except *Nse4B*. The expression of the SMC5/6 genes is elevated during early plant development, decreased in developed rosettes, during bolting and in young flowers. Then, it is elevated again during mature flower and siliques stages.

The increased expression of *Nse4A* compared to *Nse4B* and the co-expression with the other SMC5/6 complex genes suggest that *NSE4A* is the major δ -kleisin component of the SMC5/6 complex in somatic and generative cells across different developmental stages. However, the data do not exclude a putative role of *Nse4B* in embryo and endosperm cells where it is expressed.

4.1.3 *Nse4A* is co-expressed with cell division- and chromatin structure-specific genes

The *Nse4A* gene shows co-expression with the other SMC5/6 complex genes. In order to analyze whether *Nse4A* displays similar expression with other chromatin-specific genes, an analysis using the Genevestigator website was performed. The results show a high co-expression of *Nse4A* with a set of cell division- and chromatin structure-specific genes (Table 9).

Table 9 Genes showing high co-expression with *nse4A*. Scores indicate the level of correlation of expression in different anatomical samples. Gene names and their predicted coded proteins are obtained from databases of <https://genevestigator.com>. Bold gene names indicate cell division- or chromatin structure-specific genes.

Score	Gene name	Protein
0.96	<i>Med8</i>	Mediator of RNA polymerase II transcription subunit 8
0.95	<i>Smu1</i>	Suppressor of <i>mec-8</i> and <i>unc-52</i> protein homolog 1
0.95	<i>Tro</i>	Protein TRAUCO
0.95	<i>Drt111</i>	DNA-damage-repair/toleration protein
0.95	<i>Apc5</i>	Anaphase-promoting complex subunit 5
0.94	<i>Chr17</i>	Chromatin remodeling factor17
0.94	<i>Suvh4</i>	Histone-lysine N-methyltransferase
0.94	<i>Hda15</i>	Histone deacetylase 15
0.94	<i>Rfc3</i>	Replication factor C subunit 3
0.94	<i>Mlh1</i>	DNA mismatch repair protein MLH1
0.93	<i>Atr</i>	Serine/threonine-protein kinase ATR
0.93	<i>Msh3</i>	DNA mismatch repair protein MSH3
0.93	<i>Atx1</i>	Histone-lysine N-methyltransferase ATX1
0.93	<i>Aur3</i>	Serine/threonine-protein kinase Aurora-3
0.93	<i>Apc7</i>	Anaphase-promoting complex subunit 7
0.92	<i>Apc4</i>	Anaphase-promoting complex subunit 4
0.92	<i>Apc1</i>	Anaphase-promoting complex subunit 1

Nse4A is highly co-expressed with *Mlh1* and *Msh3*, two proteins required for DNA repair in mitosis and for resolving recombination intermediates in meiosis (Rogacheva et al., 2014). Furthermore, *Nse4A* is expressed together with anaphase promoting complex subunit genes (*Apc1*, 4, 5, 7), essential in triggering the transition from mitotic metaphase to anaphase. The *Nse4A* gene is also co-expressed with genes involved in histone modifications like the histone lysine N-methyltransferase *Suvh4*, the histone deacetylase 15 *Hda15*, and the histone-lysine N-methyltransferase *Atx1*, which have a role in chromatin structure and gene expression regulation (Du et al., 2014; Ding et al., 2012; Gu et al., 2017).

In addition, *Nse4A* is co-expressed with a set of DNA repair and organization proteins, which may indicate the involvement of NSE4A in these functions. This assumption is supported by literature data indicating a role of SMC5/6 in DNA repair and organization (Verver et al., 2016).

The similar gene expression values and patterns across different tissue types may indicate that these genes are involved in the same regulatory network. The network may control particular genes necessary for one or several cell functions.

4.2 Functional analysis of *Nse4* genes

To investigate the function of the *Nse4* genes, five different *A. thaliana*, ecotype Columbia T-DNA insertion mutants with insertions in *nse4A* (GK-768H08, Sail_71_A08, Salk_057130) and *nse4B* (GK_175D11, Sail_296F02) were selected and analyzed. The position of the T-DNA insertions are shown in Figure 16.

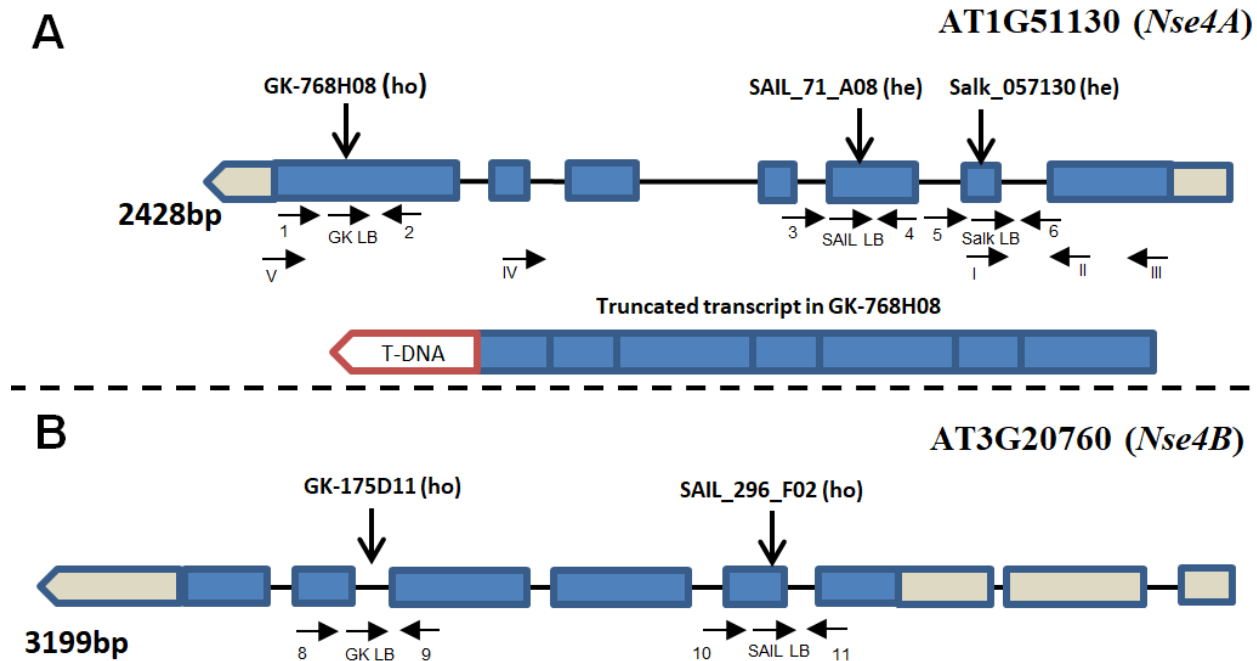


Figure 16 Scheme of the *A. thaliana* *Nse4A* and *Nse4B* gene structures (mips.helmholtz-muenchen.de, Version 10; ncbi.nlm.nih.gov; pfam.sanger.ac.uk) and of the expressed truncated transcript of *Nse4A*. Exons are shown as blue boxes. UTRs are visible in grey. The T-DNA insertions (SALK, SAIL and GK lines) and gene specific primers used for genotyping are indicated by arrows. Arabic numbers indicate gene-specific primers used for genotyping. Roman numbers denote primers applied for RT and real-time PCR (Table 5). The transcript of line GK_768H08 with indicated T-DNA insertion (red box) is truncated.

To identify T-DNA insertion homozygous plants, genomic DNA from a total of 20 mutant progeny plants were isolated and PCR-genotyped using specific primer pair combinations (Table 10).

Table 10 Primer combinations used for T-DNA line genotyping.

Gene	T-DNA insertion line	Gene specific primer pairs	Gene/T-DNA fragment
AT1G51130 (<i>Nse4A</i>)	GK-768H08	1 (GK-768H08-LP) + 2 (GK_768H08-RP)	2 (GK-768H08-RP) + GK LB
	Sail_71_A08	3 (Sail_71_A08-LP) + 4 (Sail_71_A08-RP)	4 (Sail_71_A08-RP) + SAIL LB
	Salk_057130	5 (Salk_057130-LP) + 6 (Salk_057130-RP)	6 (Salk_057130-RP) + SALK LB
AT3G20760 (<i>Nse4B</i>)	GK-175D11	7 (GK-175D11-LP) + 8 (GK_175D11-RP)	8 (GK_175D11-RP) + GABI LB
	Sail_296_F02	9 (Sail_296_F02-LP) + 10 (Sail_29_F02-RP)	10 (Sail_296_F02-RP) + SAIL LB

The PCR amplification of DNA from wild-type plants resulted exclusively in a gene-specific fragment (LP + RP). Heterozygous mutants showed gene-specific (LP + RP) and gene/T-DNA (RP + LB) amplicons. Homozygous mutants had only gene/T-DNA (RP + LB) fragments. The exclusive gene-specific amplification indicated an unchanged gene structure without T-DNA insertion, whereas the gene/T-DNA amplicons indicated a T-DNA insertion (Figure 17).

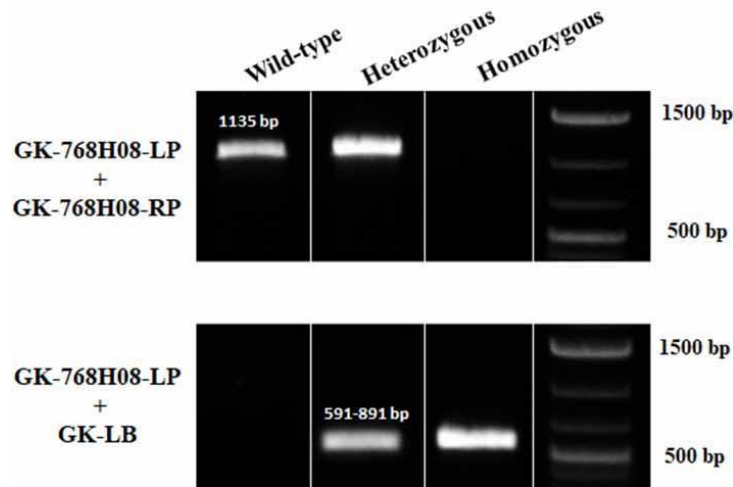


Figure 17 PCR genotyping experiment of wild-type and GK-768H08 mutant plants. Gene-specific fragment (GK-768H08-LP + GK-768H08-RP) amplification of a wild-type plant; gene-specific (GK-768H08-LP + GK-768H08-RP) and gene/T-DNA (GK-768H08-LP + GK-LB) amplification of a heterozygous mutant; and only gene/T-DNA (GK-768H08-LP + GK-LB) amplification of a homozygous T-DNA mutant.

To confirm the position of T-DNA insertions, gene/T-DNA PCR products were cloned into the pJET1.2 vector and sequenced. Based on the obtained sequences, the positions of different T-DNA insertions in all *nse4* mutants were confirmed.

The homozygous mutants were self-fertilized, seeds were collected and the offsprings were screened again for the presence of a T-DNA insertion. Only mother plants displaying a complete homozygous progeny were used in the analysis.

4.2.1 The complete inactivation of *Nse4A* is lethal

The genotyping experiments confirmed two heterozygous lines (Salk_057130, Sail_71_A08) and one homozygous (GK-768H08) T-DNA insertion line for the *Nse4A* gene (Figure 18 A). All of them are located in exon-coding regions. The Salk_057130 line has an insertion in the second exon, Sail_71_A08 in the third exon. The homozygous GK-768H08 T-DNA insertion is localized in the last exon of *Nse4A*.

Two homozygous T-DNA insertion lines (GK-175D11, Sail_294_F02) were found for the *Nse4B* gene (Figure 18 B). They are localized at the beginning of the second exon of SAIL_296_F02 and in the sixth intron of *Nse4B* of line GK-175D11. The existence of two homozygous T-DNA insertion lines for *Nse4B* indicates that the T-DNA insertion in this gene is not lethal for the plants. On the other hand, genotyping experiments did not reveal any homozygous *Nse4A* T-DNA insertion line in case of Salk_057130 and Sail_71_A08, suggesting that a homozygous T-DNA insertion into the *Nse4A* gene is lethal for the plant. However, the *nse4A* line GK-768H08 produced a homozygous progeny. Obviously, the short truncation of the gene product of this mutant does not interfere with the function of *Nse4A*.

Confirmation of the *Nse4A* gene truncation in the T-DNA insertion mutant GK-768H08

To confirm the truncation of the *Nse4A* gene transcript, RNA from GK-768H08 and wild-type plants were isolated and cDNA generated. The cDNA was used for genotyping by means of two specific primer pairs (Table 11). PCR analysis confirmed the truncation of the *Nse4A* transcript located at the end of the *Nse4A* gene of line GK-768H08 (Figure 18).

Table 11 Primer combinations used for the analysis of the T-DNA line GK-768H08.

Name of PCR product	Primers	Size of PCR product
1	nse4A(For) – nse4A(Cent)	849 bp
2	nse4A(For) – nse4A(C-Term)	2020 bp

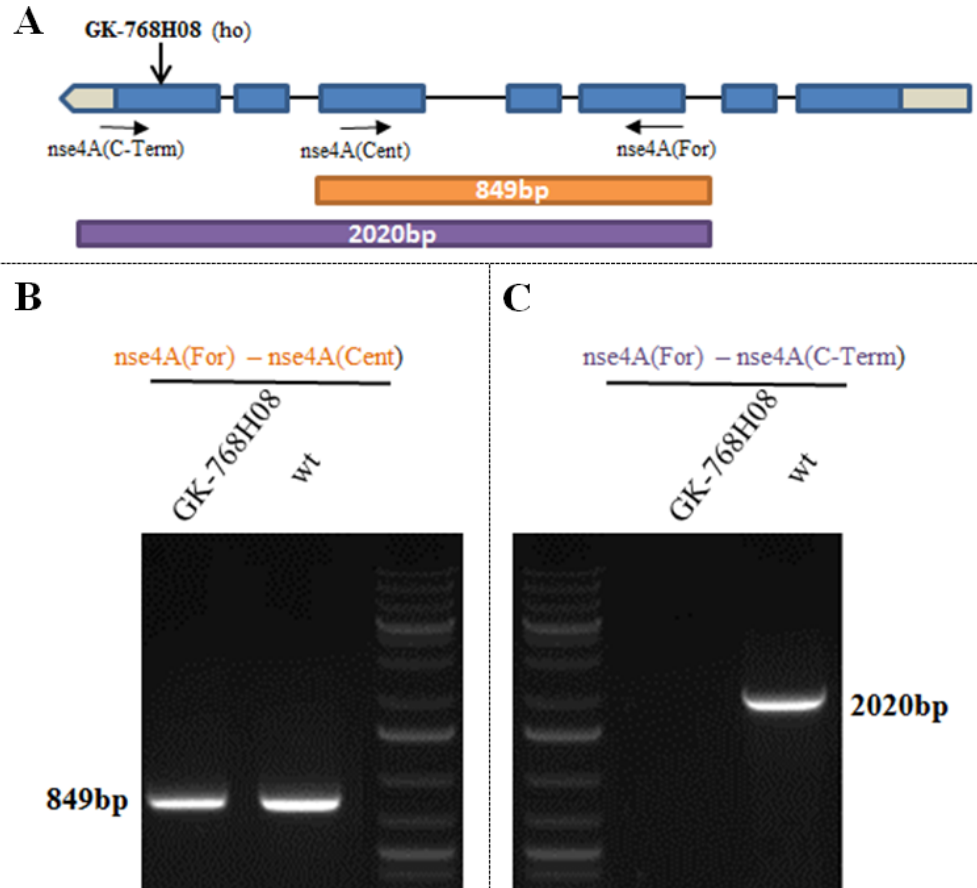


Figure 18 RT-PCR-based confirmation of the *nse4A* truncation in the T-DNA mutant line GK-768H08. (A) Schemata of gene structure and lengths of transcripts. Primers positions are indicated; the orange box indicates the PCR product of the interstitial gene region; the violet box indicates the PCR product of the central and C-terminal region. (B) RT-PCR shows the interstitial region of the *Nse4A* transcript in GK-768H08 and a wild-type plant. (C) PCR shows that the PCR product of the C-terminal region of *Nse4A* is missing in line GK-768H08.

The PCR transcript analyses of GK-768H08 proved a C-terminal truncation of the *Nse4A* transcript. Sequencing of the RT-PCR product confirmed the presence of a T-DNA insertion 13 amino acids away from the conserved NSE4-C terminal domain. This domain is essential for the binding of SMC5 to form SMC5/6 complexes (Pebernard et al., 2004). The truncation of *Nse4A* does not result in plant death. On the other hand, this truncation may effects the *Nse4A* function by changing the NSE4A structure and the N-terminus protein sequence.

4.2.2 Complementation of the *nse4A* T-DNA insertion mutant GK-768H08 with wild-type *Nse4A*

In order to confirm that the phenotype observed for the T-DNA line GK-768H08 is caused by the truncation of *Nse4A*, a complementation assay using the wild-type *Nse4A* sequence was performed.

The 2428 bp long genomic intron-exon containing *Nse4A* gene with a 1.7 kb upstream promoter sequence (pnse4A::gnse4A) was amplified by PCR using the primer pair prom_nse4A and nse4A_STOP (Table 12 and Figure 19).

Table 12 Primers combinations used for pnse4A::gnse4A amplification.

Primers	Size of PCR product
prom_nse4A – nse4A_STOP	~4200 bp

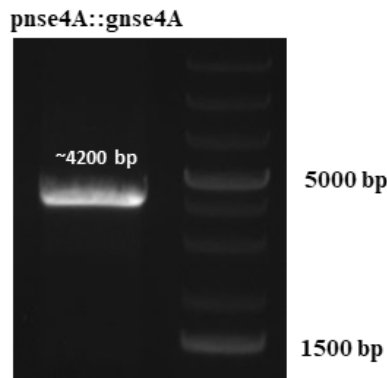


Figure 19 Full length PCR amplification of the 1.7 kb *Nse4A* promoter and genomic intron-exon sequence of the *Nse4A* gene (pnse4A::gnse4A).

The PCR product (pnse4A::gnse4A) was cloned into pJET 1.2 vector and sequenced; recloned into the vector pBWG and later transferred into *A. tumefaciens*. Transformation of the T-DNA line GK-768H08 was performed using the floral dipping method. Seeds were collected, and selected on MS plates containing PPT (BASTA). Positively selected seedlings were transferred into soil and genotyped using the GK-768H08 primers pairs (GK-768H08-RP + GK LB) for gene/T-DNA insertion and for *Nse4A* gene specific (GK-768H08-LP + GK-768H08-RP) products (Table 10). The complementation was performed on homozygous GK-768H08 plants.

The *Nse4A*-complemented GK-768H08 plants were transferred to long-day conditions and underwent self-fertilization. The seeds were collected and screened using specific primers (Table 13) to indicate the presence of the complementation construct. Only mother plants displaying a progeny with complemented constructs were used in further analysis (Figure 20).

Table 13 Primer pair used for the GK-768H08 complementation assay.

Primers	Size of PCR product
nse4A1929F – nse4A3953R	2024 bp

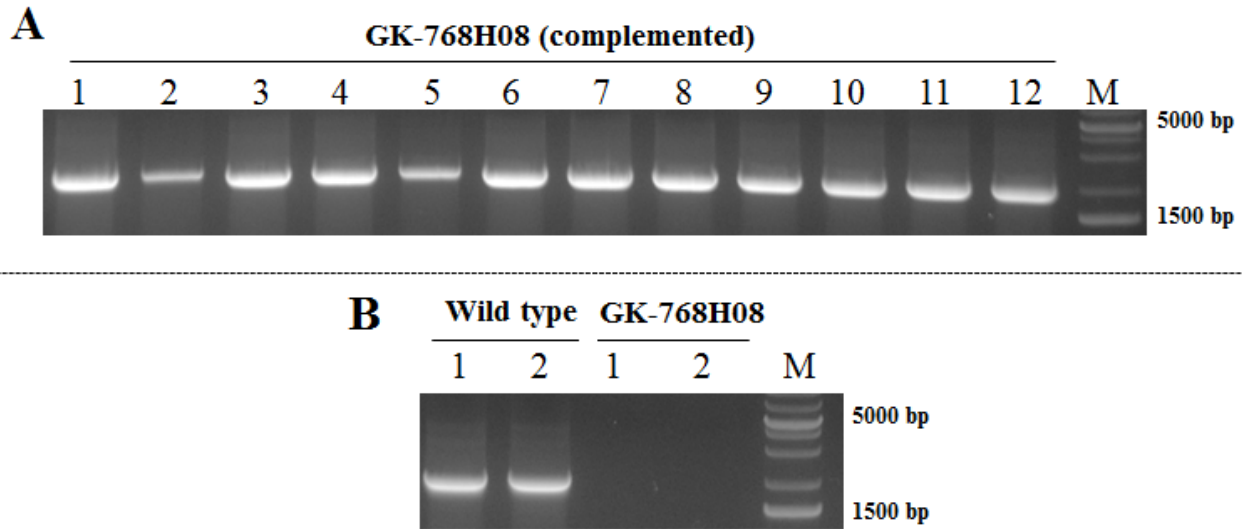


Figure 20 PCR screening of complemented GK-768H08 mutants using the nse4A1929F and nse4A3953R primer pair (2024 bp). The numbers indicate individual plants; M indicates the DNA weight marker. **(A)** PCR shows a product for complemented T2 GK-768H08 mutants. **(B)** Control PCR shows a product of wild-type and the lack of amplifications for GK-768H08 mutants.

4.2.3 Selection of a homozygous *nse4A/nse4B* T-DNA double mutant

To investigate whether the T-DNA based modification of both *Nse4* genes results in a phenotype different from wild-type, a homozygous *nse4A/nse4B* double mutant was generated by crossing homozygotes of the GK-768H08 (*nse4A*) and SAIL_296_F02 (*nse4B*) T-DNA mutants followed by subsequent selfing and screening. The crossing experiment was performed in collaboration with the group of Dr. Ales Pecinka from the Genome and Epigenome Evolution Group at the Institute of Experimental Botany AS CR in Olomouc (Czech Republic).

The crossing was bidirectional by using *nse4A* (GK-768H08) and *nse4B* (SAIL_296_F02) as pollen donor or acceptor. Selfed T2 plants were genotyped by PCR with the primer combinations

shown in table 4 for the presence of both T-DNA insertions (Figure 21). The analysis of 20 plants resulted in the identification of 11 homozygous *nse4A/nse4B* T-DNA double mutants.

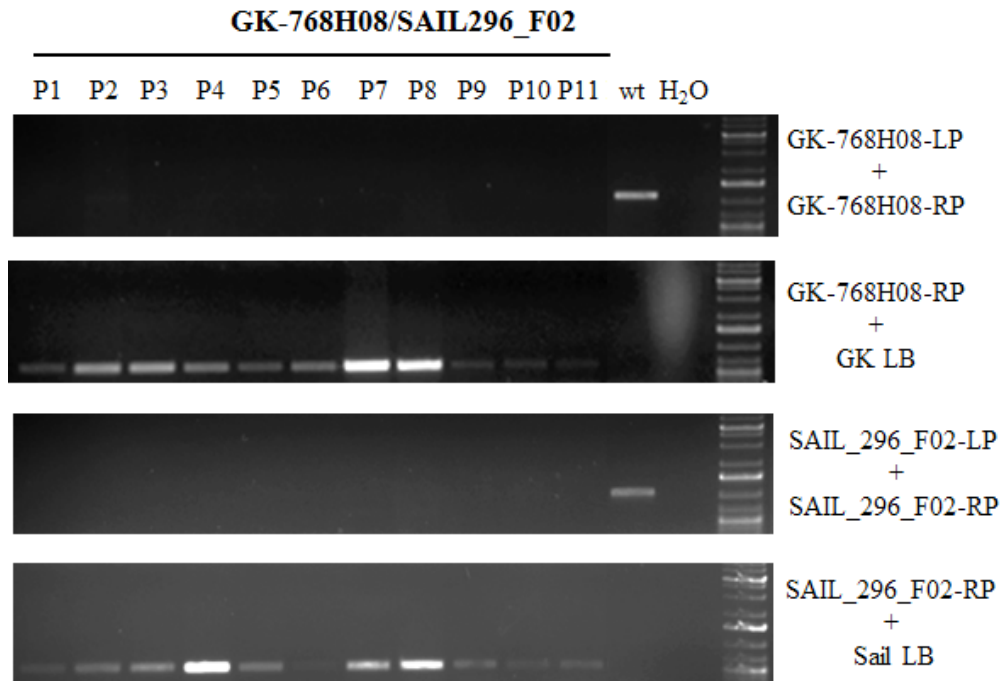


Figure 21 PCR genotyping of T2 mutants from the GK-768H08 x SAIL_296_F02 crossings. P1 – P11 T2 plants display homozygosity for T-DNA in the *Nse4A* and *Nse4B* genes. LP-RP PCR product represents the wild-type (wt) variant of the gene, whereas LB + RP identifies the T-DNA insertion. H₂O: control PCR without template. M: DNA marker.

4.2.4 *nse4A* mutants are reduced in size and branch number

In order to assay whether the mutation of *Nse4A* results in an altered growth phenotype the *A. thaliana* T-DNA lines Salk_057130, GK-768H08, GK-768H08/SAIL_296_F02 and wild-type plants were compared. The rosette development of mutant and wild-type plants did not show obvious differences. After flower induction and cultivating the plants under long-day light conditions, the vegetative phenotype differed between all three *nse4A* mutants and wild-type. Most of the T-DNA insertion lines were reduced in growth smaller and exhibited a reduced branch number (Figure 22).

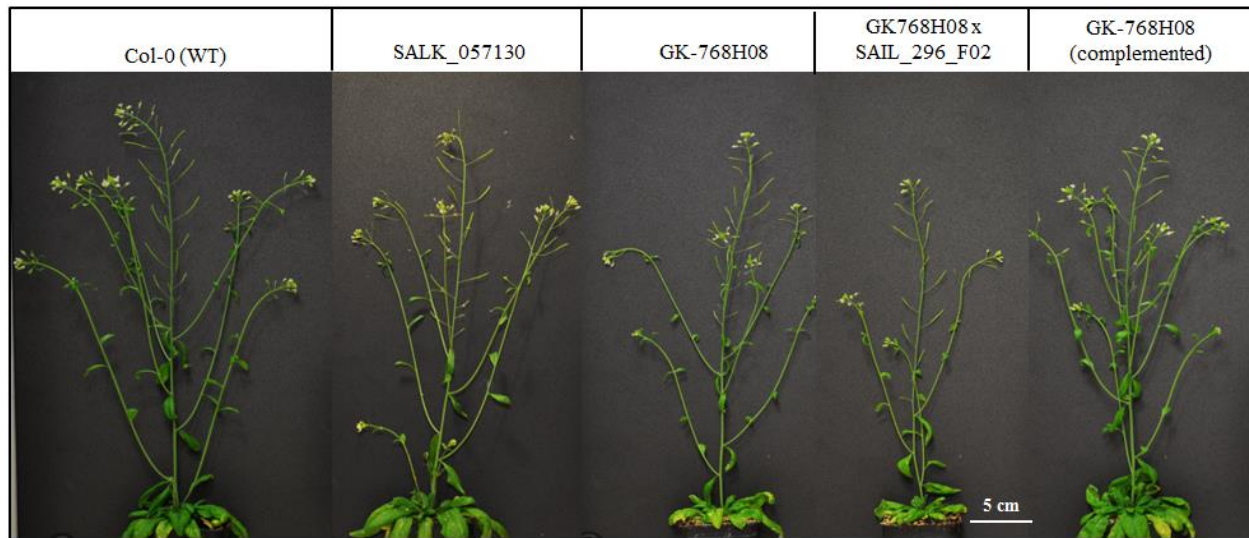


Figure 22 The *nse4A* mutant plants (heterozygous *nse4A* mutant Salk_057130, homozygous *nse4A* mutant GK-768H08 and homozygous *nse4A/nse4B* mutant GK-768H08/SAIL_296_F02) show a reduced growth and branch number compared to wild-type (wt). The wild-type phenotype of GK-768H08 was partially recovered after *pnse4A::gnse4A* complementation.

The phenotype analysis of the *nse4* mutants showed an impaired plant development. Compared to wild-type, a reduced plant growth was observed in the lines SALK_057130 and GK-768H08. In the homozygous line GK-768H08 this effect may be caused by the exclusive presence of two homologous truncated *Nse4A* genes. In the heterozygous line SALK_057130 the effect could be due to a decreased expression level of *Nse4A* caused by a knock-out of one of the two gene copies. The phenotype alteration of the GK-768H08 mutant was partially compensated by introducing the genomic *pnse4A::gnse4A* complementation construct. The homozygous *nse4B* T-DNA insertion lines GK-176D11 and SAIL_296_F02 did not display obvious phenotype alterations, although the double *nse4A/nse4B* mutation (GK-768H08/SAIL_296_F02) induced more impaired growth than the single *nse4A* mutation.

It seems that the *nse4B* mutants did not display an altered phenotype because they still have the functional wild-type *Nse4A* homologs, expressed in somatic tissues. In case of the double mutant, *nse4B* could not be complemented with the *Nse4A* gene. Knock-out of *Nse4B* (SAIL_296_F02) and the truncation of *Nse4A* (GK-768H08) obviously accumulated and resulted in increased developmental problems of the plant.

4.2.5 The mutation of *Nse4A*, but not of *Nse4B* induces mitotic defects

The reduced plant size of the *nse4A* mutants suggests an impaired mitotic division. Therefore, mitotic cells of the *nse4A* (Salk_057130 and GK-768H08) *nse4B* (GK-175D11) and *nse4A/nse4B* (GK-768H08/SAIL_296_F02) mutants were prepared from somatic flower bud cells and analyzed. A number of abnormalities, such as anaphase bridges or lagging chromosomes were found in the *nse4A* and *nse4A/nse4B* mutant lines (Figure 23 A). The mitotic defects were present in heterozygous SALK_057130 mutants (12% of 242 mitotic cells revealed division defects), and also in homozygous GK-768H08 mutants (26% of 175 mitotic cells division showed defects). The *nse4B* (GK-175D11) mutant displayed similar mitotic defects (2% of cells showed division defects in 178 mitotic cells) compared to wild-type plants (1% division defects in 412 mitotic cells). The homozygous double *nse4A/nse4B* (GK-768H08/SAIL_296_F02) mutant line showed the highest frequency of division defects (29% in 619 mitotic cells). The complementation of GK-768H08 (3% of cells showing division defects in 373 mitotic cells) recovered mainly the wild-type phenotype. The quantification of the results is summarized in Figure 24 B.

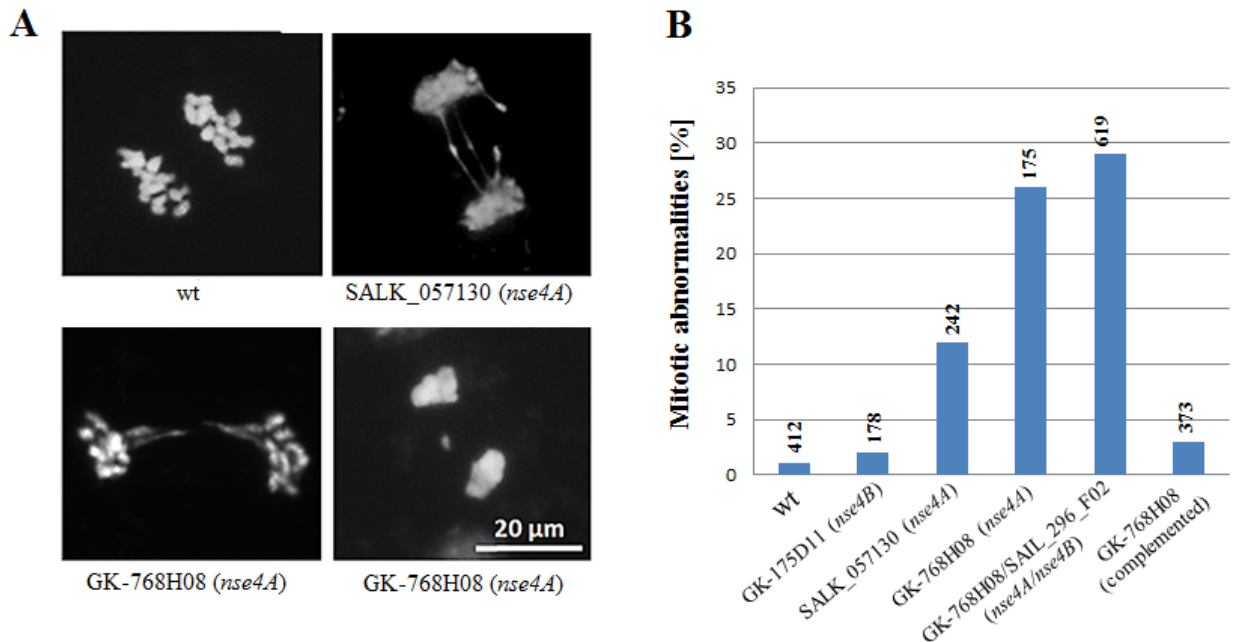


Figure 23 Mitotic defects in *A. thaliana nse4* mutants. (A) Somatic wild-type anaphase and examples of chromosome segregation abnormalities (lagging chromosomes and anaphase bridges) in the *nse4A* GK-768H08 and SALK_057130 mutants; (B) Frequency of abnormalities (anaphase bridges or lagging chromosomes) in wild-type (wt), *nse4A*, *nse4A/nse4B* double mutant and *nse4A*-complemented T-DNA lines. The numbers above the columns indicate the number of evaluated mitotic cells.

The obtained data suggest a relationship between the *Nse4A* gene mutations and the mitotic division defects. The heterozygous *nse4A* (SALK_057130) and the homozygous (GK-768H08) T-DNA lines displayed an elevated number of mitotic abnormalities compared to wild-type and the *nse4B* (GK-175D11) mutant. The complementation of the GK-768H08 mutant reduced the number of mitotic abnormalities, showing that the mitotic defects are linked to the impaired *Nse4A* function. Furthermore, the double *nse4A/nse4B* mutant displayed even a higher level of mitotic abnormalities than the single mutant lines.

4.2.6 The *Nse4* genes are essential for correct meiosis and fertility

Reduced fertility

Next we tested whether the *Nse4A* and *Nse4B* genes are required for meiosis and reproduction. In addition to an impaired growth of generative tissues in the *nse4A* mutants, a reduced fertility was observed. Compared to wild-type both *nse4A* and *nse4B* mutants displayed shorter siliques, a reduced number of seeds and pollen per anther (Figure 24). The reduced length of siliques correlated positively with a decreased seed number per silique. Additionally, abnormal dry, black and shriveled seeds occurred (Figure 24 A, B).

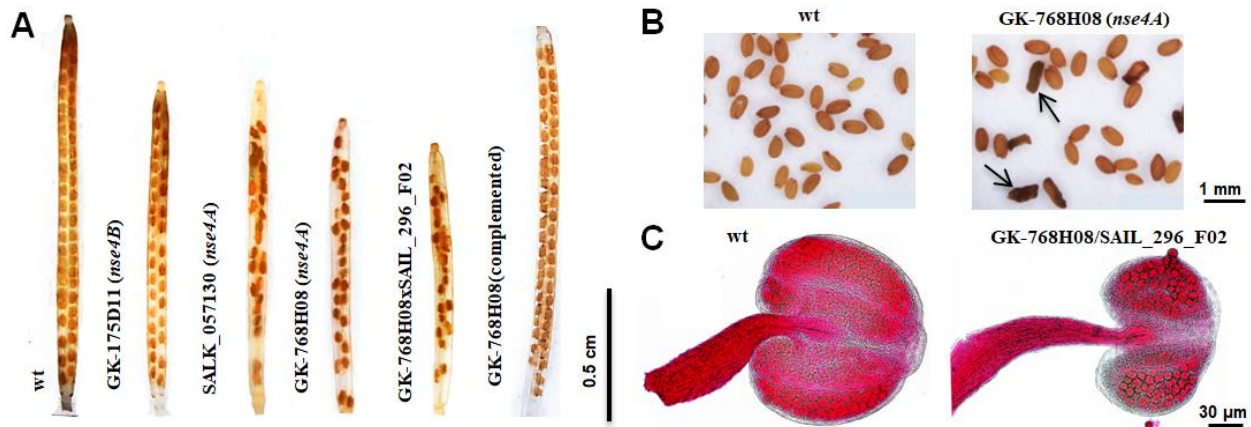


Figure 24 Reduced seed setting and fertility of *nse4* mutants compared to wild-type (wt). (A) Reduced seed number per silique in the *nse4A* and *nse4B* mutants. (B) Shriveled seeds (arrows) from the GK-768H08 mutant. (C) Reduced pollen grain number in an anther of the double mutant GK-768H08/SAIL_296_F02.

These effects were found in the heterozygous *nse4A* SALK_057130 (11.2±0.4 mm mean length of siliques, 29.3±4.5 seeds per silique) and the homozygous *nse4A* GK-768H08 (10.0±0.8 mm mean length of siliques, 21.0±4.7 seeds per silique) T-DNA lines. Defects were also found in the

homozygous *nse4B* line GK-175D11 (11.3±0.6 mm mean length of siliques, 34.8±5.9 seeds per silique) and in the homozygous *nse4A/nse4B* double mutant GK-768H08/SAIL_296_F02 (10.2±1.7 mm mean length of siliques, 17.9±7.8 seeds per silique). The complementation of GK-768H08 (12.3±0.8 mm mean length of siliques, 31.8±5.7 seeds per silique) recovered partially the silique length and seed number of wild-type plants (12.8±0.6 mm of siliques and 44.5±5.6 seeds per silique). All investigated T-DNA insertion mutants displayed an increased number of black, dry and shriveled seeds (Figure 24 B). The highest level of abnormal seeds per silique was observed in the *nse4A* GK-768H08 mutant (7.8±2.7) and in the double mutant *nse4A/nse4B* GK-768H08/SAIL_296_F02 (5.6±2.5). The complementation of GK-768H08 with the wild-type construct reduced the number of abnormal seeds up to 3.4±2.6 per silique.

Alexander staining of pollen was conducted to compare the male fertility between the *nse4* mutants and wild-type plants, and their number per anther was quantified. It was reduced in the homozygous *nse4A* (GK-768H08), *nse4B* (GK-175D11) and *nse4A/nse4B* (GK-768H08/SAIL_296_F02) mutants by 50.2%, 64.3% and 34.5%, respectively. The complementation of GK-768H08 increased the pollen grain number to the wild-type level (102%). The heterozygous SALK_057130 *nse4A* mutant did not display a significantly reduced pollen grain number (98.2%) (Figure 25).

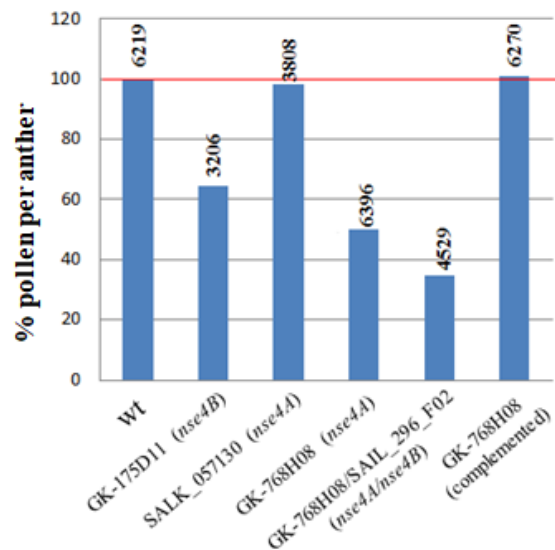


Figure 25 The mutation of the *Nse4* genes results in reduced fertility. Total pollen number per anther in wild-type (100% - red line), the *nse4A*, *nse4B*, *nse4A/nse4B* mutants and the complemented *nse4A* T-DNA line GK-768H08. The numbers of evaluated pollen grains are indicated above the diagram bars.

In summary, all evaluated *nse4* mutants displayed a reduced fertility, such as reduced silique lengths, reduced seed and pollen numbers. The strongest fertility defects were proven in the *nse4A* GK-768H08 and *nse4A/nse4B* double mutant. Minor fertility defects were also observed in the homozygous *nse4B* line GK-175D11 and the heterozygous *nse4A* line SALK_057130.

Interestingly, the high pollen number reduction in line GK768H08 (50.2%) was recovered by the presence of the native *Nse4A* gene. This complemented line did not display a reduction in pollen grain number, but has still shorter siliques and less seeds. A similar observation was true for the heterozygous *nse4A* line SALK_057130 where the mutant has less seeds and shorter siliques, but the pollen grain number reaches almost the wild-type level (98.2%).

Obviously, both *Nse4A* and *Nse4B* genes are involved in realizing complete fertility. However, *Nse4A* seems to be the more essential gene. The reduced pollen number in *nse4A* and *nse4B* mutants could be a result of disturbed meiotic processes, leading to aborted pollen grains, and in turn to reduced pollen number.

On the other hand, mutants containing a native *Nse4A* gene copy (the heterozygous *nse4A* SALK_057130 and the complemented GK768H08 mutants) showed a reduced number of seeds per silique with a normal level of pollen grains. The assumption is that in these mutants, although meiosis is disturbed and inducing impaired chromosome divisions, anaphase bridges or lagging chromosomes), the effect is not strong enough to cause a significant number of pollen abortion. But the pollen fertility and/or the embryogenesis might be negatively influenced.

4.2.7 *Nse4A* and *Nse4B* mutations result in impaired meiosis

The reduced number of seeds and pollen in *nse4* mutants suggests meiotic abnormalities. Consequently, the different stages of pollen meiosis were analyzed. All the investigated mutants; *nse4A* (SALK_057130, GK-768H08) *nse4B* (GK-175D11) and *nse4A/nse4B* (GK-768H08/SAIL_296_F02) displayed chromosome fragmentation in metaphase I, lagging chromosomes and/or chromosome bridges in anaphases I and II (Figure 26 A).

The highest number of meiotic abnormalities was found in the homozygous *nse4A* mutant GK-768H08 (25% metaphase I, 40% anaphase I and 47% anaphase II cells were abnormal).

Similarly, the double mutant *nse4A/nse4B* showed abnormal cells in 31% of metaphase I, in 65% of anaphase I and in 50% of anaphase II (Figure 26 B). Instead, the percentage of abnormal cells was clearly lower in the heterozygous *nse4A* mutant SALK_057130 (8% metaphase I, 5% anaphase I and 10% anaphase II cells were disturbed), but also in the homozygous *nse4B* GK-175D11 mutant (6% metaphase I, 18% anaphase I) showed abnormalities. Due to the complementation, the T-DNA line GK-768H08 revealed a reduced frequency of meiotic abnormalities (only 5% of metaphase I, 19% of anaphase I and 15% of anaphase II cells were abnormal).

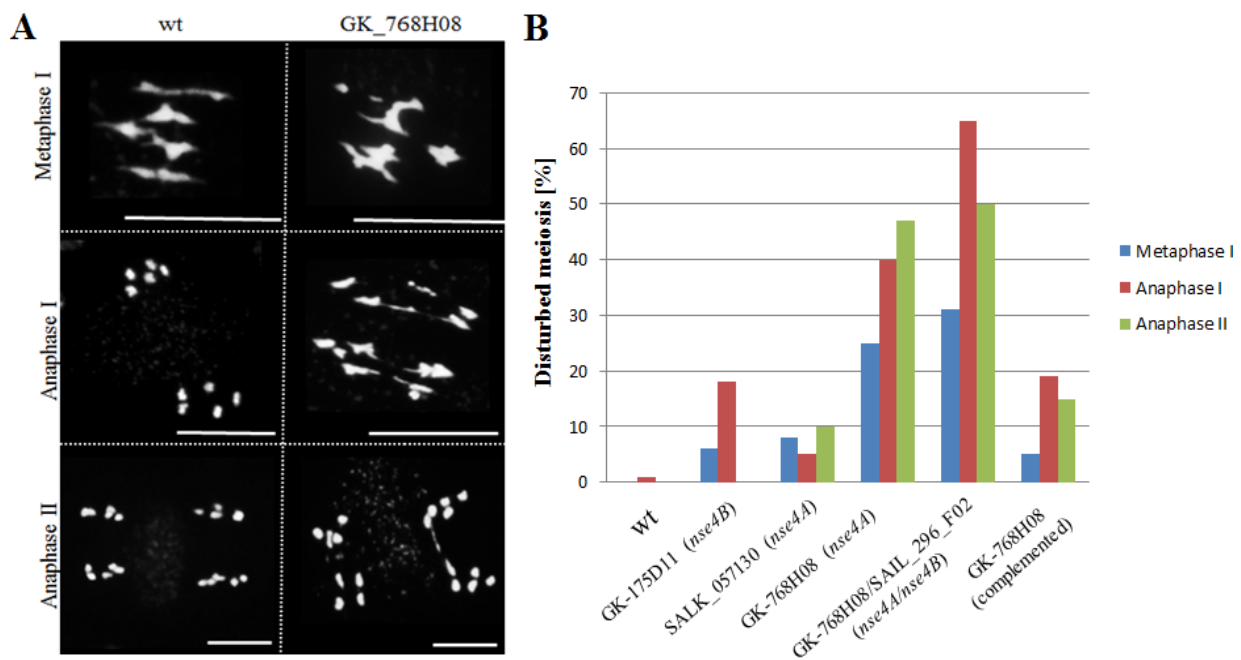


Figure 26 Mutations in *Nse4A* and *Nse4B* result in meiotic abnormalities. **(A)** The *nse4A* mutant GK-768H08 shows the fragmentation of the chromosomes at metaphase I and lagging chromosomes at anaphases I and II. The normal behavior of wild-type (wt) chromosomes during meiosis are shown for comparison. Bars = 10 μ m. **(B)** The frequencies of metaphase I, anaphase I and II abnormalities in wt, the *nse4A* and *nse4B* mutants, the *nse4A/nse4B* double mutant and the complemented *nse4A* line GK-768H08. The number of evaluated cells is shown in Table 14.

The data suggest that both *Nse4* genes are required in meiosis and for fertility. The fertility decrease is negatively correlated with the amount of meiotic defects, as obvious for the *nse4A* GK-768H08 line and the *nse4A/nse4B* double mutant. Therefore, it seems that the reduced seed and pollen number in the *nse4A* and *nse4B* mutants are caused by disturbed meiosis.

The quantification of fertility and meiotic defects is summarized in Table 14.

Table 14 Characterization of *A. thaliana nse4A* and *nse4B* T-DNA insertion mutants. Number of – analyzed pollen, seeds, siliques and cells are in parentheses.
 ** $p < 0.01$; * $p < 0.05$

Gene mutation	T-DNA mutant	Zygosity	Habit	% pollen	mm silique length	Seeds per silique	No. shriveled seeds per silique	% abnormal mitotic cells	% meiotic cells with chromosome segregation defects		
									Metaphase I	Anaphase I	Anaphase II
Wild type Col – 0	-	-	wt	100% (6219)	12.8** \pm 0.6 (28)	44.5** \pm 5.6 (1468)	0.7** \pm 1.4	1% (412)	0% (60)	1% (67)	0% (23)
<i>Nse4B</i>	SAIL-294-F02	Homozygous	wt-like	97.2% (3770)	10.8** \pm 0.7	33.5** \pm 7.4	1.6** \pm 2.9	2% (278)	0% (59)	6% (85)	8% (12)
<i>Nse4B</i>	GK-175D11	Homozygous	wt-like	64.3 (3206)	11.3** \pm 0.6 (30)	34.8** \pm 5.9 (1080)	2.9* \pm 3.8	2% (178)	6% (113)	18% (106)	0% (18)
<i>Nse4A</i>	SALK-057130	Heterozygous	Smaller	98.2 (3808)	11.2** \pm 0.4 (24)	29.3** \pm 4.5 (726)	2.7** \pm 2.5	12% (242)	8% (59)	5% (47)	10% (21)
<i>Nse4A</i>	GK-768H08	Homozygous	Smaller	50.2% (6396)	10.0** \pm 0.8 (25)	21.0** \pm 4.7 (525)	7.8** \pm 2.7	26% (175)	25% (115)	40% (114)	47% (19)
<i>Nse4A</i> and <i>Nse4B</i>	GK-768H08/SAIL_296_F02	Homozygous/Homozygous	Smaller	34.8% (4529)	10.2** \pm 1.7 (30)	17.9** \pm 7.8 (536)	5.6** \pm 2.5	29% (619)	31% (72)	65% (172)	50% (34)
<i>nse4A</i> complemented	GK-768H08 (complemented with <i>Nse4A</i>)		wt-like	102% (6270)	12.3** \pm 0.8 (25)	31.8** \pm 5.7 (795)	3.4** \pm 2.6	3% (373)	5% (121)	19% (131)	15% (20)

4.2.8 The *Nse4A* mutation induces predominantly distal acentric fragments and which are not chromosome type-specific

The analysis of the *nse4A* T-DNA line GK-768H08 demonstrated a number of meiotic defects. To investigate the chromosomal origin of the meiotic chromosome fragments, FISH was performed using differently labeled 5S and 45S rDNA probes. The unique chromosomal distribution of both repeats and the different amount of the 45S rDNA on chromosomes III and V allowed the identification of all five chromosome pairs of *A. thaliana* (Figure 27 A, B).

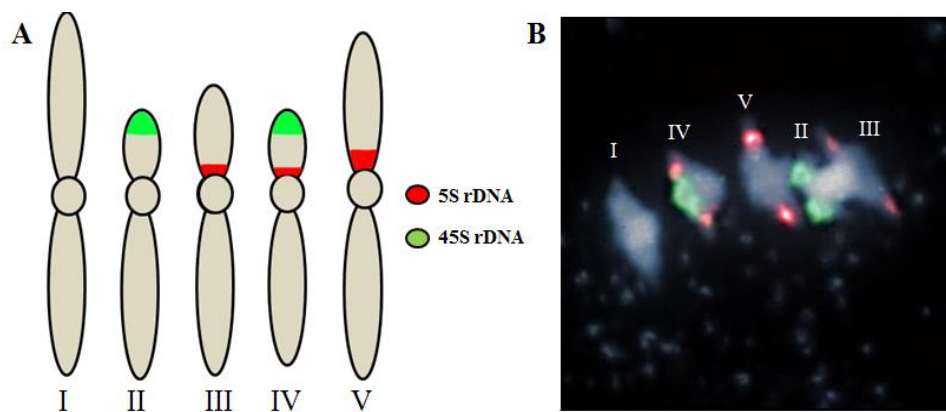


Figure 27 Chromosomal distribution of 5S and 45S rDNA repeats in wild-type *A. thaliana*. (A) Schematic drawing of the five *A. thaliana* chromosomes showing the localization of 5S and 45S rDNA, (B) Metaphase I chromosomes after FISH with 5S (red) and 45S (green) rDNA probes.

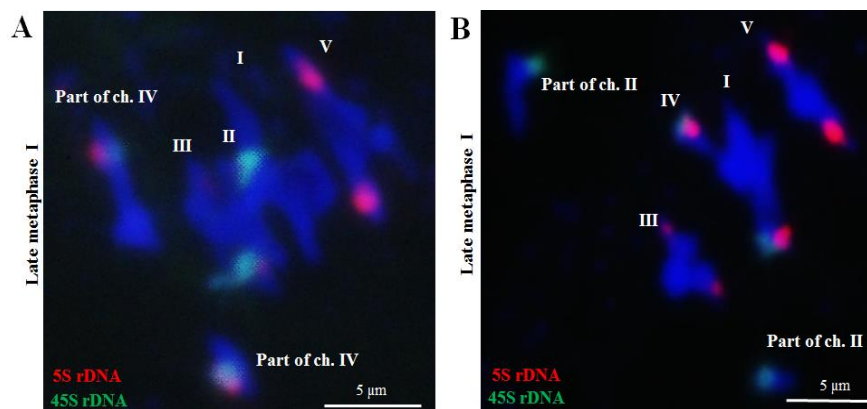


Figure 28 FISH-based analysis of metaphase I chromosomes of the *nse4A* line GK-768H08 with 5S (red) and 45S rDNA (green) repeats. (A) Fragmentation of chromosome IV, (B) Fragmentation of chromosome II.

FISH-based analysis of the *nse4A* mutant GK-768H08 displayed fragmentation of chromosome IV, II (Figure 28) and I (data not shown) in different metaphase I cells. Therefore, it is likely that the fragmentation of the chromosomes in the mutant GK-768H08 is random. Although, we name the phenomenon fragmentation, the orientation of the fragments at late metaphase I indicates, that they may still be connected via strongly decondensed, but after DAPI staining not visible chromatin threads. To further investigate the fragmentation sites, an additional FISH experiment was performed with labeled *Arabidopsis*-type (5'-CCCTAAA-3') telomere (Richards & Ausubel, 1988) and 180 bp centromere-specific (pAL) (Martinez-Zapater et al., 1986) repeats.

Preferentially acentric fragments with subtelomeric signals were found. 17 of 18 investigated metaphase I cells showed chromosome fragments with telomere signals two cells had fragments with centromeric signals only and nine cells displayed fragments without visible telomere nor centromere signals (Figure 29).

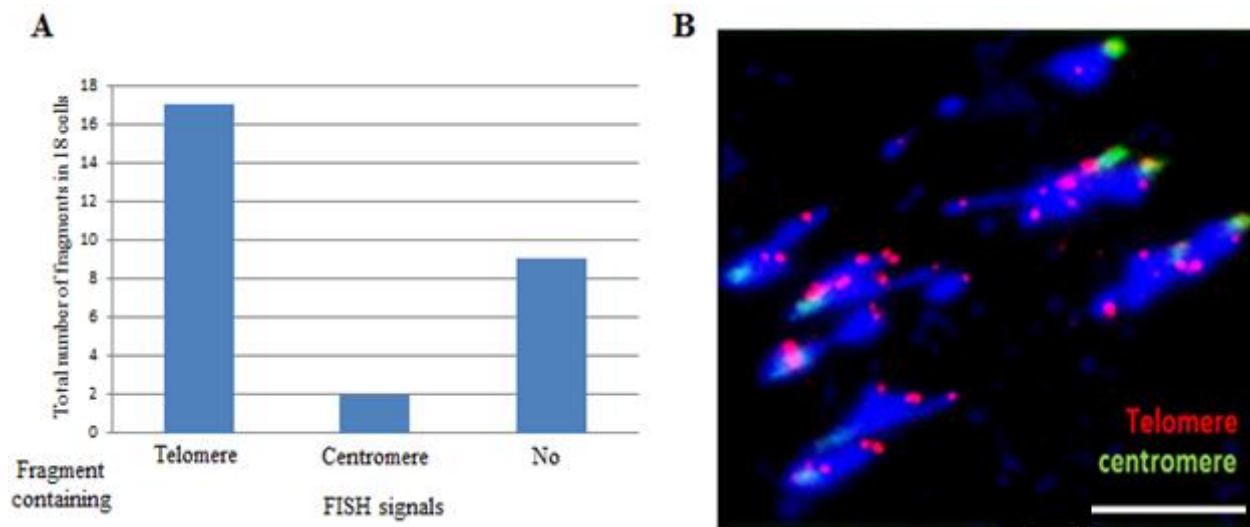


Figure 29 The chromosome fragmentation in the *nse4A* mutant GK-768H08 produces predominantly distal acentric fragments. **(A)** Quantification of chromosome fragments containing telomere and centromere signals in 18 anaphase I cells. **(B)** Anaphase I cell showing chromosome fragments after FISH with labeled telomeres (red) and centromeres (green). Bar =5 μ m

The obtained data suggest that the chromosome fragmentation of the homozygous *nse4A* mutant GK-768H06 is random at meiosis I and not assigned to a particular chromosome and chromosome region.

Chromosome fragmentation in the *nse4A* mutant GK-768H08 may result in micronuclei

Breakage in distal acentric chromosome regions may result in the formation of micronuclei. To evaluate the frequency of micronuclei formation, a screening of pollen mother cells derived from GK-768H08 was performed. Micronuclei were detected in prophase II and tetrad cells (Figure 30).

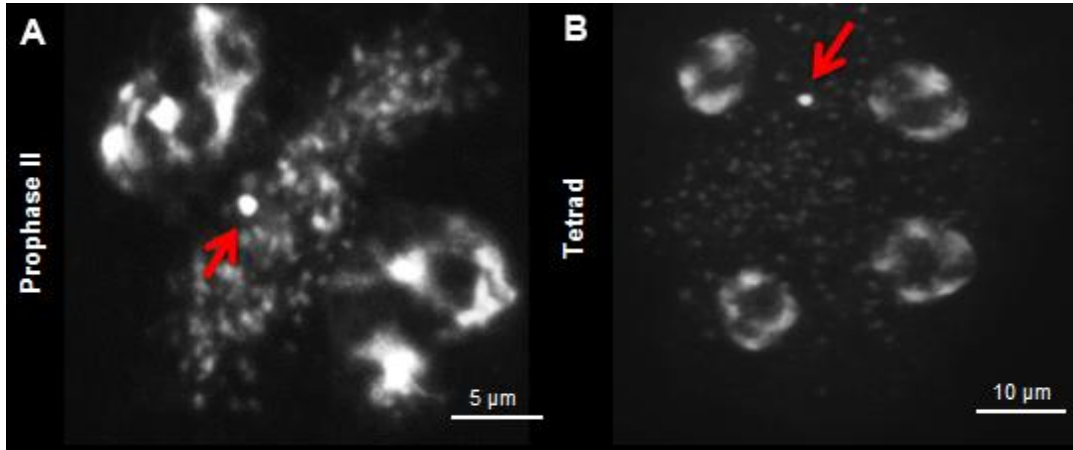


Figure 30 Micronuclei in the *nse4A* mutant GK-768H08. Micronuclei (red arrows) in (A) prophase II and (B) tetrad cells.

Unfortunately, due to the very small size of micronuclei an accurate quantification was not possible. Nevertheless, it is likely that the few detected micronuclei are a product of the observed chromosome fragmentation events.

The *nse4A* mutant GK-768H08 performs normal synapsis during prophase

One of the putative reasons for the observed meiotic chromosome fragments could be a disturbed synapsis of the homologues during prophase I. To test this assumption, prophase I chromosomes of the *nse4A* mutant GK-76H08 and wild-type plants were compared.

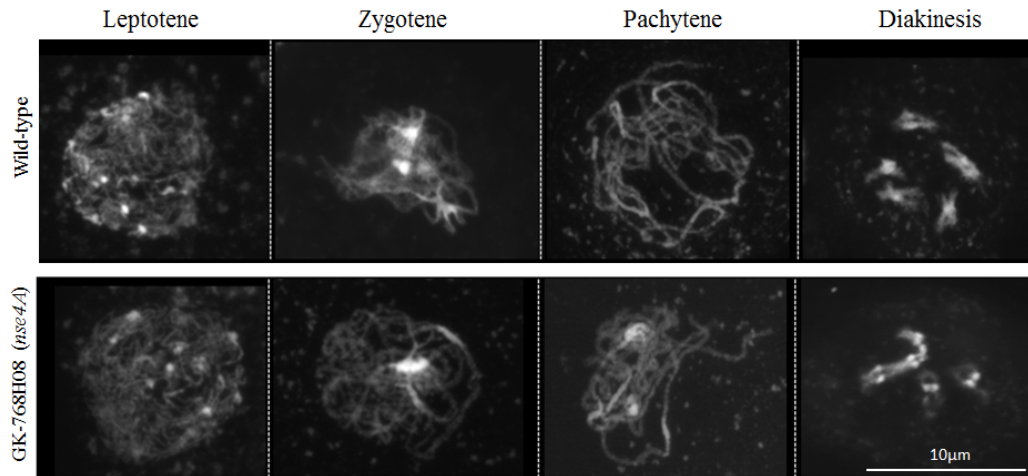


Figure 31 Comparison of the prophase I stages in wild-type and the *nse4A* mutant GK-768H08. No abnormalities were observed. Chromosomes were stained with DAPI.

No apparent differences between the mutant and wild-type were found regarding chromosome shape and condensation from leptotene until diakinesis (Figure 31). To confirm that normal homologous synapsis occurs, immunolabeling with anti-ZYP1 (transverse filament synaptonemal complex protein) was performed in ten prophase I cells of line GK-768H08 and wild-type. A continuous line-like ZYP1 signal was proven in both genotypes (Figure 32), indicating the proper assembly of the synaptonemal complex in the *nse4A* GK-768H08 mutant.

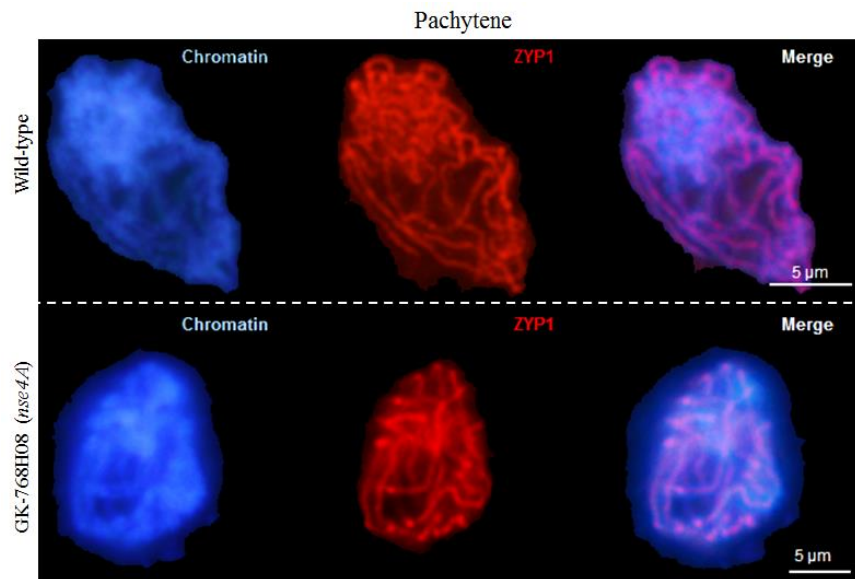


Figure 32 The *nse4A* mutant GK-768H08 shows a wild-type-like distribution of the synaptonemal complex protein ZYP1. Pachytene cells immunostained with anti-ZYP1 (red). Chromatin was counterstained with DAPI (blue).

The *Nse4A* mutation in line GK-768H08 does not influence the chiasmata frequency

Meiotic defects, such as lagging chromosomes and fragmentation, observed in the *nse4A* mutant GK-768H08 suggest unresolved crossing over intermediates and a probably altered number of chiasmata. To compare the chiasmata frequency between wild-type and mutants, FISH using 5S rDNA and 45S rDNA probes was performed in collaboration with Dr. Monica Pradillo and Prof. Juan L. Santos (University Complutense of Madrid, Spain). The rDNA probes were used as chromosome-specific markers (Figure 27). The analysis of 43 diakinesis/metaphase I cells of the *nse4A* mutant GK-768H08 revealed ~10 chiasmata per cell (Table 15). A similar number of chiasmata (~9.9) was reported for the wild-type *A. thaliana* ecotype Col-0 (Higgins et al., 2004).

Table 15 Chiasmata number of the *nse4A* mutant GK-768H08 and wild-type

Individuals	No. of diakinesis/metaphase I cells	Average number of chiasmata
GK-768H08 #1	6	9.3
GK-768H08 #2	7	9.7
GK-768H08 #3	30	10.5
Total number of cells analyzed	43	10.0
Col-0 (wt)	-	9.9*

*According to Higgins et al. (2004)

In summary, the analysis of the mutant GK-768H08 revealed no apparent abnormalities during prophase I and synapsis. However, chromosome lagging and fragmentation were observed. Random chromosome breakage occurs preferentially in acentric regions (most of the fragments have a sub-telomeric region). The fragmentation may result in micronuclei which were observed in prophase II and tetrads cells. However, these abnormalities do not influence the number of chiasmata, indicating that in this mutant the formation of crossovers is not impaired.

4.3 Dynamics and localization of NSE4A in *A. thaliana*

To investigate the dynamics and localization of the NSE4A protein, NSE4A-specific antibodies and transgenic *A. thaliana* lines processing GFP-tagged NSE4A were generated.

4.3.1 Production of NSE3, NSE4A and SMC5 recombinant proteins in *E. coli*

To investigate the localization and dynamics of the different components of the SMC5/6 complex we aimed to produce specific antibodies. Therefore, the conserved regions of *Nse3* (13-237 bp), *Nse4A* (146-867 bp) and *Smc5* (19-209 bp) were amplified by PCR. cDNA was used as PCR template and specific gene fragments with designed restriction sites (*XhoI*, *EcoRI* for *Nse3*, *Smc5* genes and *BamHI*, *XhoI* for the *Nse4A* gene) were used as primers for reaction (Table 16).

Table 16 Primers used for the amplification of SMC5/6 complex gene fragments. The sequences of restriction sites used for cloning are underlined.

Gene	Primer name	Sequence	5' Restriction site
<i>Nse3</i>	AtNse3_AB_For	<u>TGAATTCGAAGATTCTCTCTCAATTCGAT</u>	<i>EcoRI</i>
	AtNse3_AB_Rev	<u>AACTCGAGATCATTAAGCTCTACAACCTGCTACATC</u>	<i>XhoI</i>
<i>Nse4A</i>	AtNse4a_AB_For	<u>TGGATCCCCTCAGGAGGAAGAACAAGG</u>	<i>BamHI</i>
	AtSNse4a_AB_rev	<u>AACTCGAGCATGGCGAAATGAGAACCAC</u>	<i>XhoI</i>
<i>Smc5</i>	AtSmc5_AB_For	<u>TGAATTCCTTGCCTGGGAATATAATCGAAA</u>	<i>EcoRI</i>
	AtSmc5_AB_Rev	<u>AACTCGAGCTGATTCAGCGTCTCTCCATT</u>	<i>XhoI</i>

The PCR amplified gene fragments were cloned into the vector pJET 1.2, transformed into *E. coli* DH5 α cells and sequenced. After sequence verification, the plasmid DNA was extracted and enzymatically digested to release the inserts. Products of the restriction reaction were separated by agarose electrophoresis. Gene fragments were extracted from the gel and cloned into the expression vector pET23atm (a vector containing a six histidine on C-term (6xHIS)). After ligation, the vectors were transformed into electro-competent BL21pLysS *E. coli* cells. Transgenic *E. coli* were treated with 1 mM IPTG for 3 hours for induction and expression of the recombinant proteins, which were released from the cells using chemical (lysozyme) and mechanical (sonification) lysis. The recombinant proteins were separated and purified from the cell extracts using Ni-NTA agarose beads.

The obtained *E. coli* cell lysates before and after protein induction (Figure 33 A) and the elution of purified recombinant proteins (Figure 33 B) were checked using SDS-PAGE electrophoresis.

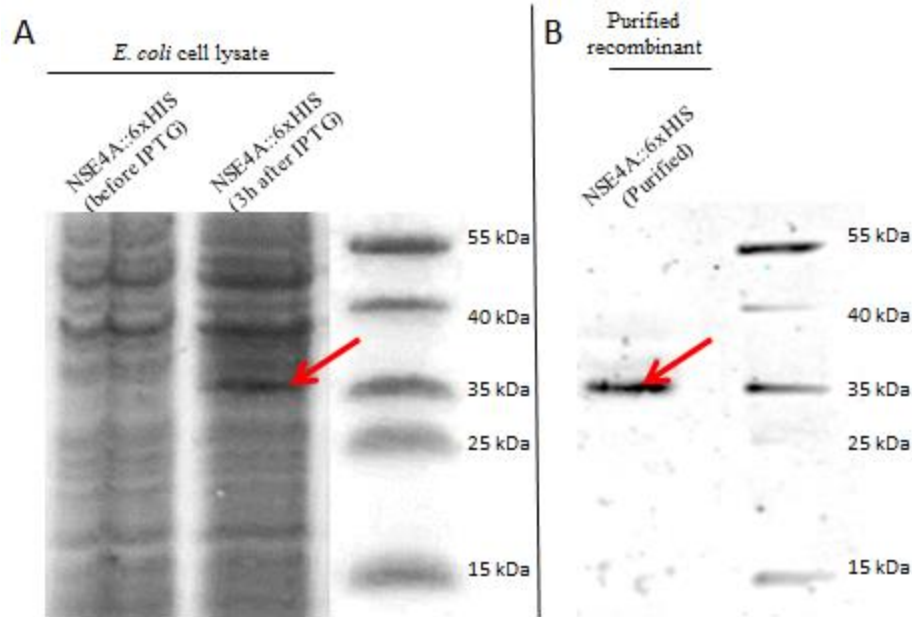


Figure 33 Expression and purification of recombinant NSE4A proteins. Coomassie stained gels after SDS-PAGE electrophoresis. Red arrows indicate recombinant protein NSE4A::6xHIS. **(A)** Total protein lysate from *E. coli* cells before and after recombinant protein expression **(B)** Recombinant protein fraction after Ni-NTA agarose purification.

The protein mass was higher (~34-36 kDa) than expected (30 kDa). This could be explained by post-translational protein modifications (e.g. SUMOylation or phosphorylation) which may influence the protein migration dynamics during SDS-PAGE electrophoresis. The isolated recombinant NSE4A::6xHIS protein displayed a high purity, without additional unspecific protein bands (Figure 33 B).

The recombinant NSE3 and SMC5 proteins were expressed and checked by the same methods as described for NSE4A (Figure 34). The purified recombinant NSE3::6xHIS, NSE4A::6xHIS and SMC5::6xHIS proteins were used to immunize rabbits to produce specific antibodies.

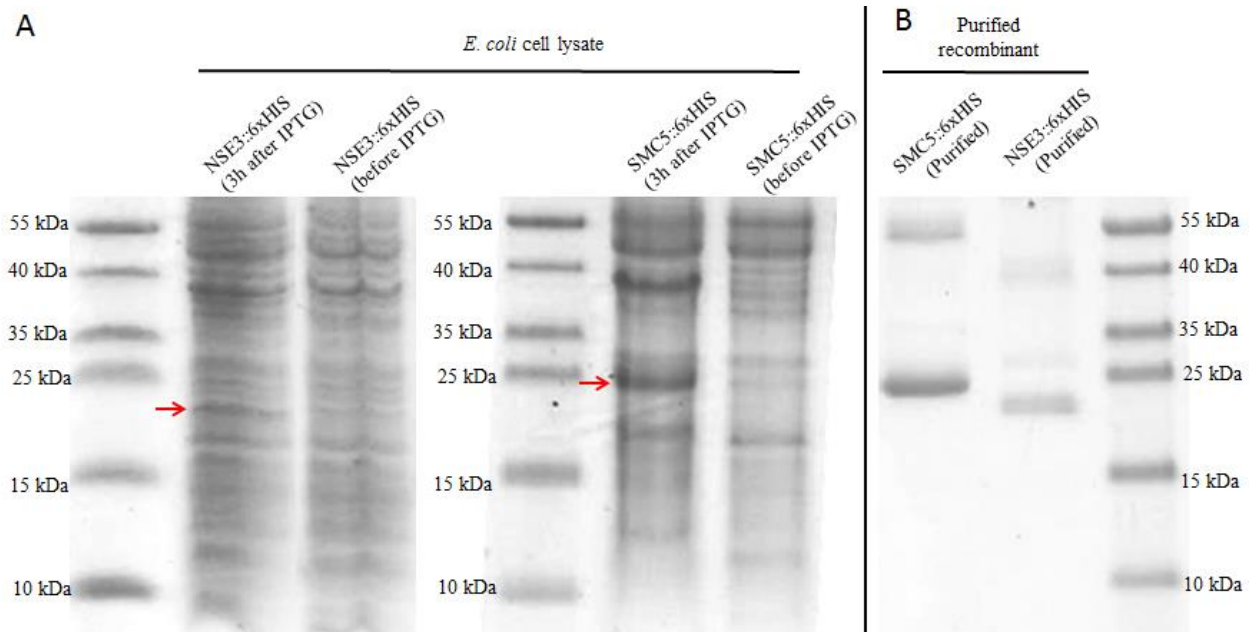


Figure 34 Expression and purification of the recombinant NSE3::6xHIS and SMC5::6xHIS proteins. Coomassie stained gels after SDS-PAGE electrophoresis. Red arrows indicate the recombinant proteins NSE3::6xHIS and SMC5::6xHIS. **(A)** Total protein lysates from *E. coli* cells before and after recombinant protein expression. **(B)** Recombinant protein fractions after Ni-NTA agarose purification.

4.3.2 Production of NSE3, NSE4A and SMC5 antibodies

The Ni-NTA purified recombinant NSE3::6xHIS, NSE4A::6xHIS and SMC5::6xHIS proteins were used as antigens. The production of antibodies was performed in collaboration with Prof. Udo Conrad (research group Phytoantibodies, IPK Gatersleben). The antibodies were raised in rabbits (per each antigen two rabbits were immunized). The antigens were injected into the neck of the rabbits in a series of injections. The first injection was performed with 0.5 mg of antigen. The second and third injection took place after 4 and 5 weeks, respectively with 0.25 mg of antigen. Six weeks after the start of immunization, the rabbits were sacrificed, their blood serum collected and the total IGG antibodies were precipitated using sodium sulfate precipitation. The pellets were resuspended in 1×PBS and dialyzed to 1×PBS with decreased concentration of sodium sulfate. The reactivity of the obtained antibodies was tested against the recombinant proteins by Western blot analysis.

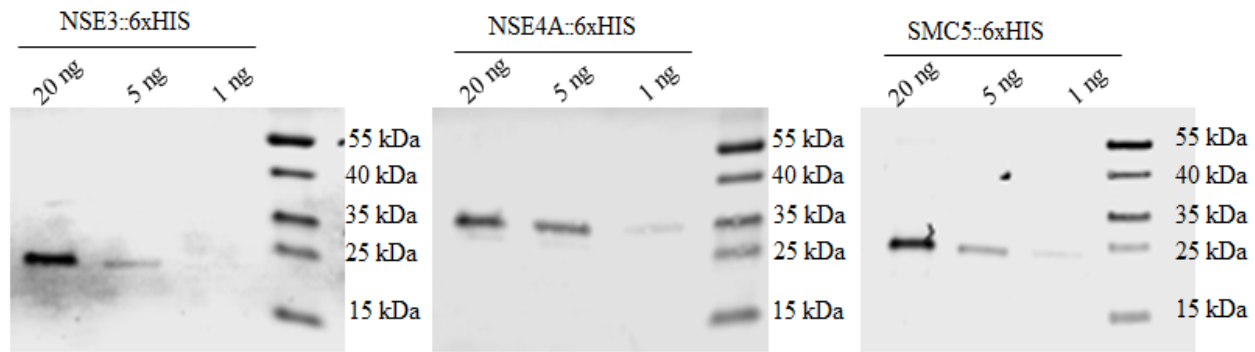


Figure 35 Western blot sensitivity test of the NSE3, NSE4A and SMC5 antibodies against different amounts (1 – 20 ng) of the recombinant proteins (NSE3::6xHIS, NSE4A::6xHIS, SMC5::6xHIS).

The obtained NSE4A and SMC5 antibodies displayed a high level of sensitivity against the recombinant proteins. The Western blot analysis showed signals for 20 ng, 5 ng and 1 ng of the tested NSE4A::6xHIS and SMC5::6xHIS antigens. Anti-NSE3 revealed a weaker sensitivity (Figure 35).

4.3.3 Generation of transgenic *A. thaliana* plants expressing SMC5/6 complex proteins containing a fluorescence tag

To investigate *in vivo* the subcellular localization of the SMC5/6 complex proteins NSE3, NSE4A, and SMC5 in *A. thaliana*, the generation of reporter constructs containing a fluorescent tag was performed. Two different reporter constructs with different types of promoters and reporters were cloned.

The strong Cauliflower Mosaic Virus (CaMV) 35S promoter (Odell et al., 1985) in combination with a C-terminal Enhanced Yellow Fluorescent Protein (EYFP) was used for the first type of a cDNA-based reporter vector. The genomic sequence of the *nse4A* gene under the control of an endogenous 1.7 kbp upstream region C-terminal fused with the Green Fluorescent Protein (GFP) was used for the second reporter construct. The structure of the reporter constructs is shown in Figure 36.

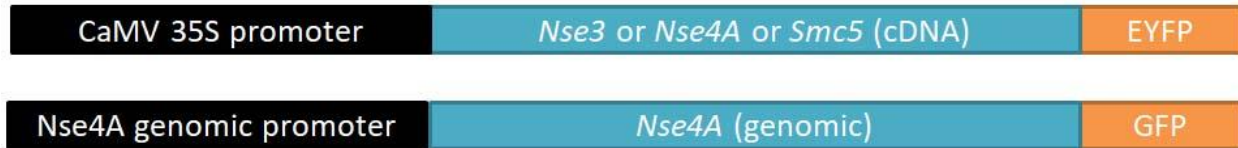


Figure 36 Structure of the *Nse3*, *Nse4A* and *Smc5* reporter constructs. Black boxes indicate the promoters, blue boxes the genes, orange boxes the fused fluorescent proteins.

The PCR amplified *Nse3*, *Nse4A* and *Smc5* genes were cloned into the vector pJET 1.2, transformed into *E. coli* DH5 α cells and sequenced. After sequence verification, the plasmid DNA were extracted from positively verified bacteria and enzymatically digested. The products of the restriction enzyme reaction were separated by agarose electrophoresis. The gene fragments were extracted from the gels and cloned into the vector pENTR A1 Gatewaytm. pENTR vectors with a desired gene of interest were used as a donor for a Gatewaytm recombination reaction. The recombination reaction was performed with the destination vectors pGWB504, pGWB604 (Nakagawa et al., 2007; Nakamura et al., 2010) Then, *E. coli* DH5 α were transformed with the destination vector constructs. The bacteria were screened by PCR for positive constructs. After verification, the vectors were isolated and tested in *N. benthamiana* leaves using a biolistic transient transformation method. Nuclear fluorescence signals were detected after 24 hours. The leaves were evaluated using a confocal microscope. An example of a cell showing NSE4A::GFP signals is shown in Figure 37.

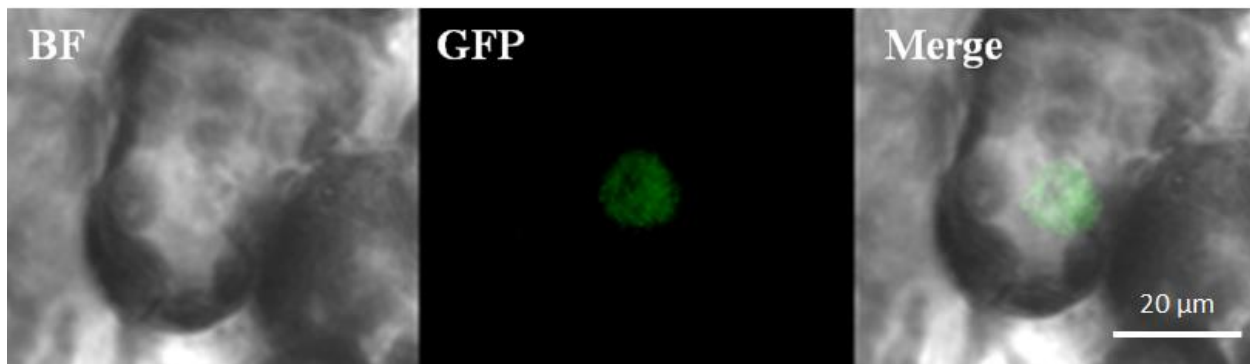


Figure 37 Nucleus of *N. benthamiana* showing NSE4A::GFP signals after transient biolistic transformation. BF - bright field illumination, GFP – Green Fluorescent Protein.

The *p*nse4A::gNse4A::GFP construct was present after biolistic transformation exclusively in *N. benthamiana* leaf cells. The 35S::Nse3::EYFP signals appeared in the nucleus and cytoplasm (Figure 38). The construct 35S::Smc5::YFP was not tested in *N. benthamiana*.

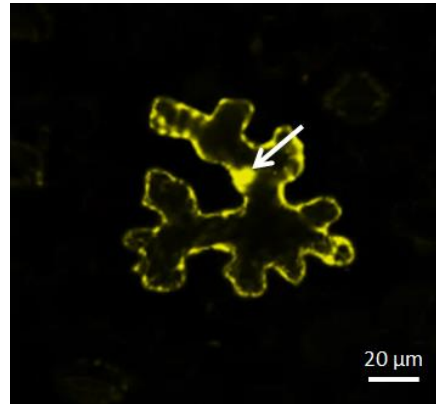


Figure 38 NSE3::EYFP signals are evident in the nucleus and cytoplasm (in yellow) after transient biolistic transformation of *N. benthamiana*. White arrow indicates the nucleus.

After verification of the constructs in *N. benthamiana*, *A. tumefaciens* containing the corresponding constructs were used to transform *A. thaliana*. T0 seeds were collected, sowed on selective medium and germinated (Figure 39).

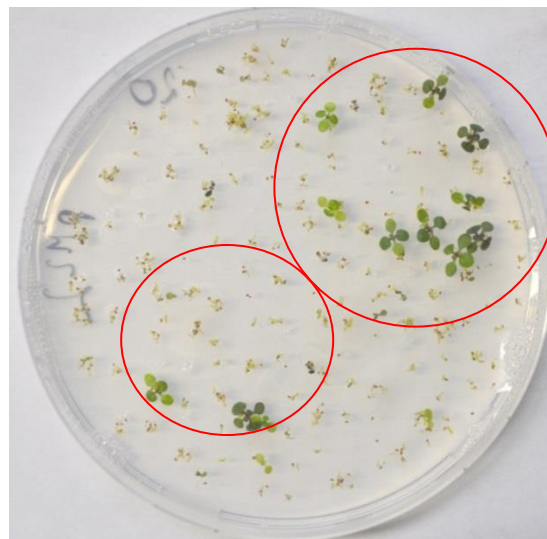


Figure 39 Selection of transgenic T0 *p*nse4A::gNse4A::GFP *A. thaliana* plants expressing BASTA resistance. Within the red circles resistant well developed green seedlings are visible.

After 10-days of selection on BASTA-containing medium, the transgenic *A. thaliana* seedlings were transferred into soil and grown under long-day conditions. For further positive verification, the plants were genotyped for the presence of the reporter constructs using PCR genotyping (Figure 40). The primers and amplicon size used in experiments listed in Table 17. The seeds of the verified transgenic plants were collected and used in further experiments.

Table 17 Primer pair used for the transgenic line genotyping.

Name of PCR product	Primers	Size of PCR product
SMC5	Smc5_Start_F – GFP (STOP)	3879 bp
NSE3	Nse3_Start_F – GFP (STOP)	1656 bp
NSE4A	Prom_Nse4A_F – GFP (STOP)	3832 bp
EYFP/GFP	GFP (START) – GFP (STOP)	720 bp

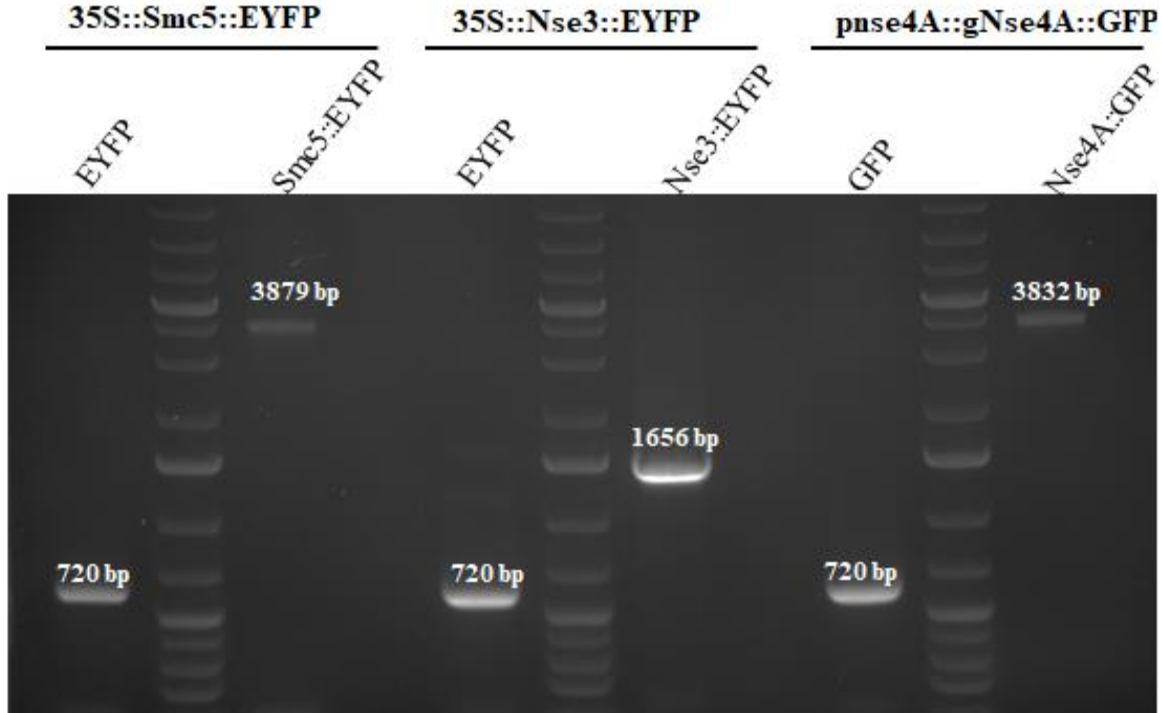


Figure 40 Genotyping of *A. thaliana* plants containing a Smc5::EYFP, Nse3::EYFP and Nse4A::GFP reporter constructs. Lanes indicate amplified gene fragment. Primers and amplicon size listed in Table 17. GeneRuler 1 kb Plus DNA Ladder used as a DNA size marker.

4.4 Localization of NSE4A in somatic cells of *A. thaliana*

4.4.1 NSE4A localizes exclusively within the euchromatin of interphase nuclei

To determine the subnuclear distribution of NSE4A, indirect immunolabeling was performed using the generated anti-NSE4A antibodies. NSE4A-signals were found exclusively within the euchromatin of somatic nuclei isolated from young flower buds (Figure 41 A) and in flow-sorted 8C leaf nuclei (Figure 41 C) of wild-type *A. thaliana*. NSE4A was not present in heterochromatin and within nucleoli. The euchromatin-specific enrichment of NSE4A was confirmed by super-resolution microscopy (SIM). A similar euchromatin-specific distribution was proven by anti-GFP immunolabeling of transgenic *pNSE4A::gNse4A::GFP* nuclei isolated from wild-type flower buds (Fig. 32B).

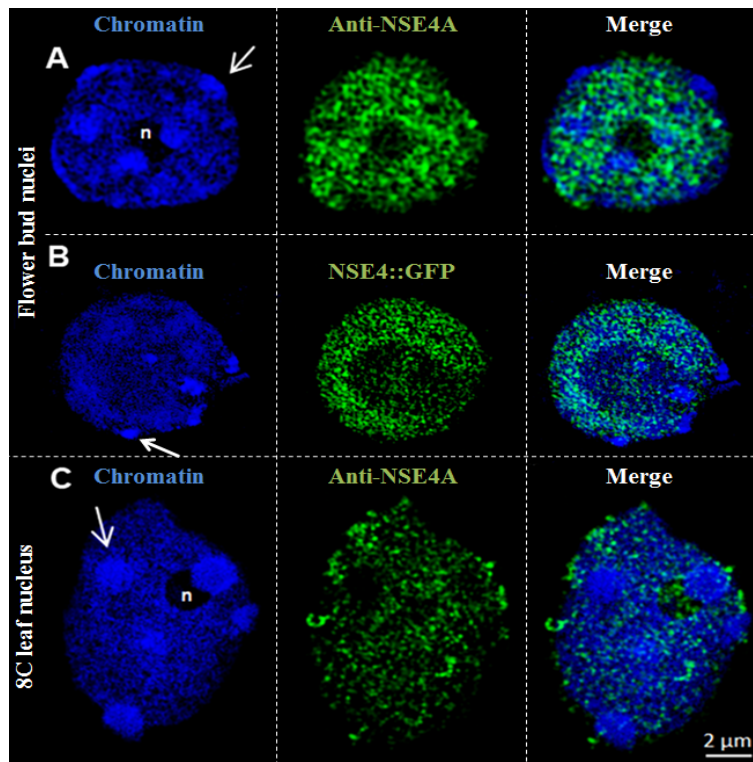


Figure 41 NSE4A localizes exclusively within the euchromatin of interphase nuclei of *A. thaliana* analyzed by super-resolution microscopy. (A, C) Distribution of NSE4A in somatic flower bud and 8C leaf interphase using the NSE4A antibody. (B) Distribution of NSE4A::GFP in somatic flower bud interphase nuclei using a GFP antibody. Both anti-NSE4A and NSE4A::GFP specific signals (in green) colocalize with euchromatin, but are absent from heterochromatin (DAPI-intense chromocenters, arrows) and nucleoli (n). The NSE4A labeling visible in the merged image of the 8C nucleus originates from optical slices outside of the nucleolus.

To investigate the localization of the other SMC5/6 subunits, immunolabeling using anti-NSE3 (Figure 42 A) and anti-SMC5 (Figure 42 B) was performed.

The anti-NSE3 signals antibody displayed a similar distribution pattern like NSE4A. Immunosignals were enriched in the euchromatin and less intense in nucleoli and heterochromatic chromocenters (Figure 42). On the other hand anti-SMC5 display euchromatin as well as heterochromatin labeling and signal reduction in nucleoli. The preferential localization of NSE4A, NSE3 and SMC5 suggests an accumulation of the SMC5/6 complex within chromatin in somatic cells nuclei.

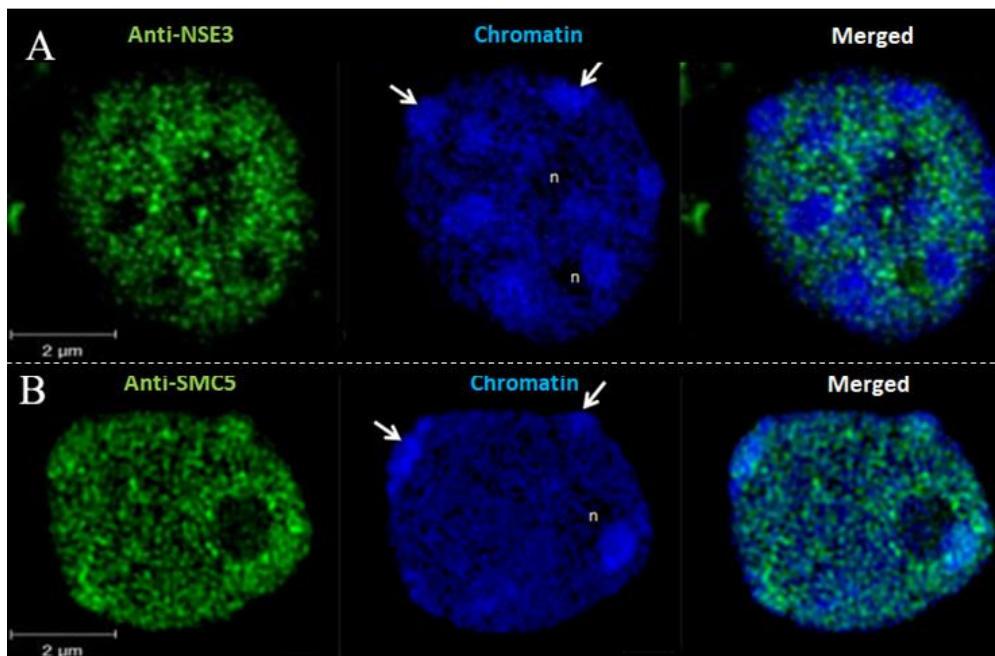


Figure 42 The localization of NSE3 and SMC5 in interphase nuclei. Distribution of NSE3 (**A**) and SMC5 (**B**) in somatic flower bud interphase nuclei of wild-type *A. thaliana* analyzed by super-resolution microscopy (SIM). The NSE3 signals are distributed within euchromatin, but were mainly absent in heterochromatic. The SMC5 display euchromatin as well as heterochromatin labeling with strong signal reduction in nucleoli. Arrows indicate heterochromatic chromocenters counterstained with DAPI and (n) indicate nucleoli.

4.4.2 NSE4A is absent from chromatin during mitosis

To investigate the dynamics and localization of the NSE4A protein during mitosis, live cell imaging of GFP signals derived from a genomic NSE4A reporter construct under the control of

the endogenous *Nse4A* promoter was performed. Signals were detected by confocal microscopy in living root meristems of wild-type *A. thaliana*.

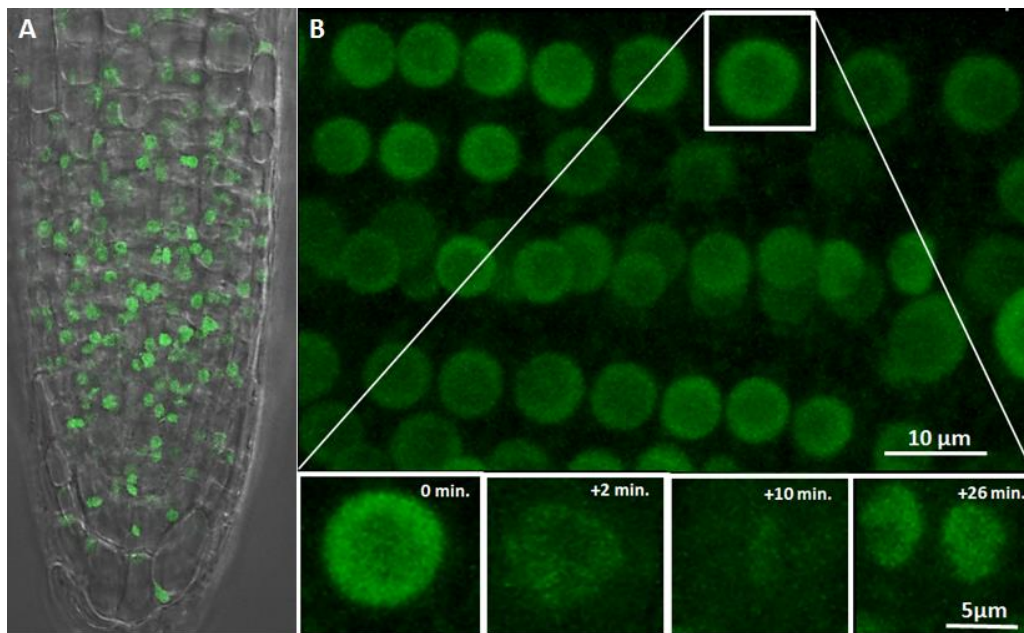


Figure 43 Dynamics of the NSE4A protein during mitosis in the root meristem of *A. thaliana*. GFP signals derived from a genomic construct of NSE4A under the control of the endogenous *Nse4A* promoter were detected by confocal microscopy. **(A)** Global view of an *A. thaliana* root expressing NSE4A::GFP. **(B)** Further enlarged cells undergoing mitosis (in the rectangle). Nuclear NSE4A::GFP signal is present in interphase (0min.), strongly reduced in mitosis (2-10min.) and recovered in telophase (+26min.).

The NSE4A::GFP signals were exclusively present within the chromatin of interphase nuclei of the root meristem cells (Figure 43 A). But the GFP signals became strongly reduced during mitosis (Figure 43 B). Nevertheless, very weak NSE4A::GFP signals remained still detectable during the cell divisions. The weak signals colocalized with the position of condensed chromatin from the entry of mitosis until telophase (Figure 44). The NSE4A-specific signals recovered after telophase during the formation of daughter nuclei.

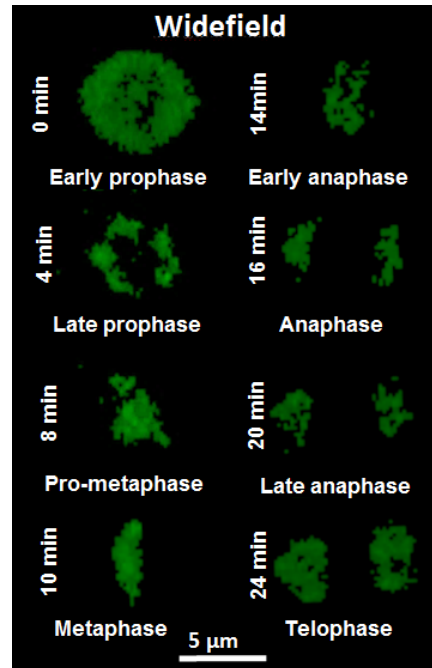


Figure 44 Maximum intensity projection of a meristematic cell of *A. thaliana* undergoing a mitotic division expressing NSE4A::GFP signals. Time progression is given in minutes.

To confirm the localization of NSE4A::GFP, immunolabeling on squashed meristematic root cells with an anti-GFP antibody was performed. Interphase nuclei revealed strong immunosignals (Figure 45 A), while mitotic chromosomes did not show NSE4::GFP signals (Figure 45 B).

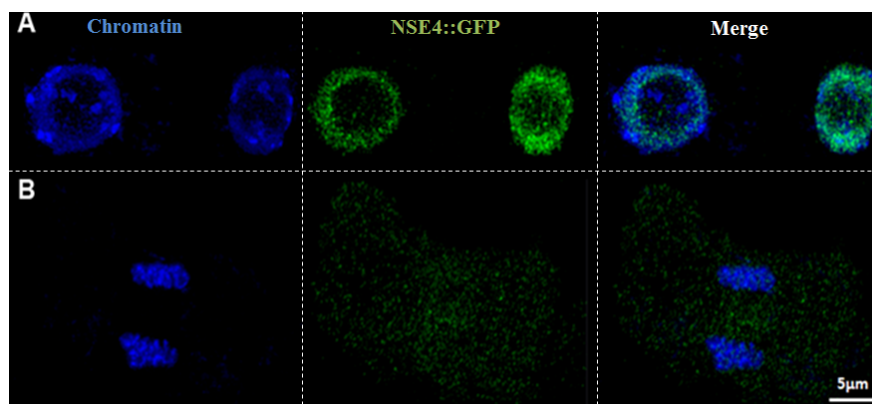


Figure 45 Detection of NSE4A::GFP signals after anti-GFP immunolabeling of mitotic cells of a transgenic *A. thaliana* plant. Cells were analyzed by super-resolution microscopy (SIM). (A) NSE4A::GFP signals (green) in somatic interphase cells colocalize with euchromatin (blue); (B) Mitotic metaphase cell without anti-GFP signals (green) at chromosomes (blue).

The immunolabeling of mitotic cells prepared from a transgenic *pns4A::gNse4A::GFP* plant with anti-GFP did not show the labeling of chromosomes. However, the live imaging of the same line demonstrated weak GFP signals at the mitotic chromosomes. This contradictory observations stimulated us to check the subcellular localization of the other SMC5/6 subunit – SMC5::EYFP.

Therefore, the localization of SMC5 was determined by confocal microscopy using an *35S::Smc5::EYFP* expressing *A. thaliana* plant.

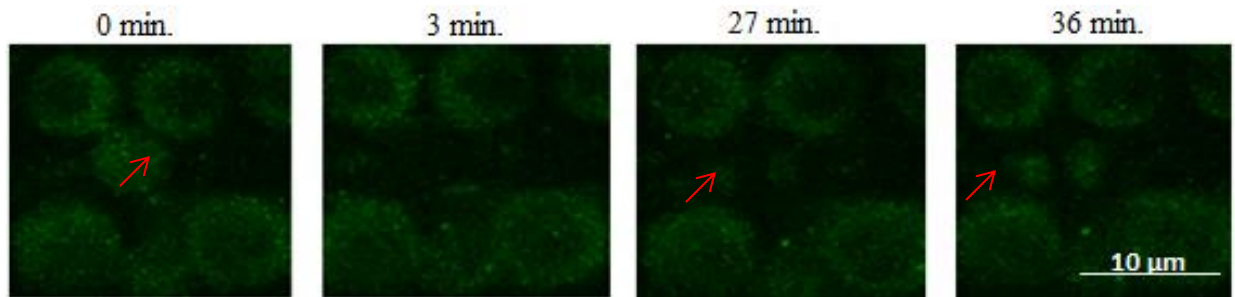


Figure 46 SMC5 is absent during mitosis in the root meristem of *A. thaliana*. A meristematic cell of a SMC5::EYFP transgenic *A. thaliana* plant undergoes a mitotic division (red arrows). Each subfigure represents another stage of mitosis. Time progression is given in minutes. 0 min – Interphase, 3min – mitosis, 27min – telophase, 36min – interphase.

The SMC5::GFP signals colocalized with the chromatin of nuclei in root meristematic cells. However, similar as NSE4A::GFP in the *pns4A::gNse4A::GFP* transgenic plants, the SMC5::EYFP signals were absent or strongly reduced from entry of mitosis until telophase, when the SMC5::EYFP signals recovered (Figure 46).

In short, based on the analysis of the reporter constructs we conclude that both NSE4A and SMC5 are present within the chromatin of meristematic interphase root nuclei. During mitosis both proteins are absent or, as in case of NSE4A, strongly reduced.

4.5 Localization of NSE4A in meiosis

4.5.1 NSE4 is present during prophase I in *A. thaliana* and *B. rapa*.

To investigate the localization and dynamics of the NSE4A protein in meiotic cells, immunolabeling of pollen mother cells of wild-type *A. thaliana* with anti-NSE4A antibodies was

performed. In addition, the localization of GFP signals was analyzed in transgenic plants expressing the genomic construct of NSE4A::GFP under the control of the endogenous *Nse4A* promoter.

Immunodetection of NSE4A resulted in a strong homogenous staining of the cytoplasm. In contrast, in the same cell, the antibodies specific for the synaptonemal complex protein ASY1 resulted in specific signals at pachytene (Figure 47). The strong immunostaining of the cytoplasm in *A. thaliana* meiocytes forced us to change the strategy for the evaluation of NSE4A localization during meiosis.

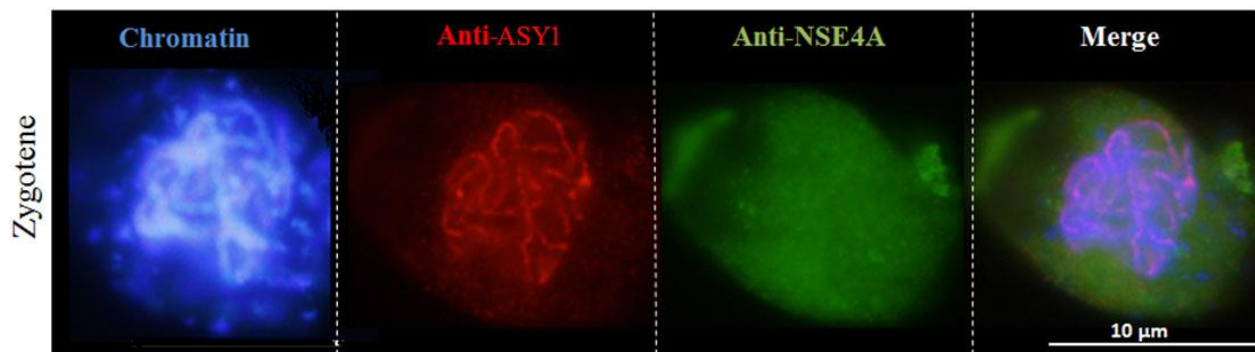


Figure 47 Immunolabeling of an *A. thaliana* cell at zygotene using anti-ASY1 (red) and anti-NSE4A (green) antibodies. Chromatin was counterstained by DAPI (blue).

***Brassica rapa* presents anti-NSE4A labeling in prophase I cells**

Pollen mother cells of *B. rapa*, a species, closely related to *Arabidopsis*, were used for the detection of NSE4A by indirect immunostaining. In parallel, the *A. thaliana* *nse4A::gNse4A::GFP* reporter line was chosen for further studies.

Protein BLAST analysis demonstrated the presence of two orthologues of NSE4A (XP_009147782 and XP_009144924) in *B. rapa*. The orthologues displays 99% coverage and 78% (XP_009147782) and 75% (XP_009144924) amino acid sequence identity (Figure 48).

```

NSE4A[Arabidopsis_thaliana] --MRKTVKRESEATGGKREADDEPEKLRSVKKEKQRKTEADSVRPDEPPPP---QEEEQG
XP_009147782[Brassica_rapa] MRRTRTVKRESEATSGGRDGEESA-RFRAVKK-EKNKGVASSVRIDEPPSQEAEEREQGG
XP_009144924[Brassica_rapa] MRMRRKVKRESEATGEGNG-----RRHVDES-AKKNKGVDDSVPIDEPPTQE----EDQG
          :.*****. .          : : :. :.*  .*  ***          :.**

NSE4A[Arabidopsis_thaliana] ISDRRILRSKYLSQLONEINDCKDDLMKIDSDKFSRIINAVENLHQQVRKPREQIADAEAL
XP_009147782[Brassica_rapa] VSDRRVLRSQLALINKISDSKDDLTVVSDKFSRIFNEFENLHQVKVQKPREQIADAEAF
XP_009144924[Brassica_rapa] ISDRRILRSQYLALIHKISHSKDDLTRVSDKFSRIFSEFENLHQVKVQKPREQVADAEAF
          :****:*:*:*:* :*:...*** :*****:..*****:*:*****:*****:

NSE4A[Arabidopsis_thaliana] LDIANITLMSVKSQSAGVSPAEFVNALISGFGQSLGIDTDETAQVSLKWKDLGFAVCS
XP_009147782[Brassica_rapa] LDIANITLMSVKSQSVNGVSPAEFVNALVNGFGQPSQRIIDTDESAPVSIKWKDLGLAVCS
XP_009144924[Brassica_rapa] LDIANITMSVKSHSANGVSPADFVNALVNGFGQASLG--VDETSFVSIKWKDLGLAVCS
          *****:*****:*:*****:*****:***** *          *:*: *:*:*****:*****

NSE4A[Arabidopsis_thaliana] TVLV-SCGCSTMLGPMDELKQKRKAPNRKRTKPGEGVRPDEVDSSQSEKIDTDKNMTI
XP_009147782[Brassica_rapa] TVLV-SCGCSTMLGPMDELKERKKAVYRKRTKPGEGVRPDEVDITQSEKIDTDKNMAI
XP_009144924[Brassica_rapa] TLFVSSFGCSTMLGPMSTELKERKRAVYRKRTKPGEGVRPEEVDITQSEKIDTDKNMAI
          *:* * *****.*****:*:* *****:*****:*****:*****:

NSE4A[Arabidopsis_thaliana] MFNIIKGGKRVQLLENLVLNRRSFAQTVENLFALSFLAKDGRVEIIVDKSGSHFAMPRNAP
XP_009147782[Brassica_rapa] MFNVLRQKKRVLENLVLNRRSFAQTVENLFALSFLSKDGRVEIIVDKNGSHFALPRNAP
XP_009144924[Brassica_rapa] MFNIIKGGKRVRLSMLNRRSFAQTVENLFALSFLVKDGRVEIIVDKTGSHFALPRNAP
          ***:* :****:*:*:*:*****:*****:*****:*****:*****:*****:*****

NSE4A[Arabidopsis_thaliana] DANVVMVSGEVIYNHFVFRFLDFKDWKLMSEMVPLGEEELMPHRQTAVASSSCPAAAPASAD
XP_009147782[Brassica_rapa] AANLVASGEVTYNHFVFRFDKDWKLMSEMVPMGEEELMPHRETAVASSSGPS-----D
XP_009144924[Brassica_rapa] AANLVMSGEVIYNHFVFRFDKDWKLMSEMVPMGEEELMPHREIAIASSSCP-----D
          **:* **** *****:*****:*****:*****:*****:***** * :

NSE4A[Arabidopsis_thaliana] FTQDTQTTPIRKLSRNRGLVVQEETVVEDTDPKEGDGTRRRCKRRLTS
XP_009147782[Brassica_rapa] FPQDSQTTPIRKLSRNRGLVVQEDTVVEDSPDVEGDGTRRRCKRRLT-
XP_009144924[Brassica_rapa] FPQDSQTTPIRKFSRNRGLVVQEDTVVEDSPDIEGDGTRKRCRRLA-
          * **:******:*****:*****:*****:* *****:*****:

```

Figure 48 Amino acids sequence alignment between NSE4A of *A. thaliana* and putative NSE4A orthologues (XP_009147782 and XP_009144924) of *B. rapa*. (*) identical amino acids, (: or .) similar amino acids, (-) missing amino acids. Alignment performed by Clustal Omega 2.1 (<https://www.ebi.ac.uk/Tools/msa/clustalo/>).

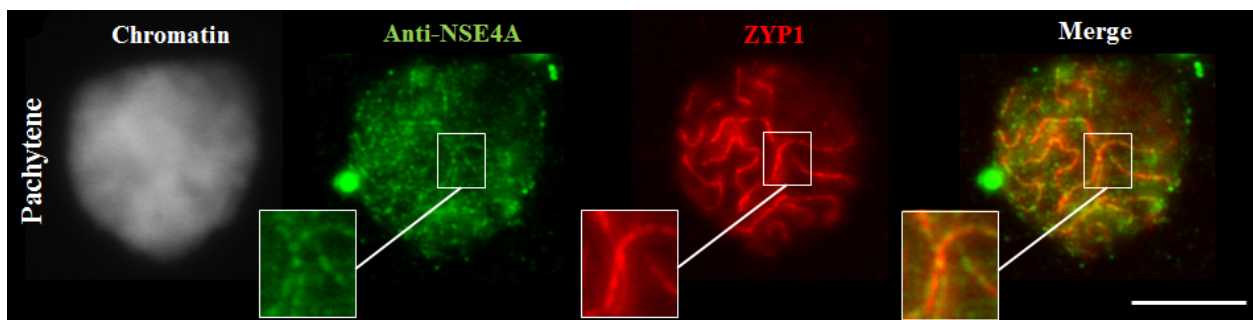


Figure 49 Immunolabelling of *B. rapa* prophase I meiocytes using anti-NSE4A (in green), the synaptonemal complex protein ZYP1 (red). The anti-NSE4A colocalizes to ZYP1 (in red) during pachytene. DNA counterstained by DAPI (blue). Bar 10µm.

The immunolocalization of NSE4A in *B. rapa* displayed ‘line-like’ fluorescence signals in cells undergoing prophase I. Furthermore, the dot-like NSE4A-signals showed the co-localization with the synaptonemal complex transverse filaments (ZYP1) (Figure 49).

4.5.2 NSE4A::GFP signals are present in meiocytes of *A. thaliana* undergoing prophase I, prophase II and tetrad formation

The high level of background staining using the NSE4A antibodies convinced us to change the strategy for the evaluation of the NSE4A proteins in meiotic cells of *A. thaliana*. To overcome the problem, we decided to use a *pNSE4A::gNSE4A::GFP* transgenic *A. thaliana* reporter line.

Therefore, flower buds were collected and screened for the presence of GFP signals in anthers (Figure 50 A). The chromatin and nucleolus of unfixed meiocytes displayed NSE4A::GFP signals in prophase I cells (Figure 50 B).

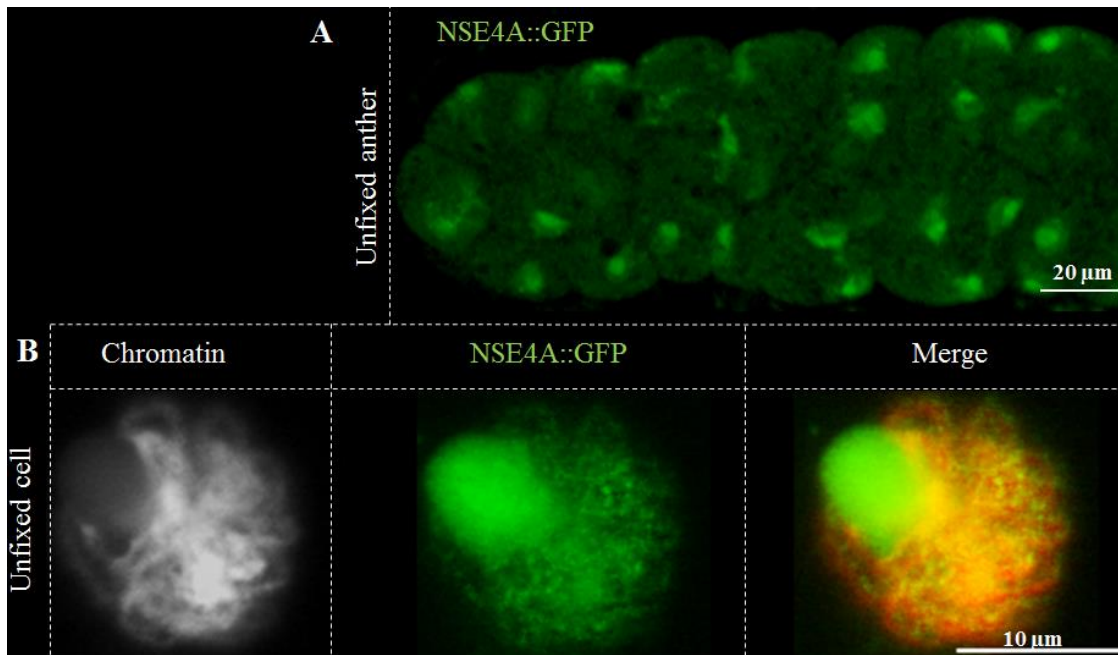


Figure 50 NSE4A::GFP signals are detectable in pollen mother cells of *pNSE4A::gNSE4A::GFP* transgenic *A. thaliana*. (A) Unfixed anther showing NSE4A::GFP signals (B) A prophase I cell shows chromatin linked ‘dot-like’ line GFP signals. Chromatin was counterstained with DAPI.

Pollen mother cells of NSE4A::GFP-signal-positive plants were selected for anti-GFP immunolabeling. NSE4A::GFP signals were visible in G2, leptotene, zygotene, pachytene, prophase II cells and tetrads. The GFP signals were very weak or undetectable on condensed metaphase I and anaphase I chromosomes but recovered at prophase II (Figure 51).

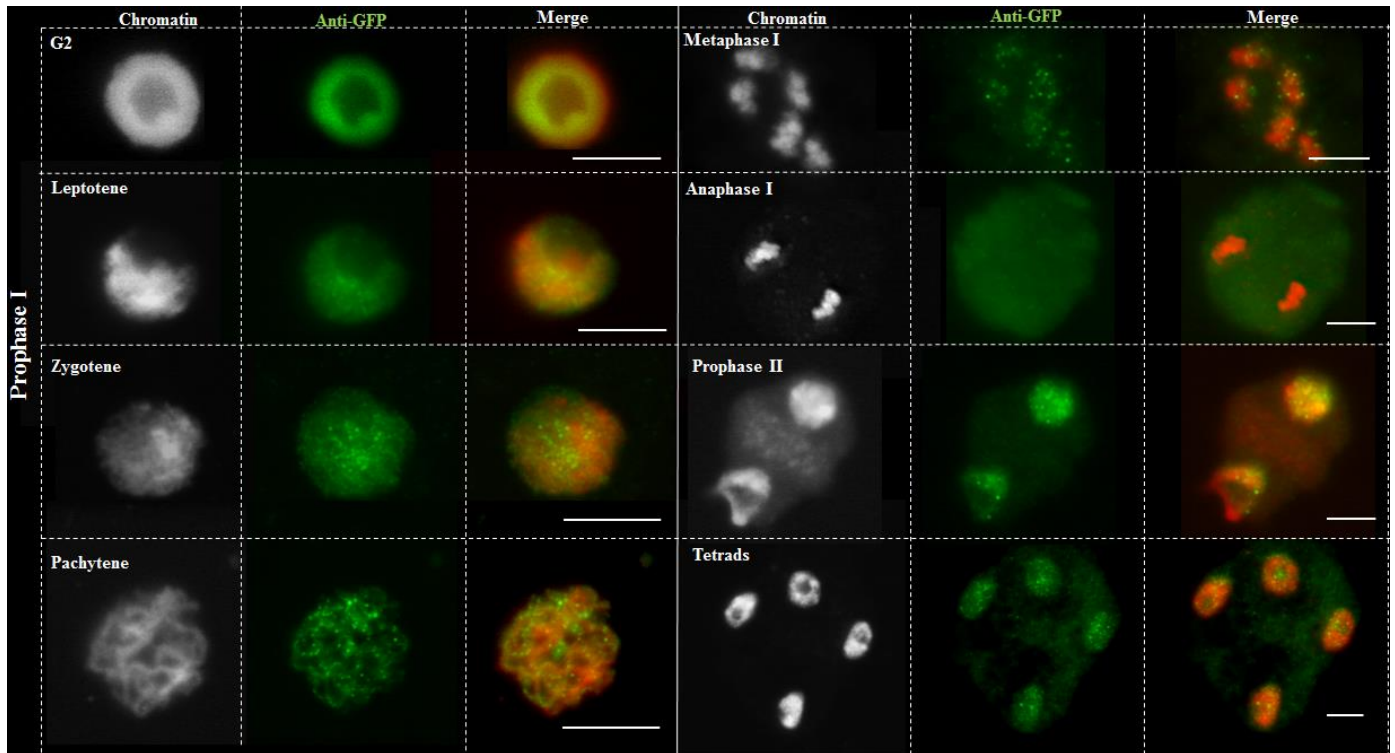


Figure 51 Dynamics and localization of NSE4A::GFP signals during meiosis of pnse4A::gNse4A::GFP transgenic *A. thaliana* plants. NSE4A::GFP signals are detectable in G2, leptotene, zygotene and pachytene cells. The signals are weak or not visible in condensed metaphase I and anaphase I chromosomes, but recover in prophase II and the tetrads stage. Gray color indicates chromatin counterstained with DAPI, green- anti-GFP. Bars = 10 μ m

In summary, the detection of NSE4A in wild-type and transgenic *A. thaliana* plants demonstrated a euchromatin-specific enrichment of NSE4A in somatic interphase nuclei. A similar distribution was found for NSE3 and SMC5. NSE4A is highly reduced or absent in somatic cells undergoing mitosis. In meiosis, NSE4A is enriched in the chromatin of G2 and leptotene cells, but reduced in the nucleolus. In zygotene and pachytene, NSE4A shows a ‘dot-like’ line colocalization with the chromatin. The synaptonemal complex proteins ZYP1 and ASY1 show a similar line-like distribution. At later stages of meiosis, in metaphase I and anaphase I, NSE4A becomes strongly reduced, but recovers at prophase II and the tetrad stage.

5. Discussion

5.1 *A. thaliana* encodes two *Nse4* variants

The results confirm that *A. thaliana* encodes two *Nse4* δ -kleisin-like variants homologous to known NSE4 proteins in non-plant organisms. Both variants contain a conserved NSE4-C terminal domain which is essential for the binding of NSE4 to SMC5, NSE1 and NSE3 (Palecek et al., 2006; Sergeant et al., 2005). Furthermore, they show 68% amino acids sequence similarity and an high intron-exon structure identity. *Nse4A* consists of 7 exons and 6 introns and *Nse4B* of 8 exons and 7 introns. The similarity of *Nse4* orthologues in plant and non-plant organisms is high (Table 7 and Figure 12) (Palecek et al., 2006). The presence of two *Nse4* gene variants exists also in other species.

The *A. thaliana* genome is a product of a large segment or even an entire genome duplication event which occurred during early evolution of this species (Simillion et al., 2002; Magadum et al., 2013). In this species the estimated frequency of gene duplications varies from 47% to 63% (Pachy et al., 2016). Most of the events occurred by whole-genome duplication, tandem duplication or retroposition of genes (Magadum et al., 2013). Genome duplication, together with rapid gene divergence, plays a fundamental role in gene evolution and the establishment of biological functions (Wang and Adams, 2015). Likely, both *A. thaliana* *Nse4* variants are the products of a gene duplication event which then underwent further evolution in the process of gene subfunctionalization (Force et al., 1999).

Gene duplication may result in multiple gene copy variants (Zmienko et al., 2014). Screening of *Nse4* orthologues in other plant species resulted in a number of putative copies (Figure 12). The analyzed plant species revealed diverse *Nse4* gene copy numbers, which varied from one in *Eucalyptus grandis* and *Cucumis sativus*. Up to three copies were found in diploid *Oryza sativa*. At least one *Nse4* gene of the investigated plant genomes is most similar to the *A. thaliana* *Nse4A* variant. Nevertheless, *Brachypodium distachyon* (monocot) and *Camelina sativa* (eudicot) have also a *Nse4B* orthologue, in addition to *Nse4A*. The dominant presence of *Nse4A* orthologues in other plant genomes suggests that *Nse4A* is an essential gene for plants.

Obviously, *Nse4A* is more important than *Nse4B*, as *Nse4B* orthologues were found only in few species.

5.2 The specializations of the *Nse4* genes

In *A. thaliana*, both *Nse4* genes display a similar sequence and gene structure, but different expression profiles based on our quantitative real-time PCR and *in silico* analysis. Both experiments demonstrated that *Nse4A* is expressed globally, across different tissue types and developmental stages. In contrast the expression of *Nse4B* is almost undetectable and limited to embryo and endosperm tissues. The endosperm and embryo restricted expression of *Nse4B* may indicate a functions of this gene during embryogenesis.

The different expression patterns of *Nse4A* and *Nse4B* may indicate gene specialization. The question of what determinates this specialization can be answered using a duplication-degradation-complementation model (DDC) (Stoltzfus, 1999; Force et al., 1999) (Figure 52). This model assumes that ancestor gene copies retain the ancestral gene function after the whole genome has been duplicated. However, over time the gene function might change due to accumulation of mutations or even becomes non-essential and undergoes elimination. As a result, one or both copies of the gene preserves the ancestral gene function in particular tissues or cell types (De Smet and Van de Peer, 2012; Feder, 2007).

The *Nse4A* homologue was found in all investigated plant genomes and is expressed widely in the different tissues of *A. thaliana*. The *Nse4B* homologue in contrast exist in few plant species only, and is expressed exclusively in the embryo and endosperm tissues. The different activity of *Nse4B* compared to *Nse4A* indicates that *Nse4B* seems to be as a paralogue. The data suggest that *Nse4A* kept all ancestral gene functions or underwent subfunctionalization, keeping only the ancestors gene function required for cells in most tissue types (Figure 52 A). On the other hand, *Nse4B* seems to be a result of subfunctionalization and it kept the ancestral gene function in embryonic and endosperm tissues only (Figure 52 B).

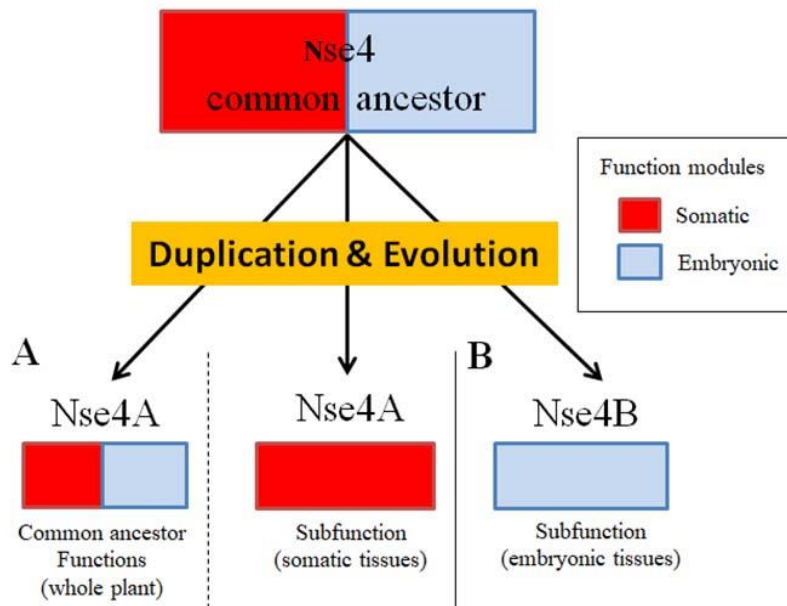


Figure 52 The origin of *Nse4* variants in *A. thaliana* explained by the duplication-degradation-complementation model according to Force et al. (1999) and Feder (2007). The *Nse4* common ancestor gene possess two functional modules, required for somatic and embryonic tissue; gene undergoes duplication and gene evolution, in effect two *Nse4* variants were formed *Nse4A* and *Nse4B*. **(A)** *Nse4A* may kept an ancestor gene function (required in different cell types) or underwent subfunctionalization (required for somatic cells), whereas **(B)** *Nse4B* gene kept only part of ancestor gene function required for embryonic tissue. The color boxes indicate gene function modules essential in: red –somatic tissue, blue- embryonic tissue. (Adapted from Feder, 2007).

Interestingly, in other plant and non-plant organisms, the expression patterns between two *Nse4* variants also differ, and a gene subfunctionalization event is suggested. In *Z. mays*, two *Nse4* homologues exist - GRMZM2G056867 and GRMZM2G026802. GRMZM2G056867 is expressed at high level and across different tissue types, whereas the GRMZM2G026802 homologue is overexpressed in embryo and seeds tissues and only weak or not expressed in other tissue types. The human genome encodes also two *Nse4* gene variants called *Hnsmc4A* and *Hnsmc4B* which are ~50% identical (Taylor et al., 2008). *Hnsmc4A*, like *A. thaliana Nse4A* is expressed globally in different tissue types, whereas *Hnsmc4B* is expressed exclusively in generative tissue (Bavner et al., 2005).

5.3 *Nse4A* gene inactivation is lethal for *A. thaliana*

The characterization of *A. thaliana nse4* T-DNA mutants supports the existence of functional differences between *Nse4A* and *Nse4B*. This is because it was not possible to select homozygous plants of the *nse4A* T-DNA insertion lines SALK_057130 and SAIL_71_A08. Therefore, we

assume that the inactivation of the *Nse4A* gene is lethal. Instead, for the T-DNA mutant line GK-768H08, which has the T-DNA insertion located in the last exon of the *Nse4A* gene, homozygous individuals could be obtained. Homozygotes of the line GK-768H08 are viable, but the transcript analysis showed a gene truncation (Figure 18). The T-DNA insertion causes a *Nse4A* translation product disturbance caused by a changed amino acid sequence (“non-sense” insertion). Furthermore, no stop codon is present in the truncated *Nse4A* gene. The insertion of the T-DNA is located behind the conserved NSE4-C terminal domain which is essential for the interaction between SMC5 and NSE1 in non-plant organisms (Pebernard et al., 2004). It might influence the protein conformation, and therefore effect the function and stability of NSE4A.

The complete inactivation of the *Nse4A* gene causes plant lethality. This indicates that *Nse4A* is essential during the plant growth in somatic tissues. The Alexander staining-based pollen analysis of heterozygous plants of line SALK_057130 did not reveal a reduced pollen quality and number after Alexander staining, suggesting that the process of male embryogenesis is affected. Evidence to support this conclusion can be found in non-plant organisms. The knock-out of *Smc5* and *Smc6* genes resulted in an abnormal early embryogenesis in the fruit fly (*Drosophila melanogaster*) (Tran et al., 2016), and embryonic lethality in the house mouse (*Mus musculus*) (Ju et al., 2013). In *A. thaliana*, the mutations in *Nse1*, *Nse3* (Tzafrir et al., 2004, Li et al., 2017) and *Nse2* (Xu et al., 2013), similar as in non-plant organisms, also induced an impaired early embryo development. Hence, we assume that the mutation of *Nse4A*, similar as *Nse1*, *Nse2* and *Nse3* mutations cause embryogenesis defects. Interestingly, the lethality was observed in homozygous SALK_057130 and SAIL_71_A08 *nse4A*, but not in SAIL_296_F02 and GK-175D11 *nse4B* mutants. The *nse4B* mutants were viable and did not display an impaired development as *nse4A* mutants.

5.4 Does the impaired mitosis cause plant developmental defects?

The analysis of the hetero- and homozygous *nse4A* mutants SALK_057130 and GK-768H08, respectively, showed mitotic defects such as anaphase bridges and lagging chromosomes. In SALK_057130 this may be caused the reduced expression of *Nse4A* because only one of both alleles is functional. In GK-768H08 the mitotic defects could be triggered by the truncation of

the *Nse4A* gene. The complementation of the mutation in GK-768H08 by the genomic *Nse4A* gene partially recovered the mitotic defects.

The increased number of mitotic defects in the *nse4A* mutants seem to correlate with the impaired development of the *nse4* mutants. Our phenotypic analysis of the mutants showed that plants with few mitotic defects like SALK_057130 display no obvious reduced plant growth. On the other hand, the mutant GK-768H08 and the double mutant GK-768H08/SAIL_296_F02, displayed high level of mitotic defects, show clearly a reduced plant size (Figure 22, 23).

Why does the mutation of *Nse4A* cause mitotic division problems?

The mitotic defects of *nse4A* mutants show mitotic defects might be explained by the fact that NSE4 is a major element of the SMC5/6 ring, which is essential for the proper function of this complex. Lack or truncation of this protein may result in an incorrect complex assembly, and consequently impaired catalytic (Figure 53) and/or topological function (Figure 54) (Verver et al., 2016; Diaz and Pecinka, 2018).

5.5 Catalytic role of the SMC5/6 complex in somatic cells

The SMC5/6 complex is one of the SMC family members having a catalytic activity. The catalytic activity is provided by the E3 SUMO-protein ligase NSE2 (Fernandez-Capetillo, 2014). In non-plant organisms this catalytic activity is essential for DNA repair and resolving double Holliday junction intermediates (Xaver et al., 2013; Bermúdez-López, 2010; Copsey, 2013; Bermundez-Lopez et al., 2016). Double strand breaks induce the activation of the SMC5/6 complex by auto SUMOylation, and thus activates the SUMOylates SGS1-TOP3-RMI (STR) complex. The STR complex is engaged in proper double strand break repair by homologous recombination (Figure 53) (Manthei and Keck, 2013; Bermúdez-López and Aragon, 2017).

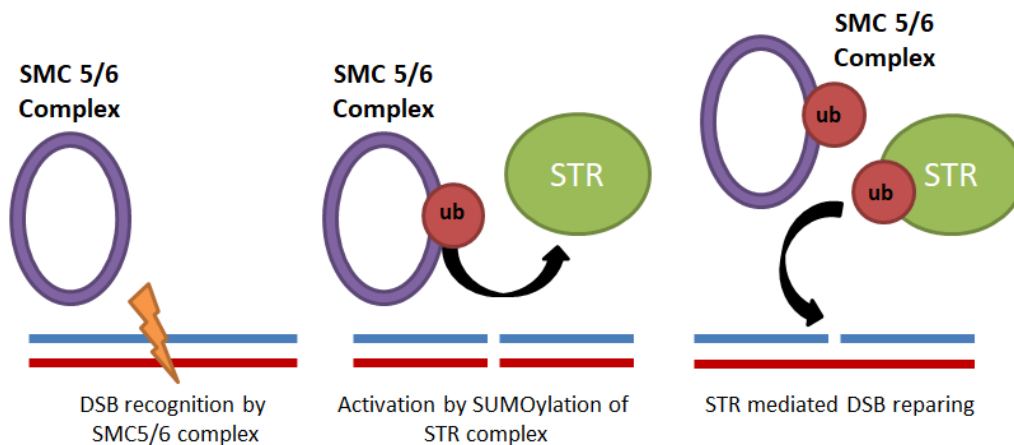


Figure 53 Putative catalytic function of the SMC5/6 complex in somatic cells. SMC5/6 catalytically mediated DSB repair by SUMOylation of the SGS1-TOP3-RMI (STR) complex. SMC5/6 recognize DSB and respond in auto SUMOylation, next activated SMC5/6 complex SUMOylate STR complex. Activated STR repair DSB. Adapted from Bermúdez-López et al. (2010).

In *A. thaliana*, a similar mechanism may exist due to the presence of the yeast STR complex orthologue called RTR (AtRECQ4A-TOP3A-AtRMI). The RTR complex is responsible for genome stability (Knoll et al., 2014). Loss of *AtRecq4A*, *AtTop3A* or *AtRmi* function results in hypersensitivity to DNA damaging agents and elevated homologous recombination (Bagherieh-Najjar et al., 2005; Hartung et al., 2007). Similar phenotypes were observed for the SMC5/6 mutants *smc6A*, *smc6B* (Watanabe et al., 2009; Hanin et al., 2000) *nse1*, *nse3* (Li et al., 2017) and *nse2* (Yuan et al., 2014; Xu et al., 2013). This suggests an engagement of these two *A. thaliana* complexes in the same DNA repair pathway.

The impaired mitotic behavior of *nse4A* mutants may be caused by unresolved DSB repair intermediates which results in mitotic anaphase bridges. However, it cannot be excluded that the SMC5/6 complex is involved in the topological organization of chromatin during mitotic condensation and decondensation.

5.6 Topological role of the SMC5/6 complex in somatic cells

Another explanation why the disturbance of the *Nse4A* gene results in mitotic defects could be answered by the topological - DNA embracing function. Similar to other SMC proteins, the SMC5/6 complex, is an ATP-dependent intermolecular DNA linker (Kanno et al., 2015). In non-plant organisms, genomic stability and DNA replication requires a functional SMC5/6 complex

(Bermúdez-López et al., 2010). The down regulation of the SMC5/6 complex components triggers the increase of replication toxic structures, such as supercoiling of DNA or sister chromatids intertwining (SCI) (Figure 54). They appear during DNA synthesis in interphase and may induce chromatin bridges during mitotic anaphase (Jeppsson et al., 2014; Diaz and Pecinka, 2018).

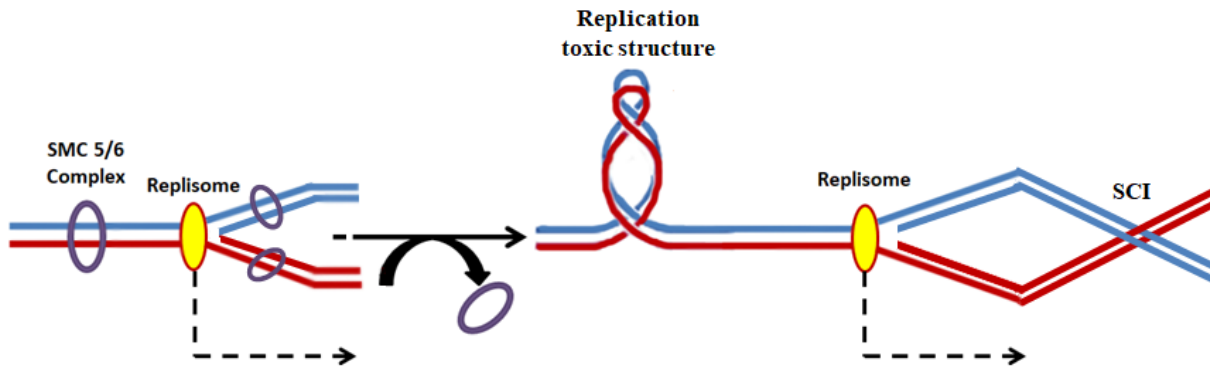


Figure 54 Putative topological function of the SMC5/6 complex in DNA synthesis and post-synthesis process. SMC5/6 is essential in DNA replication by preventing the formation of replication toxic molecules and sister chromatids intertwining (SCI) (adapted from Jeppsson et al., 2014; Diaz and Pecinka, 2018)

A similar phenotype was observed in our *nse4A* mutants, and it may be caused by similar mechanisms. In addition, our live imaging and immunolocalization experiments confirmed the localization of NSE4A proteins in interphase nuclei of somatic *A. thaliana* cells (Figure 41).

5.7 In somatic cells NSE4A is localized within euchromatin.

Live imaging of fluorescence marker tagged NSE4A and SMC5 proteins in meristematic *A. thaliana* root cells shows both proteins in interphase nuclei (Figure 43, 46). Interestingly, the interphase signals were also detectable for NSE4A and NSE3, after the transient transformation of *N. benthamiana* leaf tissues (Figure 38). Other authors observed similar results. The genomic NSE1 and NSE3 constructs show nuclear localization in *A. thaliana* embryo tissue and *N. benthamiana* leaf cells (Liu et al., 2017). The similar distribution of SMC5/6 components suggests their action in a complex.

Our super-resolution microscopy analysis using antibodies against NSE3, and NSE4A showed an euchromatin-specific labeling of somatic interphase nuclei. Signals were absent or weaker in

nucleoli and the heterochromatic chromocenters (Figure 41). Interestingly, other SMC complexes subunits from cohesins and condensins also displayed an euchromatin localization in *A. thaliana*. The cohesin subunit SMC3 and the condensing subunit CAP-D3 localized exclusively in the euchromatin of sorted leaf nuclei (Schubert et al., 2013), which may suggest a similar role of these complexes in interphase nuclei.

Why do the SMC5/6 subunits localize in euchromatin?

The reason why the SMC5, NSE4A and NSE3 SMC5/6 complex subunits localize preferentially within euchromatin could be related to their function in maintaining a topological chromatin organization. The similar composition and structure of the SMC5/6 complex compared to cohesin and condensin suggests that all SMC complexes may share a similar topological distribution in interphase chromatin. In interphase nuclei, SMC complexes interact with DNA, organize chromatin into a higher order and are responsible for the dynamics of chromatin (Carter and Sjögren, 2012). This topological distribution may contribute to organize chromatin into a transcriptional active form (euchromatin), making chromatin easily accessible for RNA polymerase II and influence the gene transcription. (Schubert and Weissart, 2015). The SMC5/6 complex similar like other SMC complexes can bind to DNA and may help structurally to organize a euchromatin in interphase nuclei (Alt et al., 2017). However, live imaging of NSE4A::GFP signals shows an uniform labeling of interphase nuclei but also reduced labeling of chromosomes during mitosis.

5.8 NSE4A is removed from chromatin during mitosis

The analysis of NSE4A::GFP expressing *A. thaliana* plants revealed an almost uniform labeling of somatic nuclei and a strong reduction of NSE4A::GFP chromatin-located signals during mitosis.

During mitosis, NSE4A::GFP signals were mainly found in the cytoplasm. In addition immunostaining with GFP-specific antibodies using the same transgenic line did not reveal a strong mitotic chromosome labeling from prophase until late anaphase (Figure 43). The strong chromatin signals recovered at telophase, together with the formation of new daughter cells. However weak signals on mitotic chromosomes were occasionally detected. Based on these

observations we developed a model showing the dynamics of NSE4A during the somatic cell cycle (Figure 55).

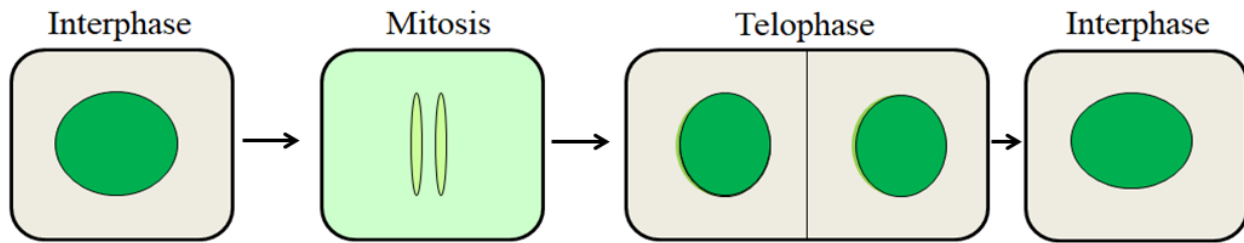


Figure 55 Dynamics of NSE4A during mitosis. At interphase NSE4A is present within chromatin. At the entry of mitosis NSE4A becomes released into cytoplasm. The chromosomes contain no or very low amount of NSE4A. At telophase the protein becomes loaded again on chromatin and is evident within euchromatin again in interphase

A similar dynamics was observed for 35S::Smc5::EYFP transgenic plants. The SMC5::EYFP signals were present in interphase nuclei and strongly reduced during mitosis.

Until now no published data exist about the dynamics of the SMC5/6 complexes during the somatic cell cycle in plants. In non-plant organisms, the localization of SMC5/6 is contradictory. In human, SMC5::GFP signals are present in interphase nuclei. SMC5 dissociates from chromosomes at mitosis and colocalizes then again with chromatin at G1 phase, a weak cytoplasmic staining was detected in mitotic cells (Gallego-Paeza et al., 2014). On the other hand, in mice SMC6 colocalized with heterochromatic centromere regions in interphase as well as in mitosis. Additional chromosome regions were also labeled (Gomez et al., 2013). The different dynamics of SMC5/6 complex components in yeast, plants and animals might be explained by different genome organization and the different methods used for analysis.

The mitotic localization of the other SMC complexes in *A. thaliana* is deviating. In contrast to the SMC5/6 complex subunits, strong cohesin and condensin-specific signals were found during mitosis (Bolaños-Villegas et al., 2017; Smith et al., 2014). The cohesin subunit SMC3 was detected at the centromeres of somatic meta- and anaphase chromosomes of *A. thaliana* (V. Schubert, unpublished). The condensin I subunit CAP-D2 shows a labeling of mitotic chromosomes with enriched signals at the centromeres (Municio et al., in prep.). The differences of localization between SMC complexes may indicate their different functions during mitosis. The function of cohesin is related to sister chromatid cohesion (Bolaños-Villegas et al., 2017)

and condensins are required to ensure normal chromosome morphogenesis and condensation (Smith et al., 2014). Our study points to the accumulation of NSE3, NSE4A and SMC5 within euchromatin of interphase nuclei. A similar distribution was found for other SMC complexes subunits such as CAP-D3 (condensin) and SMC3 (cohesin) (Schubert et al., 2013). On the other hand, live cell imaging of NSE4A::GFP and SMC5::EYFP reporters showed a strong reduction or absence of chromosomal signals during mitosis. The observed mitotic abnormalities of *A. thaliana nse4A* mutants might correlate with a function of NSE4 in DSB repair, homologous recombination and/or topological organization of euchromatic DNA during interphase. The reduction of NSE4A signals during mitosis may be explained by the replacement SMC5/6 complex components (especially required in euchromatin) by condensin and cohesin. Mitotically released SMC5/6 might be engaged in SUMO NSE2 mediated signaling pathway in the cytoplasm, which is crucial in regulating the mitotic cycle in plant and non-plant organisms (Xu et al., 2013; Park et al., 2011; Mukhopadhyay and Dasso, 2017).

5.9 *Nse4* is essential for proper male meiosis, fertility and seed development.

Our analysis of T-DNA mutants demonstrated that the disturbance of *Nse4A* and *Nse4B* results in anaphase bridges, lagging chromosomes and/or chromosome fragmentation in meiosis (Table 14). This phenotype is stronger in *Nse4A* than *Nse4B*, however double homozygote *nse4A/nse4B* mutants displayed a stronger meiotic disturbance than single mutations. Chromosome fragments could not be assigned to particular chromosomes and represent mainly distal chromosome fragments, leading to micronuclei formation (Figure 29). However, the high number of meiotic abnormalities does not influence the number of chiasmata in GK-768H08. The complementation of *nse4A* GK-768H08 T-DNA mutants by the wild type genomic *Nse4A* gene results in a reduced number of meiotic abnormalities.

Relationship between disturbed meiosis and a decreased number of pollen and seeds

The frequency of meiotic abnormalities correlate with a decreased number of viable pollen and seeds in *nse4* mutants (Table 14). A decreased seed number was previously observed also for other SMC5/6 T-DNA insertion lines, like *nse1*, *nse3* (Li et al., 2017) *nse2* (Ishida et al., 2012) and *smc6B* (Watanabe et al., 2009; Hanin et al., 2000).

The question what causes a decreased fertility in *SMC5/6* mutants might be answered by the meiotic defects in the *nse4* mutants. Our results showed a correlation between meiotic abnormalities and the reduced number of viable seeds in the *nse4* T-DNA insertion lines GK-175D11, SALK-057130, GK-768H08, GK-768H08/SAIL_296_F02 (Table 14). The meiotic abnormalities may result in non-functional meiotic products, like aborted or abnormal pollen. Fertilization of egg cells with abnormal pollen may result in lethal embryos, which in turn result in shriveled seeds (Figure 56).

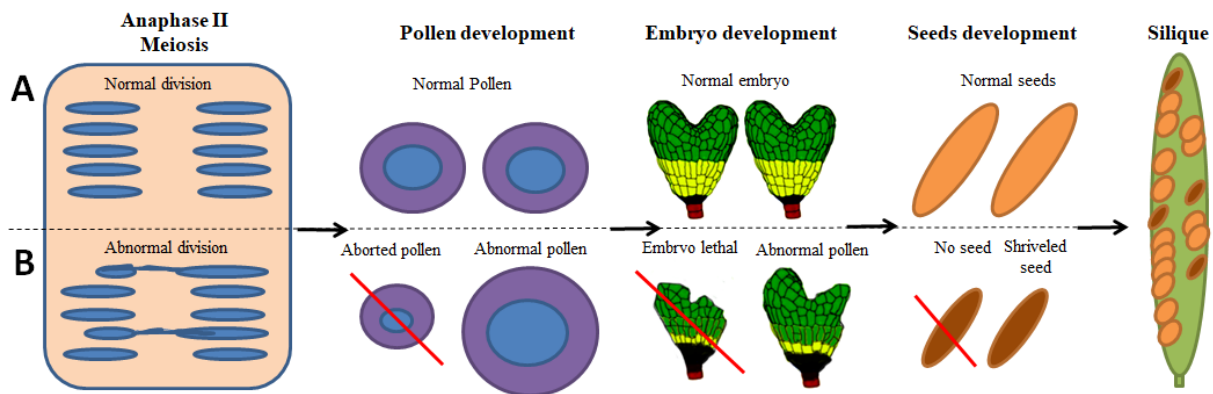


Figure 56 Model of meiosis, pollen, embryo and seeds development in *nse4* mutants. (A) The *nse4* mutant is partially able to produce viable pollen, fertilize the egg and produce viable seeds. (B) On the other hand, the *nse4* mutants display impaired meiosis and fertility, such as unequal division and chromosome damage. This damage results in pollen abortion or abnormal pollen. Abnormal pollen has an unbalanced genetic content, which after fertilization causes embryo lethality and disturbance of seeds formation.

We found that the *nse4A* mutant shows a decreased pollen and seed number and an increased number of abnormal seeds (Figure 24) as a putative outcome of a disturbed meiosis.

Embryo defects and a decreased number of pollen grains, seeds were observed also in other *A. thaliana* *SMC5/6* mutants. *nse1* and *nse3* mutations cause a disordered embryo development leading to seed abortion and lethality (McElver et al., 2001; Li et al., 2017; Watanabe et al., 2009). The authors of these investigations explained the observed embryo phenotypes by a hypersensitivity of these mutants to double strand breaks and mitotic disturbances (Li et al., 2017). However, the meiotic process of these mutants was not investigated. The mutation of *Nse2* causes a similar meiosis and fertility phenotype like *nse4A*. Furthermore, these mutants displayed a reduced pollen number together with a decreased frequency of pollen germination and growth (Liu et al., 2014). This observation supports the hypothesis about the correlation between abnormal meiosis and reduced pollen and seed number.

5.10 Is SMC5/6 essential for homologous recombination intermediates?

What causes the meiotic abnormalities observed in the *nse4* mutants? The prophase I of *A. thaliana* wild type plants and *nse4* mutants does not differ. At metaphase I, anaphase I and II the *nse4* mutants show an aberrant chromosome division, likely due to unresolved recombination intermediates between chromosomes. The agglutination of the homologues creates a tension between the chromosomes at anaphase and results in chromosome fragmentation. One explanation might be the disturbed SMC5/6 complex function in the pathway of homologous recombination.

Recent studies in plant and non-plant species demonstrate a function of the SMC5/6 complex in homologous recombination. This type of genetic recombination is engaged in DNA repair and meiotic crossing-over (Verver et al., 2016; Bermúdez-López and Aragon, 2017). Non-plant studies showed that homologous recombination requires functional *Nse2*, which is a component of the SMC5/6 complex dependent on the SGS1-TOP3-RMI1 (STR) complex activation (Bonner et al., 2016). Down-regulation of *Sgs1* and *Smc5/6* genes gives the same phenotype, as the accumulation of unresolved replication-dependent Holliday junctions and additionally increased homologous recombination (Bermúdez-López and Aragon, 2017). In yeast, SMC5/6 accumulates at cohesin binding sites and at double strand break. The deletion of *Nse4* and *Smc6* results in meiotic inter-sister and inter-homologous joined molecules (Copsey et al., 2013).

Anaphase I and II fragmentation

The characterization of *A. thaliana nse4* mutants showed that NSE4 protein is essential for the proper segregation of meiotic chromosomes. Problems might be caused by unresolved double Holliday junction intermediates, or by a disturbed cohesin dynamics, which may result in joint molecules. Then, the tension induced by attached microtubules at centromeres may cause anaphase bridges and chromosome fragments in anaphase I and II.

Metaphase I fragmentation

The mechanism of chromosome fragmentation at metaphase I cannot be explained by unresolved dHJ intermediates exclusively. A further explanation could be the participation of NSE4A in the SPO11 and meiotic recombination pathway. SPO11 is a highly conserved topoisomerase responsible for meiotic DSB formation (Hartung et al., 2007). The DSB produces 5' to 3' strand breaks which might be processed in two ways of DNA repair, forming either crossover or non-crossover products (Pawlowski and Cande, 2005). Disturbed meiotic DSB repair may result in chromosome fragments during metaphase. Similar chromosome fragmentation phenotypes have been observed in *A. thaliana* and *Z. mays* plants where proteins engaged in meiotic DSB repairing pathway, such as DMC1 and RAD51 were down-regulated (Da Ines et al., 2013; Li et al., 2004; 2007).

The *nse4A* T-DNA mutants do not show an altered chiasmata frequency compared to wild-type plants (Table 15). Hence, the engagement of the NSE4A in the formation of crossovers is less likely. On the other hand, chromosome fragmentation in *nse4* mutants occurs in the distal parts of chromosome. In *A. thaliana* and other plant species, crossover frequency in the distal parts of the chromosomes (Lambing et al., 2017; Giraut et al., 2007; Dreissig et al., 2013), which can induce the fragmentation in distal chromosome regions. This could be a hint that NSE4A is involved in crossover mechanisms. However, more detailed studies are required to clarify the situation.

5.11 NSE4::GFP is detectable at prophase I, II and the tetrads stage

The analysis of *A. thaliana* plants expressing *pnse4A::gNse4A::GFP* revealed a chromatin-specific localization of NSE4A in G2, prophase I, II and tetrad cells (Figure 57). The distribution of NSE4A in meiosis and mitosis is similar. In both, NSE4A is present in interphase, but strongly reduced during metaphase I and anaphase I. At prophase II and the tetrad stage NSE4A becomes recovered. Meta- and anaphase II cells were not found during analysis. Interestingly, at prophase I NSE4A, creates 'line-like' structures similar as ZYP1, the synaptonemal complex protein (Higgins et al., 2005). A model summarizing the described observations is visible in Figure 57.

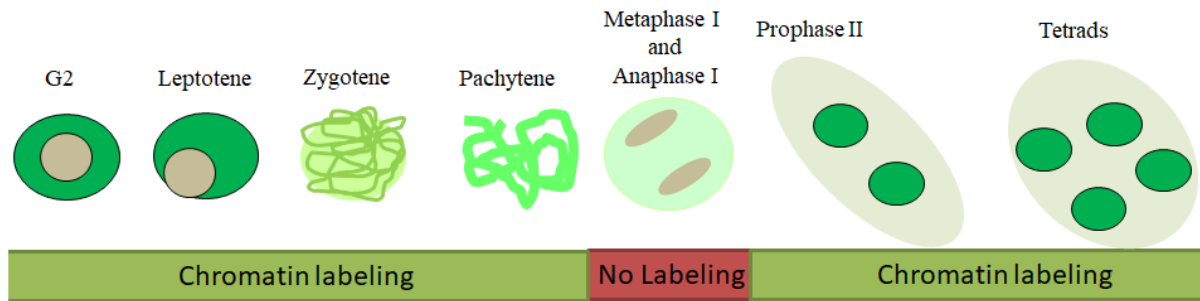


Figure 57 Dynamics of NSE4A::GFP during the meiosis of *A. thaliana* meiosis. In G2 and leptotene, NSE4A::GFP displays a strong dispersed chromatin labeling. At zygotene and pachytene, NSE4A::GFP shows ‘line-like’ signals along the chromosome axis. At metaphase I and anaphase I the protein becomes released from the chromosomes and accumulates in the cytoplasm. At prophase II and the tetrad stage NSE4A-signals reappear.

The dispersed occurrence of NSE4A within chromatin at meiotic prophase might be explained by its topological or catalytic function. As mentioned before, SMC5/6 is an ATP-dependent intermolecular DNA linker and has a genomic stabilization role and function in DNA organization (Carter and Sjögren, 2012; Kanno et al., 2015). In addition, SMC5/6 complexes of non-plant organisms have a role in meiotic double strand break repair, DNA synthesis and synaptonemal complex stability (Verver et al., 2016). The meiotic localization of NSE4A in *A. thaliana* may be connected to these functions.

5.12 Is NSE4A a synaptonemal complex component in plants?

The application of NSE4A antibodies on *A. thaliana* wild-type meiocytes did not result in a clear chromatin labeling. In order to overcome these immunostaining problems, the closely related species *B. rapa* was tested. Staining of *B. rapa* pachytene cells showed the colocalization of NSE4A with the synaptonemal complex component ZYP1 (Figure 49). Such a colocalization of SMC5/6 subunits and synaptonemal complex proteins at prophase I has already been reported in mouse (Gomez et al., 2013) and human (Verver et al., 2014). Anti-AtNSE4A signals showed ‘dotted lines’ along ZYP1 signals. However, the immunolabeling signals were not very clear due to cytoplasmic background staining (Figure 47).

Also the NSE4A immunolabeling of *A. thaliana* meiocytes resulted in a strong staining of the cytoplasm. This observation could be explained by the high amount of cytoplasm in meiotic

cells. *B. rapa* has larger chromosomes than *A. thaliana*, and therefore is easier to be characterized by cytogenetic methods, because the nuclei are more suitable for preparation.

Experiments performed by Susann Hesse (IPK, Gatersleben) using the identical NSE4A antibodies on *Secale cereale* prophase I chromosomes revealed a strict colocalization with ZYP1-specific signals from zygotene until diakinesis. In zygotene NSE4A creates ‘line-like’ signals at the paired homologues (Fig. 58A, B). At later stages NSE4A reorganizes to form finally ball-like structures in diakinesis together with ZYP1 (Fig. 58C). The ubiquitin E3 ligase HEI10 required for class I crossing-over also colocalizes to these structures (Hesse et al., submitted).

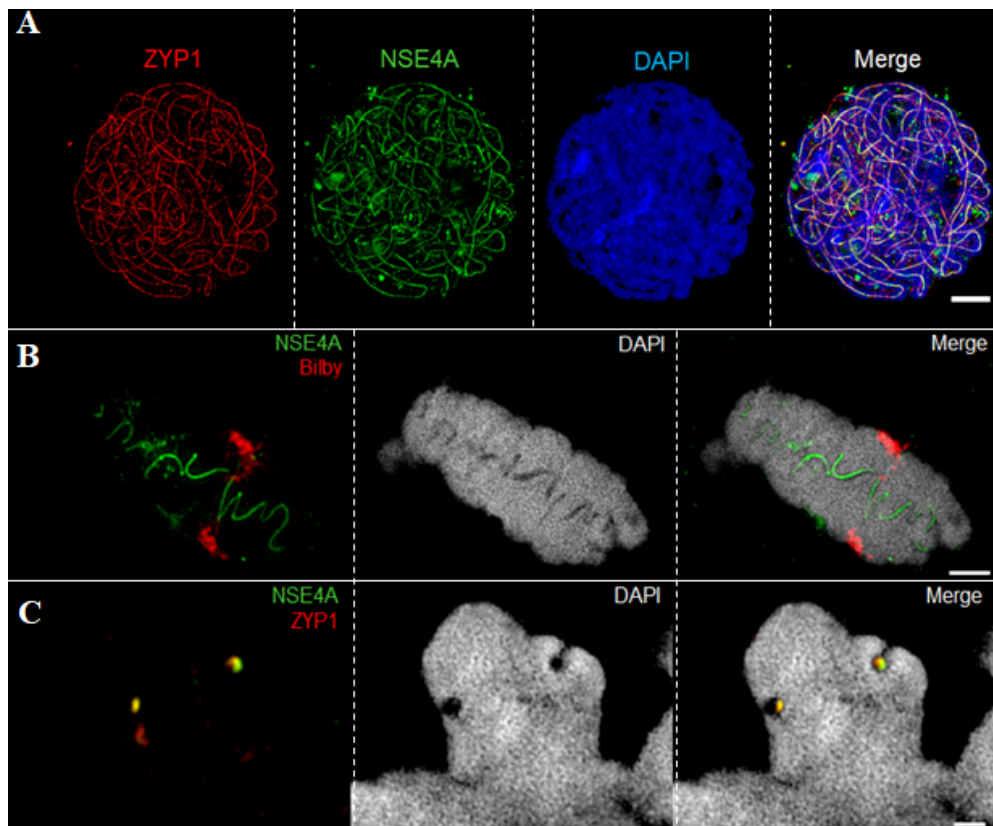


Figure 58 ZYP1 and NSE4A colocalize at the synaptonemal complex (SC) of rye. (A) Immunolocalization of NSE4A and ZYP1 shows their colocalization at the central region of the SC throughout zygotene Bars = 5 μ m. (B) NSA4A structure between bivalents in diplotene cells. The FISH probe Bilby labels the rye centromeres. Bar = 2 μ m. (C) ZYP1 and NSE4A form ball-like structure embedded in chromatin-free regions during diakinesis; Bar = 1 μ m.

The localization of NSE4A in the synaptonemal complex might be explained by the topological function of the SMC5/6 complex. Studies in mice showed that the loading of SMC6 depends on

the transverse filaments-Synaptonemal Complex Protein 1 (SYCP1) (Gomez et al., 2013). In our studies we found the colocalization between NSE4A and the transverse filament protein ZYP1 in *B. rapa* and *S. cereale*. The putative function of NSE4A in the synaptonemal complex is still enigmatic. However, it might be connected with the topological function of the SMC5/6 complex. SMC5/6 as a structural complex might link synaptonemal complex DNA or its elements. This hypothesis is supported by investigations in non-plant organisms, which revealed a connection of the SMC5/6 function with the synaptonemal complex assembly and with synapsis (Verver et al., 2014; 2016; Gomez et al., 2013). In addition, research on *C. elegans* and *S. pombe* showed a function of the SMC5/6 complex in meiotic recombination which takes place in pachytene (Bickel et al., 2010; Xavier et al., 2013). Our studies also showed strong NSE4A::GFP foci during pachytene. Furthermore, in *S. cereale* we found the colocalization of NSE4A, ZYP1 and HEI10. The colocalization between these three proteins may indicate an engagement of NSE4A in meiotic recombination.

5.13 The proposed function of NSE4 in plants

By combining the results from our work and previously published findings, we can put forward a hypothesis about the function of NSE4 in plants. NSE4A is a functional element of the SMC5/6 complex. Its function seems to be involved in the topological organization of chromatin in somatic interphase, meiotic prophase I and II, and in tetrads. In those stages, SMC5/6 may (i) interact with DNA using its ring structure and/or (ii) organize other structural proteins using the catalytic subunit NSE2. NSE4 plays a role in DNA synthesis, DSB repair and crossover intermediate resolution by supporting chromatid intertwinings or double Holliday junction resolution. The lack of proper NSE4 function results in anaphase bridges, lagging or fragmented chromosomes during mitosis and meiosis. The segregation defects correlate with abnormal development or reduced fertility caused by damaged or unequal chromosome segregation. NSE4 is present in euchromatin of somatic interphase nuclei, as well as in prophase I, II and tetrads of meiosis. In prophase I NSE4A colocalizes with the synaptonemal complex, which is conserved across different organisms including plants. NSE4A colocalizes with ZYP1, which acts as a structural element of the synaptonemal complex, and may facilitate its assembly, synapsis and meiotic recombination.

6. Outlook

1. To evaluate the origin of metaphase fragmentation in *nse4A*, a combination between between knock-out *spo11* and *nse4A* (GK-768H08) should be performed. The double mutation may explain whether the metaphase fragmentation in GK-768H08 is induced by meiosis-specific double strand breaks.
2. To determine the dynamics of NSE4A in detail, immuno co-localization between NSE4A and the synaptonemal complex proteins (ASY1 and/or ZYP1) should be performed. The labeling might reveal the loading, assembly and disassembly dynamics of NSE4A and of synaptonemal complex elements in *A. thaliana*.
3. To explore the interaction partners of NSE4A in *A. thaliana*, a protein pull-down assay might be performed. In this experiment, NSE4A::GFP might be used. The outcome might reveal interactions between NSE4A and SMC5/6 subunits or synaptonemal complex proteins.
4. To evaluate interactions and binding sites of *A. thaliana* NSE4 and SMC5/6 proteins, targeted mutagenesis combined with bimolecular fluorescence complementation or yeast two-hybrid might be performed. Such an experiment might elucidate the role of a conserved NSE4-C domain, as well as the exact SMC5 and SMC6 binding sites.

7. References

- Alt, A., Dang, H. Q., Wells, O. S., Polo, L. M., Smith, M. A., McGregor, G. A., . . . Pearl, L. H.** (2017). Specialized interfaces of Smc5/6 control hinge stability and DNA association. *Nature Communications* **8**, 14011.
- Armstrong, S.** (2013). Spreading and fluorescence in situ hybridization of male and female meiocyte chromosomes from *Arabidopsis thaliana* for cytogenetical analysis. *Plant Meiosis: Methods and Protocols* (pp. 3-11). Totowa, NJ: Humana Press.
- Bagherieh-Najjar, M. B., de Vries, O. M., Hille, J., & Dijkwel, P. P.** (2005). Arabidopsis RecQ14A suppresses homologous recombination and modulates DNA damage responses. *Plant Journal* **43**, 789-798.
- Bavner, A., Matthews, J., Sanyal, S., Gustafsson, J. A., & Treuter, E.** (2005). EID3 is a novel EID family member and an inhibitor of CBP-dependent co-activation. *Nucleic Acids Research* **33**, 3561-3569.
- Bermudez-Lopez, M., Ceschia, A., de Piccoli, G., Colomina, N., Pasero, P., Aragon, L., & Torres-Rosell, J.** (2010). The Smc5/6 complex is required for dissolution of DNA-mediated sister chromatid linkages. *Nucleic Acids Research* **38**, 6502-6512.
- Bermudez-Lopez, M., Villoria, M. T., Esteras, M., Jarmuz, A., Torres-Rosell, J., Clemente-Blanco, A., & Aragon, L.** (2016). Sgs1's roles in DNA end resection, HJ dissolution, and crossover suppression require a two-step SUMO regulation dependent on Smc5/6. *Genes & Development* **30**, 1339-1356.
- Bermúdez-López, M., & Aragon, L.** (2017). Smc5/6 complex regulates Sgs1 recombination functions. *Current Genetics* **63**, 381-388.
- Bickel, J. S., Chen, L., Hayward, J., Yeap, S. L., Alkers, A. E., & Chan, R. C.** (2010). Structural maintenance of chromosomes (SMC) proteins promote homolog-independent recombination repair in meiosis crucial for germ cell genomic stability. *PLOS Genetics* **6**, e1001028.
- Bolanos-Villegas, P., De, K., Pradillo, M., Liu, D., & Makaroff, C. A.** (2017). In favor of establishment: regulation of chromatid cohesion in plants. *Frontiers in Plant Science* **8**, 846.
- Bonner, J. N., Choi, K., Xue, X., Torres, N. P., Szakal, B., Wei, L., . . . Zhao, X.** (2016). Smc5/6 mediated sumoylation of the Sgs1-Top3-Rmi1 complex promotes removal of recombination intermediates. *Cell Reports* **16**, 368-378.
- Bowman, G. D., & Poirier, M. G.** (2015). Post-translational modifications of histones that influence nucleosome dynamics. *Chemical Reviews* **115**, 2274-2295.
- Bradford, M. M.** (1976). A rapid and sensitive method for the quantitation of microgram quantities of protein utilizing the principle of protein-dye binding. *Analytical Biochemistry* **72**, 248-254.
- Carter, S. D., & Sjogren, C.** (2012). The SMC complexes, DNA and chromosome topology: right or knot? *Critical Reviews in Biochemistry and Molecular Biology* **47**, 1-16.
- Chelysheva, L. A., Grandont, L., & Grelon, M.** (2013). Immunolocalization of meiotic proteins in *Brassicaceae*: method 1. *Methods in Molecular Biology* **990**, 93-101
- Copsey, A., Tang, S., Jordan, P. W., Blitzblau, H. G., Newcombe, S., Chan, A. C.-h., . . . Hoffmann, E.** (2013). Smc5/6 coordinates formation and resolution of joint molecules with chromosome morphology to ensure meiotic divisions. *PLOS Genetics* **9**, e1004071.

- Czechowski, T., Stitt, M., Altmann, T., Udvardi, M. K., & Scheible, W. R.** (2005). Genome-wide identification and testing of superior reference genes for transcript normalization in *Arabidopsis*. *Plant Physiology* **139**, 5-17.
- Da Ines, O., Degroote, F., Goubely, C., Amiard, S., Gallego, M. E., & White, C. I.** (2013). Meiotic recombination in *Arabidopsis* is catalysed by DMC1, with RAD51 playing a supporting role. *PLOS Genetics* **9**, e1003787.
- De Carvalho, C. E., & Colaiacovo, M. P.** (2006). SUMO-mediated regulation of synaptonemal complex formation during meiosis. *Genes & Development* **20**, 1986-1992.
- De Mey, Lambert, Bajer, Moeremans, and Brabander** (1982) Visualization of microtubules in interphase and mitotic plant cells of *Haemanthus* endosperm with the immuno-gold staining method. *Proceedings of the National Academy of Sciences of the United States of America* **79**, 1898–1902.
- De, K., Sterle, L., Krueger, L., Yang, X., & Makaroff, C. A.** (2014). *Arabidopsis thaliana* WAPL is essential for the prophase removal of cohesin during meiosis. *PLOS Genetics* **10**, e1004497.
- Dereeper, A., Guignon, V., Blanc, G., Audic, S., Buffet, S., Chevenet, F., . . . Gascuel, O.** (2008). Phylogeny.fr: robust phylogenetic analysis for the non-specialist. *Nucleic Acids Research* **36**, W465-469.
- Diaz, M., & Pecinka, A.** (2018). Scaffolding for repair: understanding molecular functions of the SMC5/6 complex. *Genes (Basel)* **9**.
- Ding, Y., Ndamukong, I., Xu, Z., Lapko, H., Fromm, M., & Avramova, Z.** (2012). ATX1-generated H3K4me3 is required for efficient elongation of transcription, not initiation, at ATX1-regulated genes. *PLOS Genetics* **8**, e1003111.
- Dreissig, S., Fuchs, J., Cápál, P., Kettles, N., Byrne, E., & Houben, A.** (2015). Measuring meiotic crossovers via multi-locus genotyping of single pollen grains in barley. *PLOS One* **10**, e0137677.
- Du, J., Johnson, L. M., Groth, M., Feng, S., Hale, C. J., Li, S., . . . Jacobsen, S. E.** (2014). Mechanism of DNA methylation-directed histone methylation by KRYPTONITE. *Molecular Cell* **55**, 495-504.
- Farmer, S., San-Segundo, P. A., & Aragón, L.** (2011). The Smc5–Smc6 complex is required to remove chromosome junctions in meiosis. *PLOS One* **6**, e20948.
- Feder, M. E.** (2007). Evolvability of physiological and biochemical traits: evolutionary mechanisms including and beyond single-nucleotide mutation. *Journal of Experimental Biology* **210**, 1653-1660.
- Fernandez-Capetillo, O.** (2016). The (elusive) role of the SMC5/6 complex. *Cell Cycle* **15**, 775-776.
- Force, A., Lynch, M., Pickett, F. B., Amores, A., Yan, Y. L., & Postlethwait, J.** (1999). Preservation of duplicate genes by complementary, degenerative mutations. *Genetic* **151**.
- Gallego-Paez, L. M., Tanaka, H., Bando, M., Takahashi, M., Nozaki, N., Nakato, R., . . . Hirota, T.** (2014). Smc5/6-mediated regulation of replication progression contributes to chromosome assembly during mitosis in human cells. *Molecular Biology of the Cell* **25**, 302-317.
- Gerlach, W. L., & Bedbrook, J. R.** (1979). Cloning and characterization of ribosomal RNA genes from wheat and barley. *Nucleic Acids Research* **7**, 1869-1885.

- Giraut, L., Falque, M., Drouaud, J., Pereira, L., Martin, O. C., & Mézard, C.** (2011). Genome-wide crossover distribution in *Arabidopsis thaliana* meiosis reveals sex-specific patterns along chromosomes. *PLOS Genetics* **7**, e1002354.
- Gómez, R., Jordan, P. W., Viera, A., Alsheimer, M., Fukuda, T., Jessberger, R., . . . Suja, J. A.** (2013). Dynamic localization of SMC5/6 complex proteins during mammalian meiosis and mitosis suggests functions in distinct chromosome processes. *Journal of Cell Science* **126**, 4239-4252.
- Gu, D., Chen, C. Y., Zhao, M., Zhao, L., Duan, X., Duan, J., . . . Liu, X.** (2017). Identification of HDA15-PIF1 as a key repression module directing the transcriptional network of seed germination in the dark. *Nucleic Acids Research* **45**, 7137-7150.
- Haering, C. H., Lowe, J., Hochwagen, A., & Nasmyth, K.** (2002). Molecular architecture of SMC proteins and the yeast cohesin complex. *Molecular Cell* **9**, 773-788
- Hanin, M., Mengiste, T., Bogucki, A., & Paszkowski, J.** (2000). Elevated levels of intrachromosomal homologous recombination in *Arabidopsis* overexpressing the *MIM* gene. *The Plant Journal* **24**, 183-189.
- Hartung, F., Wurz-Wildersinn, R., Fuchs, J., Schubert, I., Suer, S., & Puchta, H.** (2007). The catalytically active tyrosine residues of both SPO11-1 and SPO11-2 are required for meiotic double-strand break induction in *Arabidopsis*. *The Plant Cell* **19**, 3090-3099.
- Hesse S., Zekowski M., Keijzer K., Mikhailova E., Houben A., Schubert V.,** (2018) Ultrastructure and dynamics of synaptonemal complex components during meiotic pairing of rye A and B chromosomes. (Frontiers in Plant Science, submitted).
- Higgins, J. D., Sanchez-Moran, E., Armstrong, S. J., Jones, G. H., & Franklin, F. C. H.** (2005). The *Arabidopsis* synaptonemal complex protein ZYP1 is required for chromosome synapsis and normal fidelity of crossing over. *Genes & Development* **19**, 2488-2500.
- Hu, B., Liao, C., Millson, S. H., Mollapour, M., Prodromou, C., Pearl, L. H., . . . Panaretou, B.** (2005). Qri2/Nse4, a component of the essential Smc5/6 DNA repair complex. *Molecular Microbiology* **55**, 1735-1750.
- Ishida, T., Fujiwara, S., Miura, K., Stacey, N., Yoshimura, M., Schneider, K., . . . Sugimoto, K.** (2009). SUMO E3 ligase HIGH PLOIDY2 regulates endocycle onset and meristem maintenance in *Arabidopsis*. *Plant Cell* **21**, 2284-2297.
- Ishida, T., Yoshimura, M., Miura, K., & Sugimoto, K.** (2012). MMS21/HPY2 and SIZ1, two *Arabidopsis* SUMO E3 ligases, have distinct functions in development. *PLOS One* **7**, e46897.
- Jeppsson, K., Carlborg, K. K., Nakato, R., Berta, D. G., Lilienthal, I., Kanno, T., . . . Sjogren, C.** (2014). The chromosomal association of the Smc5/6 complex depends on cohesion and predicts the level of sister chromatid entanglement. *PLOS Genetics* **10**, e1004680.
- Jeppsson, K., Kanno, T., Shirahige, K., & Sjogren, C.** (2014). The maintenance of chromosome structure: positioning and functioning of SMC complexes. *Nature Reviews Molecular Cell Biology* **15**, 601-614.
- Kanno, T., Berta, D. G., & Sjogren, C.** (2015). The Smc5/6 complex is an ATP-dependent intermolecular DNA linker. *Cell Reports* **12**, 1471-1482.
- Knoll, A., Schropfer, S., & Puchta, H.** (2014). The RTR complex as caretaker of genome stability and its unique meiotic function in plants. *Frontiers in Plant Science* **5**, 33.

- Kuznetsova, M. A., & Sheval, E. V.** (2016). Chromatin fibers: from classical descriptions to modern interpretation. *Cell Biology International* **40**, 1140-1151.
- Kwak, J. S., Son, G. H., Kim, S.-I., Song, J. T., & Seo, H. S.** (2016). *Arabidopsis* HIGH PLOIDY2 sumoylates and stabilizes flowering locus C through its E3 ligase activity. *Frontiers in Plant Science* **7**.
- Lambing, C., Franklin, F. C. H., & Wang, C.-J. R.** (2017). Understanding and manipulating meiotic recombination in plants. *Plant Physiology* **173**, 1530-1542.
- Li, G., Zou, W., Jian, L., Qian, J., Deng, Y., & Zhao, J.** (2017). Non-SMC elements 1 and 3 are required for early embryo and seedling development in *Arabidopsis*. *Journal of Experimental Botany* **68**, 1039-1054.
- Li, J., Harper, L. C., Golubovskaya, I., Wang, C. R., Weber, D., Meeley, R. B., . . . Schnable, P. S.** (2007). Functional analysis of maize RAD51 in meiosis and double-strand break repair. *Genetics* **176**, 1469-1482.
- Li, W., Chen, C., Markmann-Mulisch, U., Timofejeva, L., Schmelzer, E., Ma, H., & Reiss, B.** (2004). The *Arabidopsis AtRAD51* gene is dispensable for vegetative development but required for meiosis. *Proceedings of the National Academy of Sciences of the United States of America* **101**, 10596-10601.
- Liu, M., Shi, S., Zhang, S., Xu, P., Lai, J., Liu, Y., . . . Yang, C.** (2014). SUMO E3 ligase AtMMS21 is required for normal meiosis and gametophyte development in *Arabidopsis*. *BMC Plant Biology* **14**.
- Magadum, S., Banerjee, U., Murugan, P., Gangapur, D., & Ravikesavan, R.** (2013). Gene duplication as a major force in evolution. *Journal of Genetics* **92**, 155-161.
- Manthei, K. A., & Keck, J. L.** (2013). The BLM dissolvasome in DNA replication and repair. *Cell and Molecular Life Science* **70**, 4067-4084.
- Martinez-Zapater, J. M., Estelle, M. A., & Somerville, C. R.** (1986). A highly repeated DNA sequence in *Arabidopsis thaliana*. *Molecular and General Genetics MGG* **204**, 417-423.
- McElver, J., Tzafrir, I., Aux, G., Rogers, R., Ashby, C., Smith, K., . . . Patton, D.** (2001). Insertional mutagenesis of genes required for seed development in *Arabidopsis thaliana*. *Genetics* **159**, 1751-1763.
- Mengiste, T., Revenkova, E., Bechtold, N., & Paszkowski, J.** (1999). An SMC-like protein is required for efficient homologous recombination in *Arabidopsis*. *The EMBO Journal* **18**, 4505-4512.
- Mukhopadhyay, D., & Dasso, M.** (2017). The SUMO pathway in mitosis. *Advances in Experimental Medicine and Biology* **963**, 171-184.
- Nagl W, Fusenig HP.** (1979) Types of chromatin organization in plant nuclei. *Plant Systematics and Evolution Supplement* **2**, (pg. 221-233).
- Nakagawa, T., Suzuki, T., Murata, S., Nakamura, S., Hino, T., Maeo, K., . . . Ishiguro, S.** (2007). Improved gateway binary vectors: high-performance vectors for creation of fusion constructs in transgenic analysis of plants. *Bioscience, Biotechnology, and Biochemistry* **71**, 2095-2100.
- Nakamura, S., Mano, S., Tanaka, Y., Ohnishi, M., Nakamori, C., Araki, M., . . . Ishiguro, S.** (2010). Gateway binary vectors with the bialaphos resistance gene, bar, as a selection marker for plant transformation. *Bioscience, Biotechnology, and Biochemistry* **74**, 1315-1319.
- Nasmyth, K., & Haering, C. H.** (2005). The structure and function of SMC and kleisin complexes. *Annual Review of Biochemistry* **74**, 595-648.

- Niki, H., Imamura, R., Kitaoka, M., Yamanaka, K., Ogura, T., & Hiraga, S.** (1992). *E. coli* MukB protein involved in chromosome partition forms a homodimer with a rod-and-hinge structure having DNA binding and ATP/GTP binding activities. *EMBO Journal* **11**, 5101-5109.
- O'Connor, C.** (2008) Cell division: stages of mitosis. *Nature Education* **1**,188.
- O'Connor, C.** (2008) Meiosis, genetic recombination, and sexual reproduction. *Nature Education* **1**,174.
- Odell, J. T., Nagy, F., & Chua, N. H.** (1985). Identification of DNA sequences required for activity of the cauliflower mosaic virus 35S promoter. *Nature* **313**, 810-812.
- Olins, A. L., & Olins, D. E.** (1974). Spheroid chromatin units (v bodies). *Science* **183**, 330-332.
- Palecek, J., Vidot, S., Feng, M., Doherty, A. J., & Lehmann, A. R.** (2006). The Smc5-Smc6 DNA repair complex. bridging of the Smc5-Smc6 heads by the KLEISIN, Nse4, and non-Kleisin subunits. *Journal of Biological Chemistry* **281**, 36952-36959.
- Panchy, N., Lehti-Shiu, M., & Shiu, S. H.** (2016). Evolution of gene duplication in plants. *Plant Physiology* **171**, 2294-2316.
- Park, H. J., Kim, W. Y., Park, H. C., Lee, S. Y., Bohnert, H. J., & Yun, D. J.** (2011). SUMO and SUMOylation in plants. *Molecular Cells* **32**, 305-316.
- Pawlowski, W. P., & Cande, W. Z.** (2005) Coordinating the events of the meiotic prophase. *Trends in Cell Biology* **15**, 674-681.
- Pebernard, S., McDonald, W. H., Pavlova, Y., Yates, J. R., 3rd, & Boddy, M. N.** (2004). Nse1, Nse2, and a novel subunit of the Smc5-Smc6 complex, Nse3, play a crucial role in meiosis. *Molecular Biology of the Cell* **15**, 4866-4876.
- Rattner, J. B., Hendzel, M. J., Furbee, C. S., Muller, M. T., & Bazett-Jones, D. P.** (1996). Topoisomerase II alpha is associated with the mammalian centromere in a cell cycle- and species-specific manner and is required for proper centromere/kinetochore structure. *Journal of Cell Biology* **134**, 1097-1107.
- Richards, E. J., & Ausubel, F. M.** (1988). Isolation of a higher eukaryotic telomere from *Arabidopsis thaliana*. *Cell* **53**, 127-136.
- Rogacheva, M. V., Manhart, C. M., Chen, C., Guarne, A., Surtees, J., & Alani, E.** (2014). Mlh1-Mlh3, a meiotic crossover and DNA mismatch repair factor, is a Msh2-Msh3-stimulated endonuclease. *Journal of Biological Chemistry* **289**, 5664-5673.
- Sanchez Moran, E., Armstrong, S. J., Santos, J. L., Franklin, F. C., & Jones, G. H.** (2001). Chiasma formation in *Arabidopsis thaliana* accession Wassileskija and in two meiotic mutants. *Chromosome Research* **9**, 121-128.
- Sanger, F., Nicklen, S., & Coulson, A. R.** (1977). DNA sequencing with chain-terminating inhibitors. *Proceedings of the National Academy of Sciences of the United States of America* **74**, 5463-5467.
- Schmittgen, T. D., & Livak, K. J.** (2008). Analyzing real-time PCR data by the comparative C(T) method. *Nature Protocols* **3**, 1101-1108.
- Schubert, V.** (2009). SMC proteins and their multiple functions in higher plants. *Cytogenetic Genome Research* **124**, 202-214.
- Schubert, V., & Weisshart, K.** (2015). Abundance and distribution of RNA polymerase II in *Arabidopsis* interphase nuclei. *Journal of Experimental Botany* **66**, 1687-1698.
- Schubert, V., Lermontova, I., & Schubert, I.** (2013). The *Arabidopsis* CAP-D proteins are required for correct chromatin organisation, growth and fertility. *Chromosoma* **122**, 517-533.

- Schubert, V., & Weisshart, K.** (2015). Abundance and distribution of RNA polymerase II in *Arabidopsis* interphase nuclei. *Journal of Experimental Botany* **66**, 1687-1698.
- Sergeant, J., Taylor, E., Palecek, J., Foustari, M., Andrews, E. A., Sweeney, S., . . . Lehmann, A. R.** (2005). Composition and architecture of the *Schizosaccharomyces pombe* Rad18 (Smc5-6) complex. *Molecular Cell Biology* **25**, 172-184.
- Simillion, C., Vandepoele, K., Van Montagu, M. C., Zabeau, M., & Van de Peer, Y.** (2002). The hidden duplication past of *Arabidopsis thaliana*. *Proceedings of the National Academy of Sciences of the United States of America* **99**, 13627-13632.
- Smith, S. J., Osman, K., & Franklin, F. C.** (2014). The condensin complexes play distinct roles to ensure normal chromosome morphogenesis during meiotic division in *Arabidopsis*. *Plant Journal* **80**, 255-268.
- Stoltzfus, A.** (1999). On the possibility of constructive neutral evolution. *Journal of Molecular Evolution* **49**, 169-181.
- Smyth, D. R., Bowman, J. L., & Meyerowitz, E. M.** (1990). Early flower development in *Arabidopsis*. *Plant Cell* **2**, 755-767.
- Strunnikov, A. V., Larionov, V. L., & Koshland, D.** (1993). *Smc1*: an essential yeast gene encoding a putative head-rod-tail protein is required for nuclear division and defines a new ubiquitous protein family. *Journal of Cell Biology* **123**, 1635-1648.
- Taylor, E. M., Copsey, A. C., Hudson, J. J. R., Vidot, S., & Lehmann, A. R.** (2008). Identification of the proteins, including MAGEG1, that make up the human SMC5-6 protein complex. *Molecular and Cellular Biology* **28**, 1197-1206.
- Tran, M., Tsarouhas, V., & Kegel, A.** (2016). Early development of *Drosophila* embryos requires Smc5/6 function during oogenesis. *5*, 928-941.
- Tzafirir, I., Pena-Muralla, R., Dickerman, A., Berg, M., Rogers, R., Hutchens, S., . . . Meinke, D.** (2004). Identification of genes required for embryo development in *Arabidopsis*. *Plant Physiology* **135**, 1206-1220.
- Verver, D. E., Hwang, G. H., Jordan, P. W., & Hamer, G.** (2016). Resolving complex chromosome structures during meiosis: versatile deployment of Smc5/6. *Chromosoma* **125**, 15-27.
- Verver, D. E., Langedijk, N. S., Jordan, P. W., Repping, S., & Hamer, G.** (2014). The SMC5/6 complex is involved in crucial processes during human spermatogenesis. *Biology of Reproduction* **91**, 22.
- Voelkel-Meiman, K., Taylor, L. F., Mukherjee, P., Humphries, N., Tsubouchi, H., & MacQueen, A. J.** (2013). SUMO localizes to the central element of synaptonemal complex and is required for the full Synapsis of meiotic chromosomes in budding yeast. *PLOS Genetics* **9**, e1003837.
- Wang, S., & Adams, K. L.** (2015). Duplicate gene divergence by changes in microRNA binding sites in *Arabidopsis* and *Brassica*. *Genome Biology and Evolution* **7**, 646-655.
- Watanabe, K., Pacher, M., Dukowic, S., Schubert, V., Puchta, H., & Schubert, I.** (2009). The STRUCTURAL MAINTENANCE OF CHROMOSOMES 5/6 complex promotes sister chromatid alignment and homologous recombination after DNA damage in *Arabidopsis thaliana*. *Plant Cell* **21**, 2688-2699.
- Wilhelm, L., Burmann, F., Minnen, A., Shin, H. C., Toseland, C. P., Oh, B. H., & Gruber, S.** (2015). SMC condensin entraps chromosomal DNA by an ATP hydrolysis dependent loading mechanism in *Bacillus subtilis*. *Elife* **4**.

- Woodcock, C. L., & Ghosh, R. P.** (2010). Chromatin higher-order structure and dynamics. *Cold Spring Harbor Perspectives in Biology* **2**, a000596.
- Xaver, M., Huang, L., Chen, D., & Klein, F.** (2013). Smc5/6-Mms21 prevents and eliminates inappropriate recombination intermediates in meiosis. *PLOS Genetics* **9**, e1004067.
- Xu, P., & Yang, C.** (2013). Emerging role of SUMOylation in plant development. *Plant Signaling & Behavior* **8**, e24727.
- Xu, P., Yuan, D., Liu, M., Li, C., Liu, Y., Zhang, S., . . . Yang, C.** (2013). AtMMS21, an SMC5/6 complex subunit, is involved in stem cell niche maintenance and DNA damage responses in *Arabidopsis* roots. *Plant Physiology* **161**, 1755-1768.
- Xu X, Kanai R, Nakazawa N, Wang L, Toyoshima C, Yanagida M** (2018) Suppressor mutation analysis combined with 3D modeling explains cohesin's capacity to hold and release DNA. *Proceedings of the National Academy of Sciences of the United States of America* **115**, E4833-E4842.
- Yan, S., Wang, W., Marques, J., Mohan, R., Saleh, A., Durrant, W.E., Song, J., and Dong, X.** (2013). Salicylic acid activates DNA damage responses to potentiate plant immunity. *Molecular Cell* **52**, 602-610.
- Yong-Gonzales, V., Hang, L. E., Castellucci, F., Branzei, D., & Zhao, X.** (2012). The Smc5-Smc6 complex regulates recombination at centromeric regions and affects kinetochore protein sumoylation during normal growth. *PLOS One* **7**, e51540.
- Yuan, D., Lai, J., Xu, P., Zhang, S., Zhang, J., Li, C., . . . Yang, C.** (2014). AtMMS21 regulates DNA damage response and homologous recombination repair in *Arabidopsis*. *DNA Repair (Amst)* **21**, 140-147.
- Zhang, S., Qi, Y., Liu, M., & Yang, C.** (2013). SUMO E3 ligase AtMMS21 regulates drought tolerance in *Arabidopsis thaliana* (F). *Journal of Integrative Plant Biology* **55**, 83-95.
- Zmienko, A., Samelak, A., Kozłowski, P., & Figlerowicz, M.** (2014). Copy number polymorphism in plant genomes. *TAG. Theoretical and Applied Genetics. Theoretische und Angewandte Genetik* **127**, 1-18.

Publications in connection with the submitted dissertation

Zelkowski M., Zelkowska K., Pradillo M., Santos J.L., Marzec M., Houben A., Schubert V. (2018). Arabidopsis NSE4 proteins act in somatic nuclei and meiosis to ensure plant viability and fertility. (in preparation).

Hesse S., **Zelkowski M.**, Keijzer K., Mikhailova E., Houben A., Schubert V. (2018). Ultrastructure and dynamics of synaptonemal complex components during meiotic pairing of rye A and B chromosomes. *Frontiers in Plant Science*.

Declarations

Eidesstattliche Erklärung / Declaration under Oath

Ich erkläre an Eides statt, dass ich die Arbeit selbstständig und ohne fremde Hilfe verfasst, keine anderen als die von mir angegebenen Quellen und Hilfsmittel benutzt und die den benutzten Werken wörtlich oder inhaltlich entnommenen Stellen als solche kenntlich gemacht habe.

I declare under penalty of perjury that this thesis is my own work entirely and has been written without any help from other people. I used only the sources mentioned and included all the citations correctly both in word or content.

25.06.2018

Matthias Zellwies

Datum / Date

Unterschrift des Antragstellers / Signature of the applicant

Erklärung über bestehende Vorstrafen und anhängige Ermittlungsverfahren / Declaration concerning Criminal Record and Pending Investigations

Hiermit erkläre ich, dass ich weder vorbestraft bin noch dass gegen mich Ermittlungsverfahren anhängig sind. / *I hereby declare that I have no criminal record and that no preliminary investigations are pending against me.*

25.06.2018

Matthias Zellwies

Datum / Date

Unterschrift des Antragstellers / Signature of the applicant

Curriculum Vitae

Personal Details:

Name Mateusz Zelkowski
Gender Male
Nationality Polish
Present address 426 Winthrop dr. Apt. 10
14850 Ithaca NY, United States of America
Date of birth 11 June 1988

Contact information:

Phone +48 730 412 123
E-mail mateusz.zelkowski@gmail.com

Education

2014 – 2018 Leibniz Institute of Plant Genetics and Crop Plant Research, Laboratory of Chromosome Structure and Function in Gatersleben (Germany) – **PhD candidate**

2015 – 2017 University of Amsterdam (Netherlands) and Complutense University of Madrid (Spain) – **Internship**

2012 – 2013 University of Bergen (Norway), Brain Tumor Immunology & Therapy lab - Leonardo da Vinci program **Internship**

2013 Polish Academy of Science (IITD), Laboratory of Molecular Biology of Microorganisms in Wroclaw (Poland) - **Contract researcher**

2010 – 2012 **MSc in Chemistry and Biotechnology** at the Polish Academy of Science (IITD) and Wroclaw University of Technology in Wroclaw (Poland)

2011 École Normale Supérieure de Cachan, Laboratory of Biology and Applied Pharmacology in Cachan/Paris (France) - **Internship**

2007 - 2010 **Engineer of Biotechnology** at the Wroclaw University of Technology

Publications

Zelkowski M., Zelkowska K., Marzec M., Houben A., Schubert V. (2018). Arabidopsis NSE4 proteins are involved in mitosis and meiosis to ensure plant viability and fertility. (article in preparation).

Hesse S., **Zelkowski M.**, Keijzer K., Mikhailova E., Houben A., Schubert V. (2018). Ultrastructure and dynamics of synaptonemal complex components during meiotic pairing of rye A and B chromosomes. *Frontiers in Plant Science*.

Schubert V., **Zelkowski M.**, Klemme S., Houben A. (2016). Similar sister chromatid arrangement in mono- and holocentric plant chromosomes. *Cytogenetics and Genome Research* **149**, 218-225.

Gras Navarro A., Kmiecik J., Leiss L., **Zelkowski M.**, Engelsen A., Bruserud Ø., Zimmer J., Enger PØ., Chekenya M. (2014). NK cells with KIR2DS2 immunogenotype have a functional activation advantage to efficiently kill glioblastoma and prolong animal survival. *Journal of Immunology* **193**, 6192-6206.

Awards

Scientific poster distinction	“The role of the SMC5/6 complex in <i>Arabidopsis thaliana</i> “ 21 st ICC, Foz Iguazu, Brazil
EDU inspiration award	Ministry of Higher Education, Warsaw, Poland
Master Thesis distinction	Polish Science Academy, IITD PAN, Wroclaw, Poland

